Harmonic behavior and modeling of grid components and devices

Hooijmans, M.A.J.T.

Award date:
2005

TU/e technische universiteit eindhoven

Capaciteitsgroep Elektrische Energietechniek
Electrical Power Systems

Harmonic behavior and modeling of grid components and devices

door: M.A.J.T. Hooijmans
EPS.05.A.176

Afstudeerwerk verricht o.l.v.:

prof.ir. W.L. Kling
ir. J.F.G. Cobben
ir. J.G.J. Sloot

mei 2005

/ faculteit elektrotechniek

Summary

Harmonic distortion is caused by electrical equipment with non-linear current/voltage characteristics or periodically switched loads. This equipment injects current harmonics into the network. These current harmonics induce voltage harmonics in the network impedances, which are superimposed upon the existing supply voltage. Usually these harmonic voltages are no problem, because they are relatively small compared to the amplitude of the fundamental voltage. However, it is possible that resonance circuits existing within the network amplify the voltage harmonics to such an extent that they have a relatively large influence on the fundamental voltage. This results in a distorted supply voltage.
A first step into examining this distortion is determining the harmonic emission of the equipment present in the net.

Harmonic emission in the grid can consist of different amplitudes and frequencies. The most common harmonics in power systems are sinusoidal components of a periodic waveform that have frequencies which can be resolved in to multiples of the fundamental frequency. Fourier analysis is the mathematical tool employed for such an analysis. Next to these common harmonics power systems can also contain harmonics that are non-integer multiples of the fundamental frequency and have a-periodic waveforms. These are less common then the ones that are integer multiples.
Now the harmonics which are present in the grid are known, the sort of equipment causing the harmonic distortion can be examined.

It was found that the main causes of harmonics in the net are non-linear loads. From this collection of non-linear loads the inverters and lighting ballasts are the main sources of harmonic distortion in the net. Other, less significant, causes of harmonic distortion are power transformers and electrical machines. It must be taken in mind that approximately more than 90% of the harmonic distortions in the grid are caused by inverters and the huge numbers of lighting ballasts. Electrical machines and transformers only contribute a small percentage to the total harmonic distortions.
Now the main causes of harmonic distortion in the gird are known, the harmonic model can be presented.

This basic harmonic model contains information on grid and load parameters and can be extended to incorporate more complex grid topologies and loads.
The basic harmonic model elements are a harmonic voltage source, the resistance and inductance of the cabling and transformers and a universal harmonic model to incorporate typical loads. To make a proper estimation of a possible harmonic problem this model needs to consist of an accurate frequency description of each of the individual elements. If this is present, problems can be estimated by an instability analysis of this model.

A frequency description model for the resistance and inductance of two typically used medium voltage and low voltage cables is presented. The construction of these cables is discussed, followed by a general explanation of the three-phase cable impedance with insight in the cable resistance and inductance. Next the practical acquisition of the resistance and reactance of the cable is presented, followed by results of practical measurements. These measurements are then combined with the theoretical resistance and inductance to validate the acquired theory with the practical results.
From this follows that the resistance part of the harmonic model for the cable corresponds well with the measured values. The inductance part of the model is not jet complete. The inductances due to proximity effects and losses in the sheath still have to be incorporated in the theory. This can be done with the given analytical method.

With the currently used method of measurement and modelling it is possible to expand the model in a simple way to incorporate the capacitance of the cable in it if this is necessary in the future.

A basic theoretical harmonic model for a single-phase and three-phase transformer is given, which can be deducted from 50Hz manufacturer's data. If needed this basic model can be extended to incorporate the non-linear elements of a transformer. The model can also incorporate the resonating of a transformer by adding shunt capacitors to the model. This only has to be done if the transformer resonates in the harmonic frequency range of interest. Also a measurement method is given to validate the given model.

The modeling of the loads is studied. Of each appliance the frequency dependent parameters G, C and I_{inv} of the load model are determined. Measurement results of standard electrical equipment are presented. This tested equipment consists of common Dutch household appliances like television sets, video recorders, computers, etc. Next to the individual measurements there are measurements done on combinations of the equipment. This gives information on whether or not the summation of the loads is possible for the extended harmonic model.
The results imply the possibility that the load parameters are dependent on grid topologies. They also tell us that that the element G in the model is mainly positive and that element C in the model can range from positive to negative.

Samenvatting

Harmonische vervorming wordt veroorzaakt door elektrische apparaten met niet lineaire stroom/voltage karakteristieken of door periodieke geschakelde belastingen. Deze belastingen injecteren harmonische stromen in het netwerk. Deze harmonische stromen induceren harmonische voltages in de netwerkimpedanties, welke worden gesuperponeerd op de bestaande voedingsspanning. Normaal vormen deze harmonische spanningen geen probleem, omdat ze relatief klein zijn ten opzichte van de amplitude van de voedingsspanning. Het is echter mogelijk dat resonantiecircuits, bestaande in het netwerk, de harmonische spanningen versterken in zo'n mate dat ze een relatief grote invloed hebben op de voedingsspanning. Dit resulteert in een verstoorde voedingsspanning.
Een eerste stap voor een onderzoek naar deze vervormingen is het bepalen van de harmonische emissie van de apparaten in het net.

Harmonische emissie in het netwerk bestaat uit verschillende amplitudes en frequenties. De meest voorkomende harmonischen zijn sinusoïdale componenten van een periodieke golfvorm die bestaan uit frequenties die kunnen worden ontbonden in veelvouden van de fundamentele frequentie. Fourier theorie is het mathematische werktuig wat gebruikt wordt voor een dergelijke analyse. Naast deze veelvoorkomende harmonischen, kan het netwerk ook niet-gehele veelvouden van de fundamentele frequentie bevatten en a-periodieke golfvormen. Deze zijn echter minder voorkomend dan de gehele veelvouden.
Nu de bestaande harmonische vervormingen in het netwerk bekend zijn, kunnen de apparaten bepaald worden welke de belangrijkste bron zijn van de verstoringen.

Het is bevonden dat de voornamelijke bronnen van harmonischen in het netwerk niet-lineaire belastingen zijn. Van deze collectie van niet-lineaire belastingen zijn inverters en (TL) verlichting de voornamelijkste oorzaken van harmonische vervorming in het net. Andere, minder belangrijke oorzaken van vervorming zijn transformatoren en elektrische machines. Het moet in gedachten genomen worden dat ongeveer meer dan 90% van de harmonische vervorming in het netwerk worden veroorzaakt door inverters en het enorme aantal (TL) verlichting. Elektrische machines en transformatoren contribueren maar een klein percentage aan de totale harmonische vervorming.
Nu zijn de belangrijkste veroorzakers van harmonische vervorming bekend en kan het harmonische model worden gevormd.

Het harmonische model bevat informatie over netwerk en belasting parameters en kan worden uitgebreid tot een model dat meer complexe netwerk- en belasting-topologieën kan bevatten.
De elementen van het harmonische model zijn een harmonische spanningsbron, de weerstand en inductie van de bekabeling en transformatoren en een universeel harmonisch model van een standaard belasting. Om een degelijke voorspelling te doen van een mogelijk harmonisch probleem moet dit model een juiste frequentiebeschrijving van elk individueel element van bevatten. Als dit is gedaan, kan een mogelijk probleem worden geschat door een instabiliteitanalyse van het model.

Het frequentiemodel voor de weerstand en inductie van twee typerend gebruikte kabels voor middenspanning en laagspanning wordt gepresenteerd. De constructie van deze kabels wordt besproken, gevolgd door een algemene uitleg van de drie fase kabel impedantie met inzicht op de kabel zijn weerstand en inductie. Hierop volgend wordt de praktische acquisitie van de weerstand en de inductie gegeven, gevolgd door de resultaten van de praktische metingen. Deze metingen worden dan gecombineerd met de theoretische weerstand en inductie om de verkregen theorie te valideren met de praktische resultaten.

Hieruit volgt dat het weerstandsgedeelte van het harmonisch model voor de kabel goed overeenkomt met de gemeten waarden. Het inductieve deel van het model is echter nog niet compleet. De inductanties veroorzaakt door nabijheidseffecten en verliezen in de mantel van de kabel moeten nog worden opgenomen in de theorie. Dit kan worden gedaan met de gegeven analytische methode.
Met de huidige manier van meten en modelleren is het echter ook nog mogelijk om het model op een simpele manier uit te breiden, zodat het de capaciteit van de kabel kan bevatten, mocht dit mogelijk zijn in de toekomst.

Een basis harmonisch model voor een eenfase en driefase transformator wordt gegeven. Dit model kan worden afgeleid van de informatie die door de fabrikant wordt gegeven voor de transformator bij 50Hz. Mocht het nodig zijn, dan kan dit model worden uitgebreid, zodat het niet-lineaire elementen van de transformator bevat. Het model kan ook de resonantiefrequentie van een transformator simuleren door shunt capaciteiten op te nemen in het model. Dit is echter alleen maar nodig als deze resonantiefrequentie binnen de frequentieband van interesse ligt. Afsluitend wordt een meetmethode gegeven om het model te valideren.

De modellering van de belastingen is bestudeerd. Van elke toestel zijn de frequentie afhankelijk parameters G, C en I_{inv} voor het belastingmodel bepaald. Meetresultaten van standaard elektrische apparaten worden gepresenteerd. De geteste apparaten bestaan uit veel voorkomende Nederlandse apparatuur in huishoudens, zoals televisies, video's, computers, enz. Naast individuele metingen van deze apparatuur zijn ook metingen gedaan met combinaties van de apparatuur. Dit geeft informatie over het feit of de belastingen wel of niet opgeteld kunnen worden voor het uitgebreide harmonische model.
De resultaten impliceren de mogelijk dat het model voor de belastingen afhankelijk kan zijn van de netwerk topologie. De resultaten vertellen ook dat het element G in het model voornamelijk positief is en dat het element C zowel positief als negatief kan zijn.

Table of contents

1 Introduction

1.1 Problem Definition

The research into power quality has increased the last years due to the development and still growing applications of power electronics and microelectronics. This research has produced several standards for the power quality, which relate to deviations in the supply voltage. The five most important power quality aspects mentioned are voltage magnitude, voltage unbalance, harmonic distortion, flicker and dips. For the first four power quality aspects mentioned the Dutch regulator DTe ("Dienst uitvoering en Toezicht Energie") has defined criteria.

Continuon is aware of the importance of these power quality aspects in the future and has proposed research activity in this direction. One of these research activities consists of research into harmonic distortion in the grid. Continuon has chosen this field of research, because it can give insight into a theoretical estimation of a harmonic problem in the grid. With this insight it is possible to control this harmonic problem between its boundaries so that the impact on the grid and its customers can be minimized.

Harmonic distortion is caused by electrical equipment with non-linear current/voltage characteristics or periodically switched loads. This equipment injects current harmonics into the network. These current harmonics induce voltage harmonics in the network impedances, which are superimposed upon the existing supply voltage. Usually these harmonic voltages are no problem, because they are relatively small compared to the amplitude of the fundamental voltage. However, it is possible that resonance circuits existing within the network amplify the voltage harmonics to such an extent that they have a relatively large influence on the fundamental voltage. This results in a distorted supply voltage.

At the current time the impact of these harmonic voltages on the Dutch network and loads has not been fully worked out. For harmonic calculations, models of the net and the most common loads are necessary. Therefore research has to be done into the modeling of different network elements for harmonics. In the end these models can be used to predict the harmonic impact on the net with simulation.

1.2 Objectives

In this report causes and effects of harmonic distortions are determined and solutions to improve the voltage shape are analysed.
A model is presented for the combination of the net with the most common loads. For this model the behaviour of several network components at frequencies up to 2500 Hz is investigated. Among these components are cables and transformers. With these new models simulations can be carried out in the future to predict possible problems with harmonics and resonance in medium voltage and low voltage networks.

2 Theory of harmonic voltages

This chapter discusses the nature of harmonics, the theory of Fourier, the definition of harmonic voltages and an example on how a voltage waveform can be split up into harmonic waveforms with the theory of Fourier.

2.1 Nature of harmonics

The term 'harmonic' originates from acoustics, where it signifies the vibration of a string or a column of air at a frequency which is a multiple of the basic repetition (or fundamental) frequency. Similarly with electrical signals, a harmonic is defined as the content of the signal whose frequency is an integer multiple of the actual system frequency, i.e. the main frequency produced by the generators.
When a complex signal is viewed on an oscilloscope its shape is observed in the time domain; that is, for any given instant in time, the amplitude of the waveform is displayed. If the same signal is applied to a hi-fi amplifier, then the ear hears the resultant sound as a mixture of frequencies; that is, it sounds like a full musical chord. The waveform may therefore be described by its time domain or frequency domain data. The transfer between these two domains can be accomplished with the so-called Fourier transform.
It must be made clear from the outset that such a transfer is only perfectly applicable when the distorted waveform is maintained for an infinite number of cycles. This is not the case in practice, where variations in loading conditions will alter the system harmonic content. However, this problem presents no difficulty provided that the condition to be analysed persists for a reasonable time. It is thus necessary to distinguish between a harmonic, where the wave shape remains unaltered, and a transient where there is significant cycle-to-cycle variation in the wave shape.
Finally the phase relationship of the harmonic to the fundamental frequency is significant in determining the wave shape. The amplitude of the harmonic and the relative phase of the same harmonic may alter the overall effect considerably.

2.2 Theory of Fourier

The key to understanding harmonic voltages lies within the understanding of how any function, and thus also the supply voltage of a network, can be split up into a fundamental wave and the appropriate harmonics.
Following the theory of Fourier (2.1) any periodic function that obeys the following conditions can be written as a sum of cosines and sines:

1. The function must be finite
2. The number of discontinuities in the function must be finite
3. The derivative of the function may be discontinuous at a finite number of places.

Theory of Fourier:

$$f(x) = a_0 + a_1\cos(x) + a_2\cos(2x) + a_3\cos(3x) + \ldots + b_1\sin(x) + b_2\sin(2x) + b_3\sin(3x) + \ldots$$

or

$$f(x) = a_0 + \sum_{1}^{\infty}\left[a_n\cos(nx) + b_n\sin(nx)\right] \qquad (2.1)$$

For a given function f(x), the constant coefficient a_0 from equation (2.1) can be found by integrating both sides of the equation over one period:

$$\int_{-\pi}^{\pi} f(x)dx = \int_{-\pi}^{\pi}\left[a_0 + \sum_{n=1}^{\infty}\left[a_n\cos(nx) + b_n\sin(nx)\right]\right]dx$$

$$\int_{-\pi}^{\pi} f(x)dx = a_0\int_{-\pi}^{\pi}dx + \sum_{n=1}^{\infty}\left[a_n\int_{-\pi}^{\pi}\cos(nx)dx + b_n\int_{-\pi}^{\pi}\sin(nx)dx\right] \qquad (2.2)$$

$$a_0 = \frac{1}{2\pi}\int_{-\pi}^{\pi} f(x)dx$$

The a_n coefficients can be determined by multiplying equation (2.1) with cos(mx), where m is any fixed positive integer, and again integrating over one period:

$$\int_{-\pi}^{\pi} f(x)\cos(mx)dx = \int_{-\pi}^{\pi}\left[a_0 + \sum_{n=1}^{\infty}\left[a_n\cos(nx) + b_n\sin(nx)\right]\right]\cos(mx)dx$$

$$\int_{-\pi}^{\pi} f(x)\cos(mx)dx = a_0\int_{-\pi}^{\pi}\cos(mx)dx + \sum_{n=1}^{\infty}\left[a_n\int_{-\pi}^{\pi}\cos(nx)\cos(mx)dx + b_n\int_{-\pi}^{\pi}\sin(nx)\cos(mx)dx\right] \qquad (2.3)$$

The first term on the right hand side is zero, as are all the terms in b_n, since sin(nx) and cos(mx) are orthogonal functions for all n and m. Similarly, the terms in a_n are orthogonal and thus zero, unless m=n. In this case equation (2.3) becomes:

$$\int_{-\pi}^{\pi} f(x)\cos(mx)dx = a_n\int_{-\pi}^{\pi}\cos^2(nx)dx$$

$$\int_{-\pi}^{\pi} f(x)\cos(mx)dx = \frac{a_n}{2}\int_{-\pi}^{\pi}\cos(2nx)dx + \frac{a_n}{2}\int_{-\pi}^{\pi}dx \qquad (2.4)$$

$$a_n = \frac{1}{\pi}\int_{-\pi}^{\pi} f(x)\cos(nx)dx$$

To determine the coefficients b_n, the equation (2.1) is multiplied by sin(mx). By similar method as above:

$$b_n = \frac{1}{\pi}\int_{-\pi}^{\pi} f(x)\sin(nx)dx \qquad (2.5)$$

Now the coefficients are known.
If the equation of Euler (2.6) and the time ($x=\omega t$) are introduced into equation (2.1), the complex theory of Fourier (2.7) is obtained:

Euler:

$$e^{jx} = \cos x + j\sin x \qquad \cos x = \frac{e^{jx} + e^{-jx}}{2}$$

$$e^{-jx} = \cos x - j\sin x \qquad \sin x = \frac{e^{jx} - e^{-jx}}{2j} \qquad (2.6)$$

Complex theory of Fourier:

$$f(t) = \sum_{n=-\infty}^{\infty} c_n e^{jn\omega t}$$

$$with \qquad c_n = \frac{1}{T}\int_{-T/2}^{T/2} f(t)e^{-jn\omega t}dt \tag{2.7}$$

The coefficient c_n follows directly from coefficients a_n and b_n and equation (2.6):

$$a_n \cos(n\omega t) + b_n \sin(n\omega t) = a_n \frac{e^{jn\omega t} + e^{-jn\omega t}}{2} + b_n \frac{e^{jn\omega t} - e^{-jn\omega t}}{2j}$$

$$a_n \frac{e^{jn\omega t} + e^{-jn\omega t}}{2} + b_n \frac{e^{jn\omega t} - e^{-jn\omega t}}{2j} = \left(\frac{a_n}{2} + \frac{b_n}{2j}\right)e^{jn\omega t} + \left(\frac{a_n}{2} - \frac{b_n}{2j}\right)e^{-jn\omega t}$$

$$\left(\frac{a_n}{2} + \frac{b_n}{2j}\right)e^{jn\omega t} + \left(\frac{a_n}{2} - \frac{b_n}{2j}\right)e^{-jn\omega t} = c_n e^{jn\omega t} - c_{-n}e^{-jn\omega t}$$

$$thus \qquad c_n = \frac{1}{2}\frac{2}{T}\int_{-\frac{T}{2}}^{\frac{T}{2}} f(t)\cos(n\omega t)dt + \frac{1}{2j}\frac{2}{T}\int_{-\frac{T}{2}}^{\frac{T}{2}} f(t)\sin(n\omega t)dt$$

$$c_n = \frac{1}{T}\int_{-\frac{T}{2}}^{\frac{T}{2}} f(t)\left[\cos(n\omega t) - j\sin(n\omega t)\right]dt = \frac{1}{T}\int_{-\frac{T}{2}}^{\frac{T}{2}} f(t)e^{jn\omega t}dt \tag{2.8}$$

The above equation (2.7) can only be used with periodic functions. If it is to be used with non-periodic functions the period time has to be brought to infinity. For c_n this means:

$$c_n = \frac{\Delta\omega}{2\pi}\int_{-\infty}^{\infty} f(t)e^{-jn\Delta\omega t}dt \tag{2.9}$$

This reflects on f(t) as:

$$f(t) = \sum_{n=-\infty}^{\infty} c_n e^{jn\omega t} = \sum_{n=-\infty}^{\infty}\left[\frac{\Delta\omega}{2\pi}\int_{-\infty}^{\infty} f(t)e^{-jn\Delta\omega t}dt\right]e^{jn\omega t} = \frac{1}{2\pi}\sum_{n=-\infty}^{\infty}\left[\int_{-\infty}^{\infty} f(t)e^{-jn\Delta\omega t}dt\right]e^{jn\omega t}\Delta\omega \tag{2.10}$$

So the result is:

$$f(t) = \frac{1}{2\pi}\int_{-\infty}^{\infty} F(\omega)e^{j\omega t}d\omega$$

$$with \qquad F(\omega) = \int_{-\infty}^{\infty} f(t)e^{-j\omega t}dt \tag{2.11}$$

F(ω) is known as the Fourier integral, which gives the spectral content of the function f(t). The Fourier transform is unequivocal; Out of f(t) follows unequivocally F(ω) and visa versa.
The Fourier series establishes a relationship between a time domain function and that function in the frequency domain.

2.3 Definition of harmonic voltages

Harmonic voltage is a sinusoidal voltage with a frequency equal to an integer multiple of the fundamental frequency of the fundamental voltage.

This means the h^{th}-order harmonic is equal to hf_o, with f_o the fundamental frequency of the system. So in a 50Hz system the harmonics of the system can consist of a 100Hz component (2^{nd} harmonic), a 150Hz component (3^{rd} harmonic), a 200 Hz component (4^{th} harmonic), and so on. The amplitude of these harmonics can be different.

2.4 Example which clarifies the theory of Fourier and harmonics

Consider the extremely distorted supply voltage given in Figure 2.1 and it's Fourier transform in Figure 2.2.

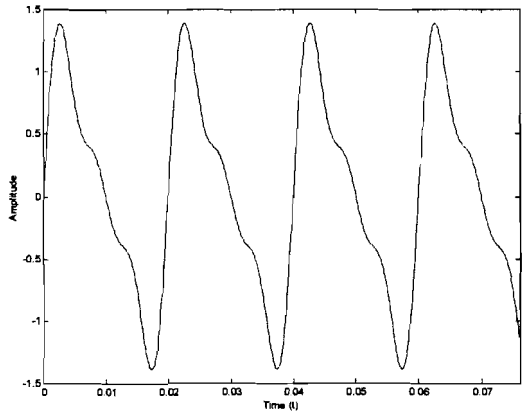

Figure 2.1: Distorted supply voltage

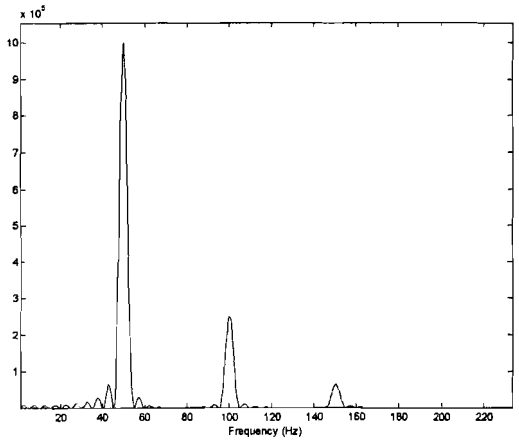

Figure 2.2: Fourier spectrum of the distorted supply voltage

As can be seen from Figure 2.2 the supply voltage contains frequency components of 50 Hz, 100 Hz and 150 Hz. This means the supply voltage in the time domain can be split up into three sinusoidal functions of these frequencies, each with different amplitude. This is depicted in Figure 2.3. The amplitude of each component is relative to the amount of power each frequency contains in Figure 2.2. It must be taken in mind that the power is displayed on the y-axis of Figure 2.2 as the amplitude of the signal is displayed in Figure 2.1 and Figure 2.3.

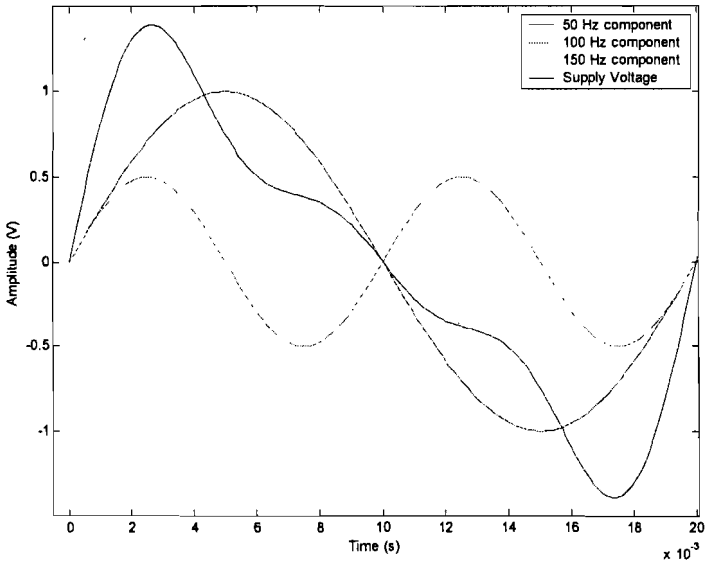

Figure 2.3: Supply voltage plus it's basic frequency components

3 Causes of harmonic distortions

Harmonic injection in the grid causes distortions of the voltage and current waveforms, which have adverse effects on electrical equipment.
Harmonic emission can consist of different amplitudes and frequencies. The most common harmonics in power systems are sinusoidal components of a periodic waveform that have frequencies which can be resolved in to multiples of the fundamental frequency. Fourier analysis is the mathematical tool employed for such analysis. Next to these common harmonics power systems can also contain harmonics that are non-integer multiples of the fundamental frequency and have a-periodic waveforms. These are less common then the ones that are integer multiples.
The estimation of this harmonic emission is the first step in a harmonic analysis. This estimation is not straightforward. There is an interaction between the harmonic producing equipment and the electrical system.
So, before any harmonic model can be introduced, it is important to get an idea of which sort of equipment introduces harmonics in the electrical system. Therefore in this chapter the nature of harmonics and their generation by electrical equipment will be discussed. The first thing to do is to split the generators of harmonics into two distinct types of loads:

Linear time-invariant loads:
Linear time-invariant loads are characterized so that an application of a sinusoidal voltage results in a sinusoidal flow of current. The load displays constant steady state impedance during the applied sinusoidal voltage. If the voltage is increased, the current also increases in direct proportion. Incandescent light is an example of such a load. Next to incandescent light rotating machines and transformers approximately meet this definition under normal operating conditions, though the flux in the air gap of the rotating machine is not sinusoidal and the magnetic circuits in the transformer can saturate and generate harmonics. Saturation in the transformer due to operation on an abnormally high voltage produces harmonics, because the relationship between the magnetic flux density B and the magnetic field intensity H in the core is not linear. Also the inrush current of a transformer contains odd and even harmonics. Yet, under normal operating conditions, these effects for transformers and rotating machines are small. Another element to consider in power systems are synchronous generators as they also produce sinusoidal voltages. However, the harmonic pollution produced for this type of load is also small.

Non-linear time-invariant loads:
The second category of loads is described as non-linear. In a non-linear device the application of a sinusoidal voltage does not result in a sinusoidal flow of current. These loads do not exhibit constant impedance during the entire cycle of applied sinusoidal voltage. Non-linear loads can draw a current that may even be discontinuous, or flow in pulses for a part of the sinusoidal voltage cycle. Some examples of non-linear loads are:

- Adjustable drive systems
- Arc furnaces
- Switched mode power supplies
- Computers, copy machines, television sets, micro-waves, ...
- Static var compensators
- Wind and solar power generators
- Battery charging and fuel cells
- Slip recovery schemes of induction motors
- Fluorescent lighting and electronic ballast

The distortion produced by non-linear loads can be resolved into a number of categories:

- A distorted waveform having a Fourier series with fundamental frequency equal to power system frequency, and a periodic steady state exists. This is the most common in harmonic studies.
- A distorted waveform having a sub-multiple of power system frequency, and a periodic steady state exists. Certain types of pulsed loads and integral cycle controllers produce these types of waveforms.
- The waveform is a-periodic, but perhaps almost periodic. Examples are arc furnaces and fluorescent, mercury and sodium vapour lighting. The process in not periodic in nature. A periodic waveform is obtained if the operating conditions are kept constant for a length of time.

With the distinction of linear and non-linear loads in mind, the rest of the chapter will focus in on some important linear and especially non-linear loads which produce harmonics. It must be taken in mind that approximately more than 90% of the harmonic distortions in the grid are caused by inverters and the huge numbers of lighting ballasts. Electrical machines and transformers only contribute a small percentage to the total harmonic distortions. They are included to get a broader picture on the diversity of devices in the grid which can cause harmonic distortions.

3.1 Electrical machines

3.1.1 Three-phase windings in electrical machines

The armature windings of a machine consist of phase coils which span approximately a pole-pitch. A phase winding consists of a number of coils connected in series, and the emf generated in these coils is time displaced in phase by a certain angle. The air gap is bounded on either side by iron surfaces which accommodate slots. Simple methods for estimating the reluctance of the air gap for carrying flux across it are not straightforward and the flux density in the air gap is not sinusoidal. This is shown in Figure 3.1, where the magneto magnetic flux is shown.

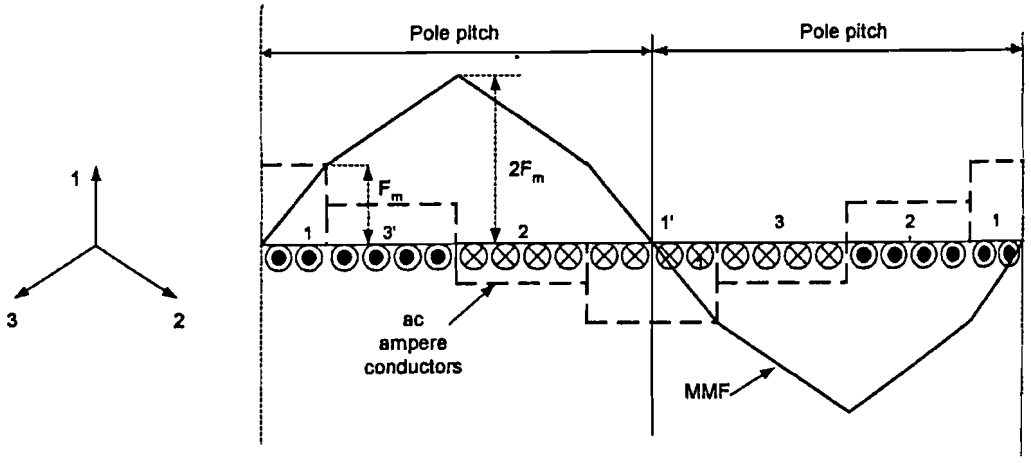

Figure 3.1: Magneto magnetic flux of a three-phase winding

This magneto magnetic flux has a constant fundamental, and harmonics of the order 5, 7, 11, 13 or 6m±1, where m is any positive integer. The third harmonic and it's multiples are absent. As this flux is coupled with the magnetisation current, these harmonics in the magneto magnetic flux will also be found in the magnetisation current. As the electrical machine is connected to grid this current is injected into the grid, causing harmonic distortions.

3.1.2 Tooth ripples in electrical machines

Tooth ripples in electrical machines are produced by slotting as these effect air-gap permeance.

Figure 3.2 shows ripples in the air-gap flux distribution (exaggerated) because of variation in gap permeance. The frequency of flux pulsation corresponds to the rate at which slots cross the pole face.

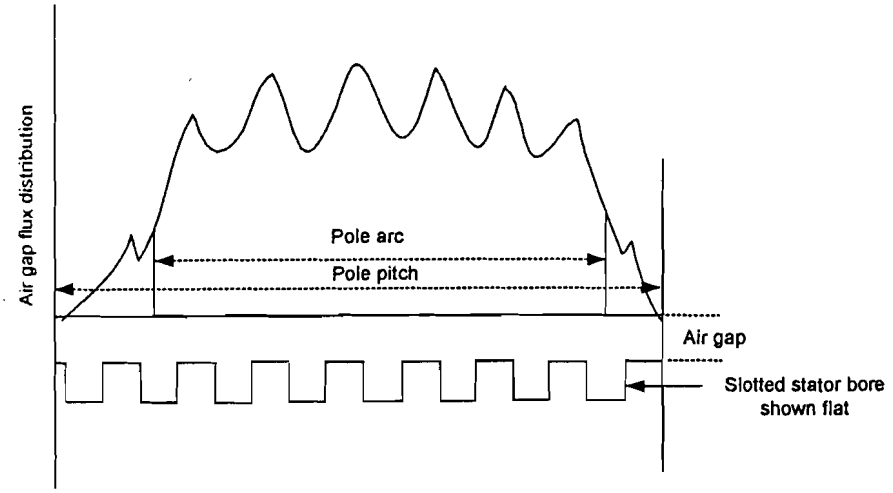

Figure 3.2: Gap flux distribution due to tooth ripples

As can be seen the gap flux is far from sinusoidal and as this flux is coupled with the magnetisation current it results in a magnetization current that is also far from sinusoidal. This far from sinusoidal current is injected into the grid causing harmonic distortions.

3.2 Transformers

Harmonics in transformers originate as a result of saturation, switching and high flux densities. The following summarizes the main factors in respect of harmonic generation:

1. For economical reasons transformers are operated close to the knee point of saturation characteristics of magnetic materials. This causes a non-sinusoidal magnetization current as will be explained.

At no-load the primary voltage of a transformer is practically balanced by the back e.m.f. because the effect of winding resistance and leakage reactance is negligible at low currents. At any instance, therefore, the impressed voltage v_1 for a sinusoidal supply is:

$$v_1 = -e_1 = -E_m \sin \omega t = N_1 \frac{d\phi}{dt} \tag{3.1}$$

From equation (3.1) the following expression is obtained for the main flux:

$$\phi = -\int \frac{e_1}{N_1} dt = \frac{E_m}{N_1 \omega} \cos \omega t = \phi_m \cos \omega t \tag{3.2}$$

This means a sinusoidal primary voltage produces a sinusoidal flux at no-load. The primary current, however, will not be purely sinusoidal, because the flux is not linearly proportional to the magnetizing current. In an ideal core without hysteresis loss the flux ϕ and the magnetizing current i_m needed to produce it are related to each other by the

magnetizing curve of the material used in the laminations as shown in Figure 3.3(a). In Figure 3.3(b), where ϕ represents the sinusoidal flux necessary to balance the primary voltage, the magnetizing current is plotted against time for each value of ϕ and the resulting waveform is far from sinusoidal.

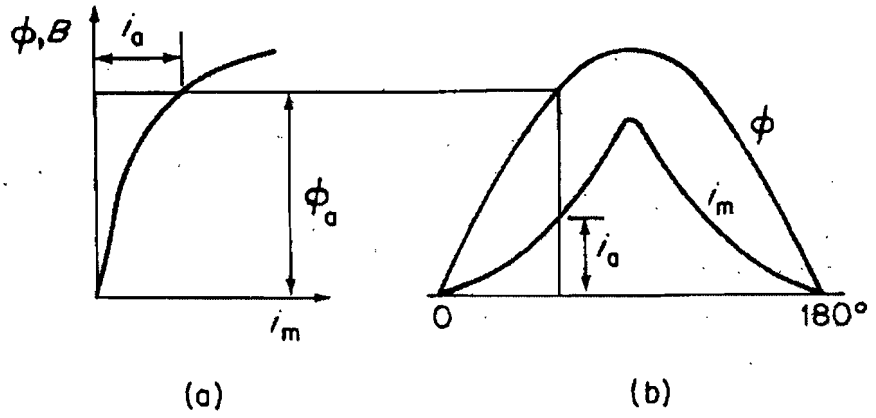

Figure 3.3: Transformer magnetization (without hysteresis): (a) magnetization curve; (b) flux and magnetization current waveform

When the hysteresis effect is included, as can be seen in Figure 3.4, the non-sinusoidal magnetization current is no longer symmetrical about it's maximum value. In this case the current corresponding to any point on the flux density wave of Figure 3.4 is determined from the new magnetization curve. The ascending portion of the hysteresis being used for the ascending portion of the flux density wave, and the descending portion of the loop for the descending portion of the flux density wave.

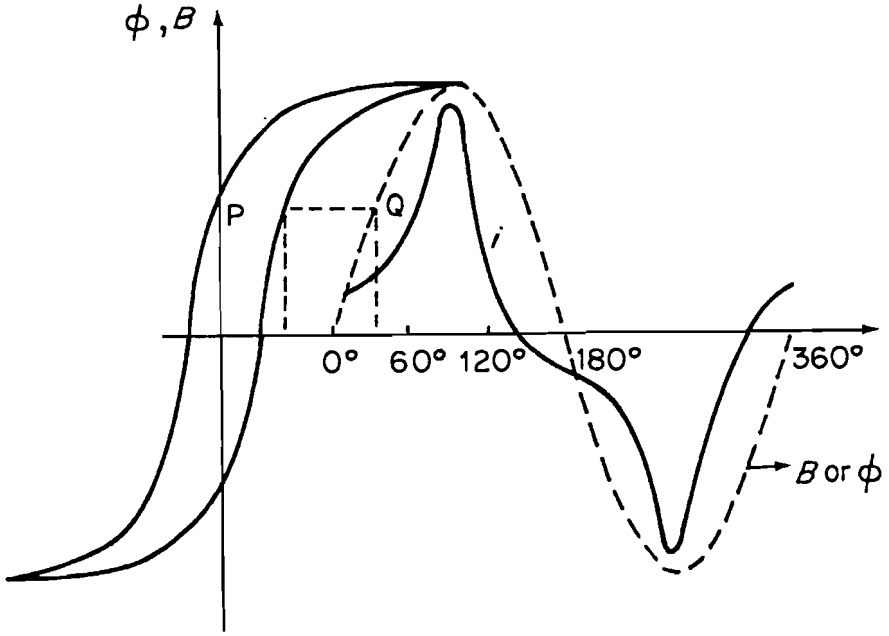

Figure 3.4: Transformer magnetization including hysteresis

The distortions in the current waveform are clearly visible. This means the transformer produces harmonics, because it introduces non-sinusoidal currents in the network.

2. It can be said that power transformers generate very low levels of harmonic currents in steady-state operation. Design and transformer winding connections control the harmonics. The higher-order harmonics may be less then 0.1% of the transformers full-load current. An example is a three-phase core-type transformer, which has

magnetically interlinked phases and a return path of triplet harmonic fluxes which lies outside the core, through the tank and transformer fluids, which have high reluctance.

3. Energizing a power transformer does generate a high order of harmonics including a dc component. Figure 3.5 shows three conditions of the energizing of a power transformer: (a) the switch closed at the peak value of the voltage, (b) the switch closed at zero value of the voltage, and (c) energizing with some residual trapped flux in the magnetic core due to the retentivity of the magnetic materials. Figure 3.5(d) shows the spectrum of magnetizing inrush current, which resembles a rectified current and it's peak value may reach 8-15 times the transformer full-load current, mainly depending on the transformer size. Typical harmonics generated by the transformer inrush current are shown in Figure 3.6.

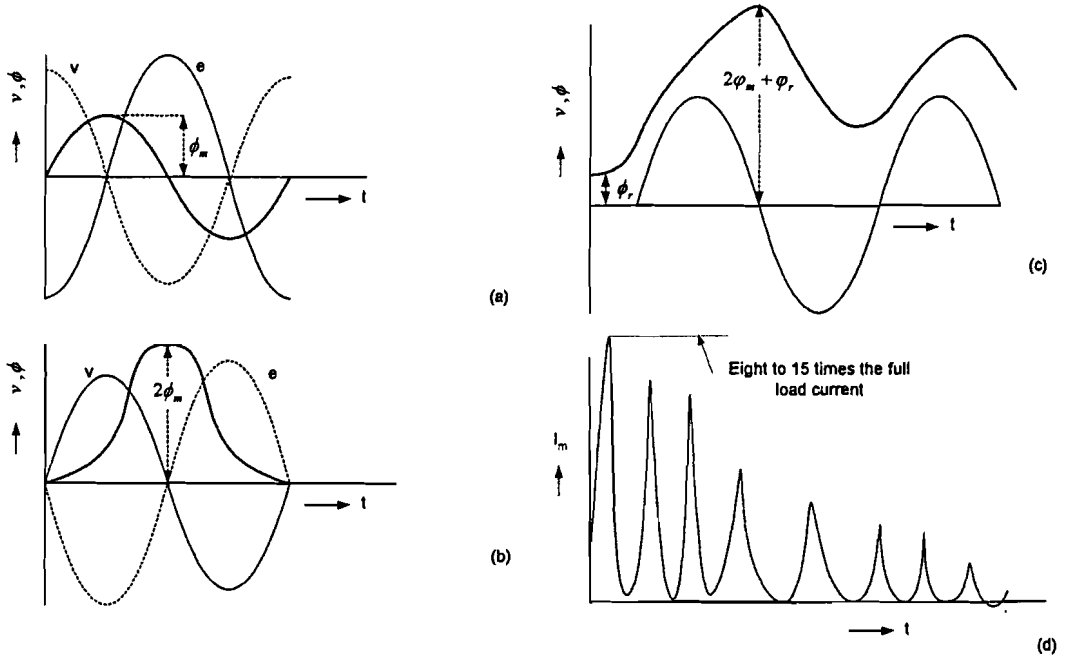

Figure 3.5: Switching inrush current transients in a transformer

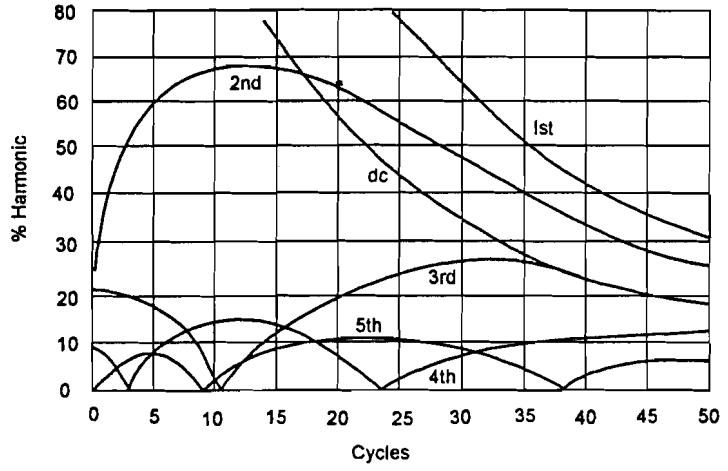

Figure 3.6: Harmonic components of the inrush current of a transformer

3.3 Static power converters

The primary sources of harmonics in the power system are power converters, rectifiers and adjustable speed drives. The characteristic harmonics are those produced by the power electronic converters during normal operation and these harmonic are integer multiples of the fundamental frequency of the power system.
Non-characteristic harmonics are usually produced by sources other than power electronic devices and may be at frequencies other than the integer multiple of the fundamental power frequency. However, the converters do produce some non-characteristic harmonics, as ideal conditions of commutation and control are not achieved in practice.

3.3.1 Single-phase bridge circuit

The single-phase rectifier full-bridge circuit of Figure 3.7 is first considered.

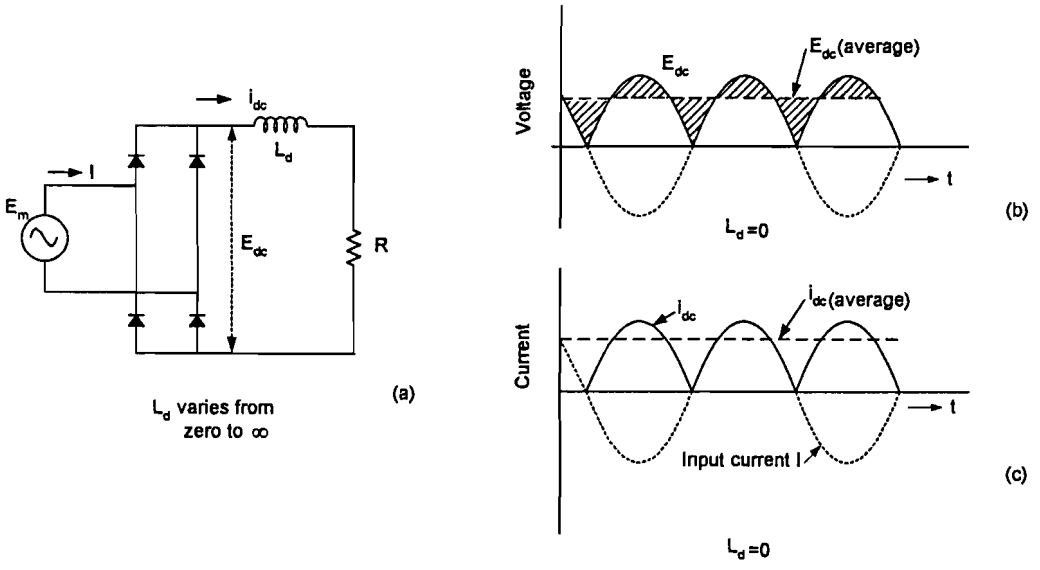

Figure 3.7: A single-phase full rectifier bridge circuit with resistive load

It is considered that there is no voltage drop or leakage current, the switching is instantaneous, the voltage source is sinusoidal, and the load is resistive. For normal operation, the waveforms of input and output currents are than as in Figure 3.7(b) and (c). The average dc current is:

$$I_{dc} = \frac{1}{2\pi}\int_0^{\pi}\frac{E_m}{R}\sin\omega t d\omega t = \frac{2E_m}{\pi R} \tag{3.3}$$

and the rms value or the effective value of the output current, including all harmonics, is:

$$I_{rms} = \sqrt{\frac{1}{2\pi}\int_0^{\pi}\left(\frac{E_m}{R}\right)^2 \sin^2\omega t d\omega t} = \frac{E_m}{\sqrt{2}}R \tag{3.4}$$

The input current has no harmonics. The average dc voltage is given by:

$$E_{dc} = \frac{2E_m}{\pi} \tag{3.5}$$

The output ac power is defined as:

$$P_{ac} = E_{rms} I_{rms} \tag{3.6}$$

where E_{rms} considers the effect of harmonics on the output. The dc output power is:

$$P_{dc} = E_{dc} I_{dc} \tag{3.7}$$

The efficiency of rectification is given by P_{dc}/P_{ac}. The form factor is a measure of the shape of the output voltage or current and it is defined as:

$$FF = \frac{I_{rms}}{I_{dc}} \tag{3.8}$$

The ripple factor, which is a measure of the ripple content of the output current or voltage, is defined as the rms value of output voltage or current, including all harmonics, divided by the average value:

$$RF = \sqrt{\frac{I_{rms}}{I_{dc}} - 1} = \sqrt{FF - 1} \tag{3.9}$$

For the single-phase bridge circuit with resistive load (and thus L=0), the ripple factor is:

$$RF = \sqrt{\frac{I_{rms}}{I_{dc}} - 1} = 0.48 \tag{3.10}$$

This shows that the ripple content of the dc output voltage is high, Figure 3.7(b). This is not acceptable even for the simplest applications. Let a series reactor be added in the dc circuit. The load current is no longer a sine wave but the average current is still equal to $2E_m/\pi R$. The ac line current is no longer a sinusoidal, but approximately a poorly defined square wave with superimposed ripples, Figure 3.8(a). The inductance has reduced the harmonic content of the load current by increasing the harmonic content of the ac line current. When the inductance is large, the ripple across the load is insignificant and can be assumed constant. The ac current wave is now a square wave, Figure 3.8(b).

As now can be concluded from the above the overall purpose of the single-phase bridge circuit, creating a DC current, also creates an ac current at the connection points of the inverter which resembles a square. As can be calculated with the theory of Fourier presented in chapter 2 this square wave I(t) contains the following harmonics:

$$I(t) = I_{amp} + \frac{4I_{amp}}{\pi}\sin(\omega t) + \frac{4I_{amp}}{3\pi}\sin(3\omega t) + \frac{4I_{amp}}{5\pi}\sin(5\omega t) + \ldots + \frac{4I_{amp}}{n\pi}\sin(n\omega t) \quad \text{for } n = 9,11,13,15,\ldots \tag{3.11}$$

These harmonic currents are injected back into the grid causing harmonic distortion. This harmonic distortion mainly depends on the value of L_d, as this inductance mainly controls the " form" of the current drawn from the grid.

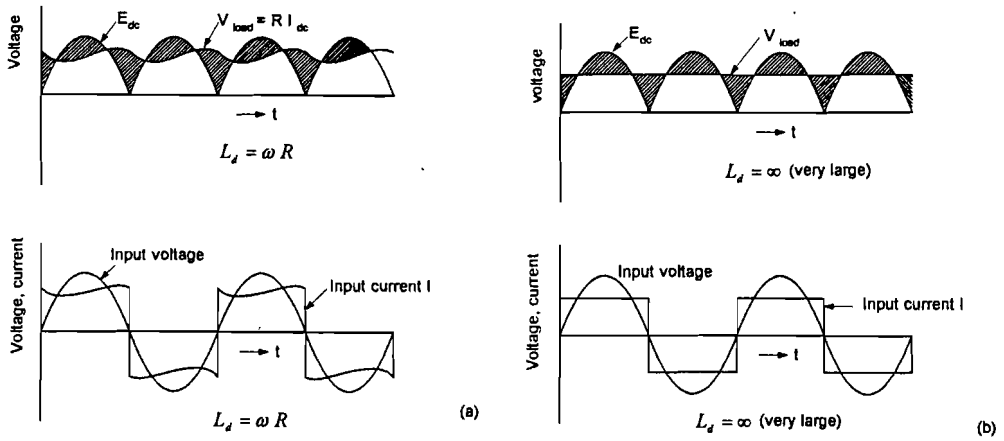

Figure 3.8: A single-phase full rectifier bridge circuit with resistive load and L_d small and large

3.3.1.1 Phase control

A silicon controlled rectifier (SCR) can be turned on by applying a short pulse to its gate and turned of due to natural or line commutation. The term thyristor pertains to the family of semi-conducting devices for power control. The angle by which the conduction is delayed after the input voltage starts to go positive until the thyristor is fired is called the delay angle. Figure 3.9(b) shows waveforms with a large dc reactance, and Figure 3.9(c) shows waveform with no dc reactance but identical firing angle.

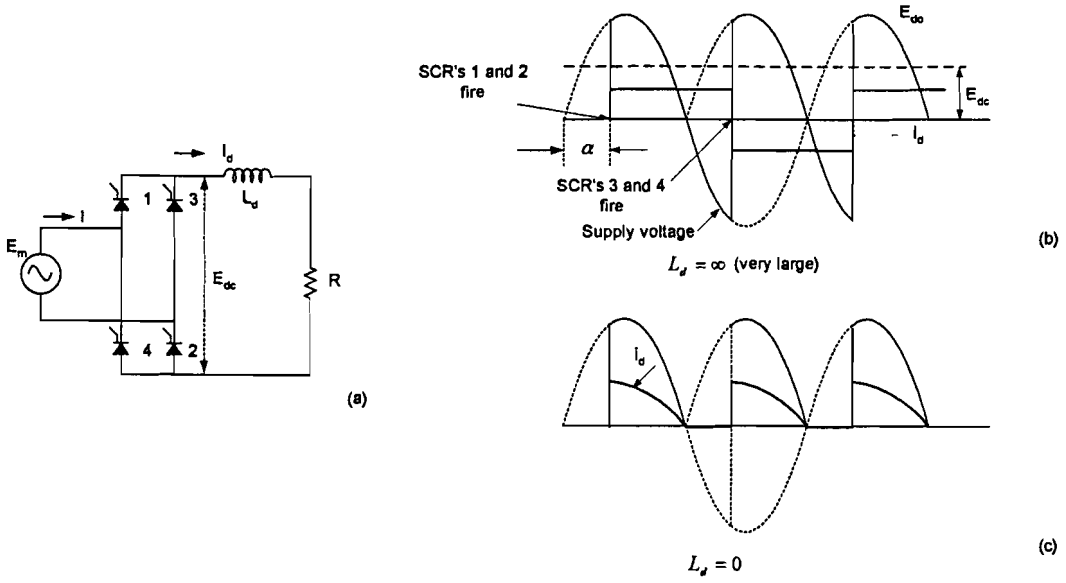

Figure 3.9: A single-phase full rectifier bridge circuit with phase control

Thyristors 1 and 2 and 3 and 4 are fired in pairs as shown in Figure 3.9(b). Firing of thyristors 3 and 4 reverse biases thyristors 1 and 2 and turns them off. The average dc voltage is:

$$E_{dc} = \frac{1}{\pi}\int_{\alpha}^{\pi+\alpha} E_m \sin\omega t d(\omega t) = \frac{2E_m}{\pi}\cos\alpha \qquad (3.12)$$

and the Fouries analysis of the rectangular current wave in Figure 3.9(b) gives:

$$I = \sum_{h=1,2,...}^{\infty} \left[a_h \cos(h\omega t) + b_h \sin(h\omega t) \right] \tag{3.13}$$

with

$$a_h = -\frac{4I_a}{h\pi} \sin(\mathrm{h}\,\alpha), \qquad \begin{matrix} h = 1,3,5,... \\ h = 0 \quad h = 2,4,6,... \end{matrix} \tag{3.14}$$

$$b_h = \frac{4I_a}{h\pi} \cos(\mathrm{h}\,\alpha), \qquad \begin{matrix} h = 1,3,5,... \\ h = 0 \quad h = 2,4,6,... \end{matrix} \tag{3.15}$$

The rms input current is given by:

$$I = \frac{4}{\pi} I_d \left[\sin(\omega t - \alpha) + \frac{1}{3} \sin 3(\omega t - \alpha) + \frac{1}{5} \sin 5(\omega t - \alpha) + ... \right] \tag{3.16}$$

Triple harmonics are present. Figure 3.10 shows harmonics as a function of the delay angle for a resistive load. The overlap angle decreases the magnitude of the harmonics. When the output reactor is small, the current goes to zero, the input current wave is no longer rectangular and the line harmonics increase.

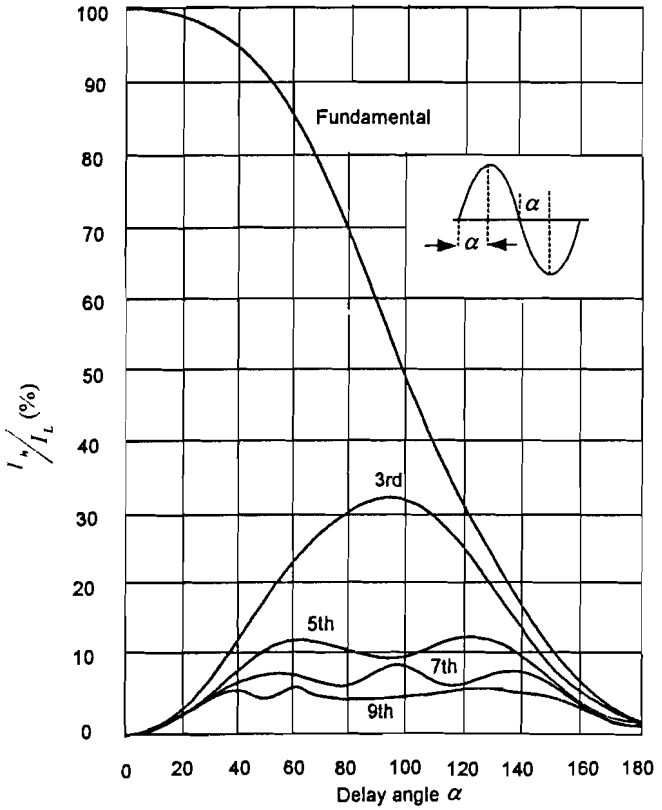

Figure 3.10: Harmonic generation as a function of delay angle

3.3.2 Three-phase bridge circuit

A three-phase bridge has two forms: (1) half-controlled and (2) fully controlled. The three-phase fully controlled bridge is described, as it is most commonly used.

Figure 3.11(a) shows a three-phase fully controlled bridge circuit, and Figure 3.11(b) shows it current and voltage waveforms.

The firing sequence of thyristors is shown in Table 1. At any time two thyristors are conducting. The firing frequency is six times the fundamental frequency and the firing angle can be measured from point O shown in Figure 3.11(b). With a large output reactor the output dc current is continuous and the input current is a rectangular pulse of $2\pi/3$ duration and amplitude I_d. The average dc voltage is:

$$E_d = 2\left[\frac{3}{2\pi}\int_{-\pi/3+\alpha}^{\pi/3+\alpha} E_m \cos\omega t d(\omega t)\right] = \frac{3\sqrt{3}}{\pi} E_m \cos\alpha \qquad (3.17)$$

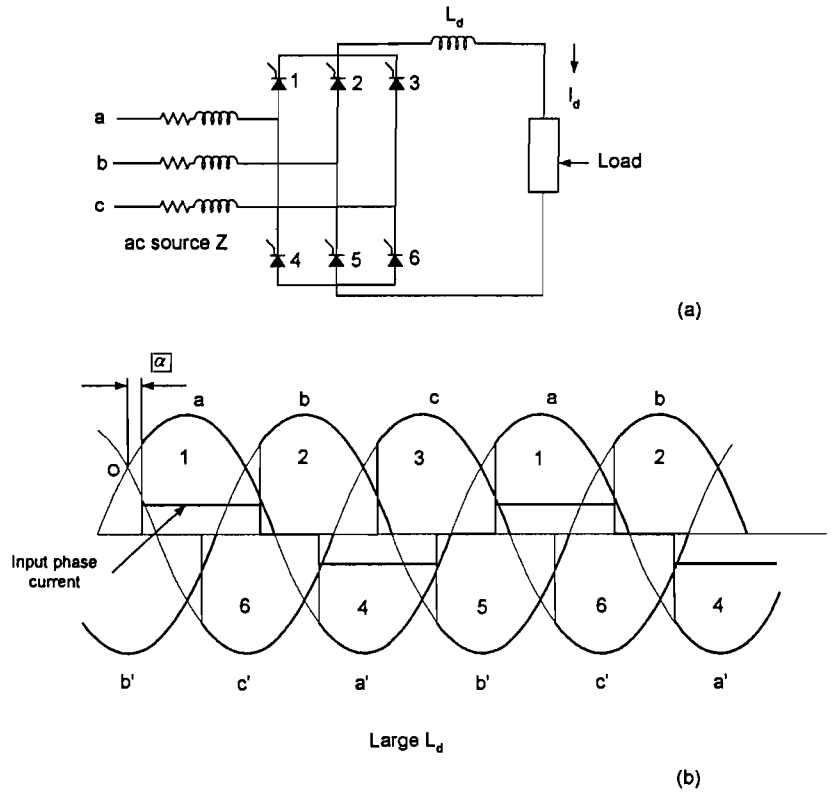

Figure 3.11: A three–phase fully controlled bridge with large L_d

Conducting thyristors	5, 3	1, 5	6, 1	2, 6	4, 2	3, 4
Thyristors to be fired	1	6	2	4	3	5
Thyristors turning off	3	5	1	6	2	4

Table 1: Firing sequence of thyristors in six-pulse converter

As the current drawn from the grid is again rectangular, as it was for the single-phase bride and phase-controlled bridge, it introduces harmonic distortions in the grid as a rectangular current form contains a lot of harmonics as explained in chapter 3.3.1.

3.4 Switch-mode power (smp) supplies

Single-phase rectifiers are used for power supplies in copiers, computers, TV sets, and household appliances. In these applications the rectifiers use a dc filter capacitor and draw impulsive current from the ac supply. The harmonics current is worse than that given by equation (3.16). Figure 3.12(a) and (b) show conventional and switch mode power supplies. The input current wave for a switch mode power supply is highly non-linear, flowing in pulses for part of the sinusoidal ac voltage cycle, Figure 3.12(c). The spectrum of a switch mode power supply is given in Table 2 and shows a high magnitude of the third and fifth harmonic. Overall the switch-mode power supplies are an important producer of harmonics in the network.

Harmonic	Magnitude	Harmonic	Magnitude
1	1.000	9	0.157
3	0.810	11	0.024
5	0.606	13	0.063
7	0.370	15	0.07

Table 2: Spectrum of typical switch mode power supply

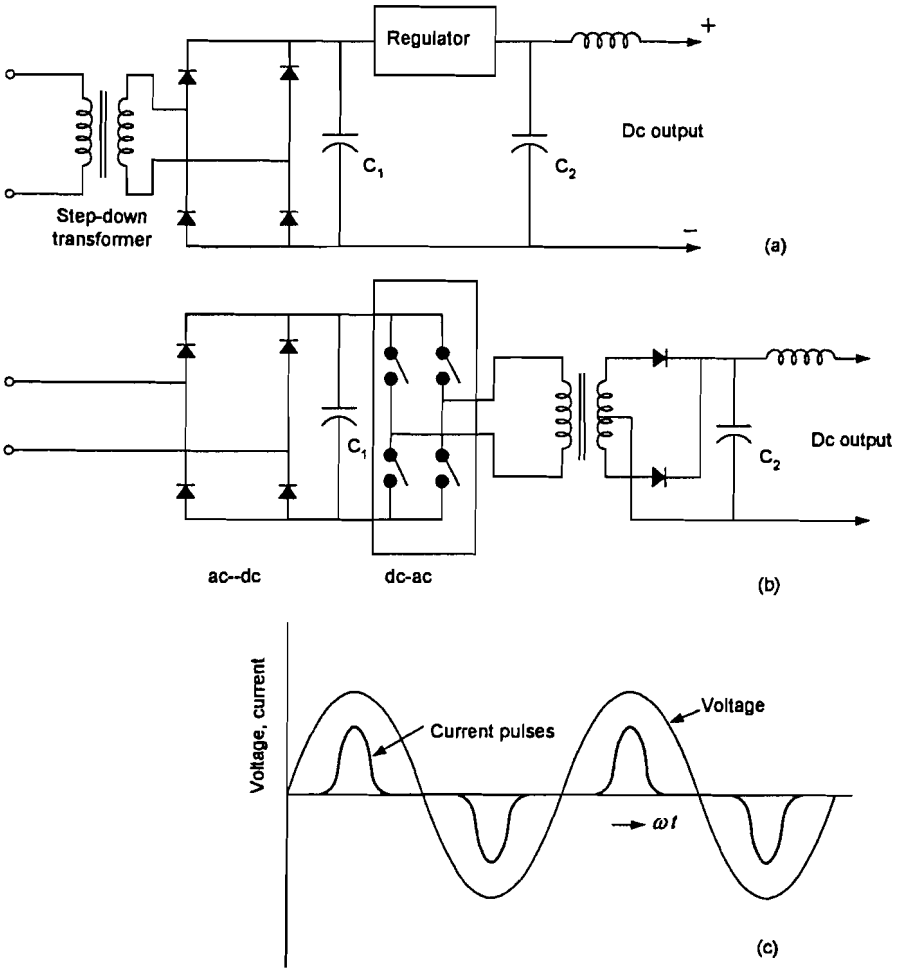

Figure 3.12: Conventional (a) and switch mode power supply (b) circuits

3.5 Adjustable speed drives

Adjustable speed drives account for the largest percentage of non-linear loads in the industry. Most drive systems require that the incoming ac power supply be converted into dc. The dc power is then inverted back to ac at a frequency demanded by the speed reference of the ac variable-frequency drive or the dc feeds directly to dc drive systems through two or four quadrant converters. These converters are the main cause of the harmonic pollution for adjustable speed drives.

3.6 Lighting ballasts

Lighting ballasts may produce large harmonic distortions and third harmonic currents. The newer rapid start ballast has a much lower harmonic distortion. The current harmonic limits for lighting ballasts are given in Table 3 and Table 4.

Harmonic	Maximum value (%)
Fundamental	100
2^{nd} harmonic	5
3^{rd} harmonic	30
Individual harmonics > 11^{th}	7
Odd triplens	30

Table 3: Harmonic limits for lighting ballasts

Device type	THD (%)
Older rapid start magnetic ballast	10-29
Electronic IC-based ballast	4-10
Electronic discrete based ballast	18-30
Newer rapid start electronic ballast	< 10
Newer instant start electronic ballast	15-27
High intensity discharge ballast	15-27
Office equipment	50-150

Table 4: THD ranges for different types of lighting ballasts

Because of there large numbers lighting ballasts are still a contribution to be taken into account for the harmonic distortions in the network.

3.7 Typical pollution produced by non-linear loads

Figure 3.13 gives an overview of some typical non-linear loads and the pollution produced by these loads.

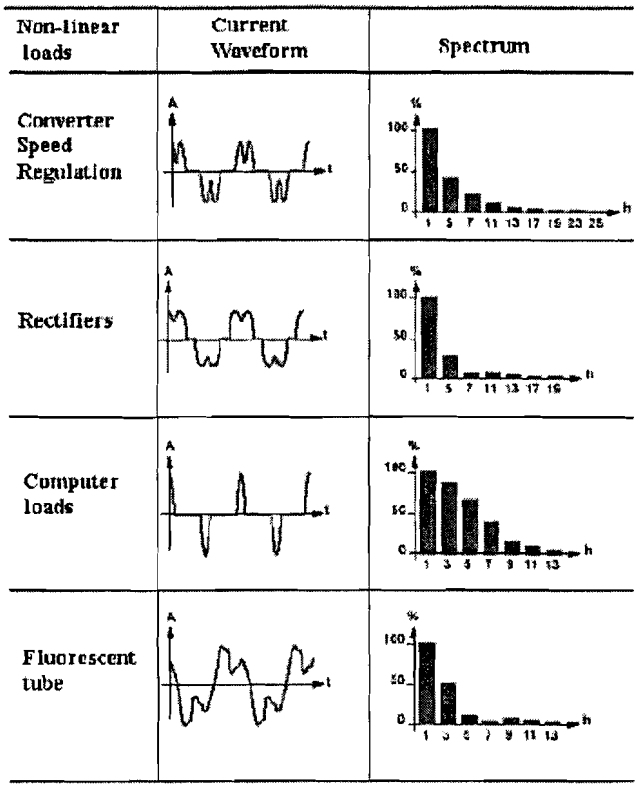

Figure 3.13: Spectrum of typical loads

As can be seen the most erratic current waveform has the most harmonic content. In this case that is the computer load.

4 Harmonic Modeling

In this chapter a basic harmonic model containing information on grid and load parameters is presented. To make a proper estimation of a possible harmonic problem this model needs to consist of an accurate frequency description of each of the individual elements. If this is present, problems can be estimated by an instability analysis of this model.

4.1 The simplest harmonic model

The simplest harmonic model is shown in Figure 4.1.

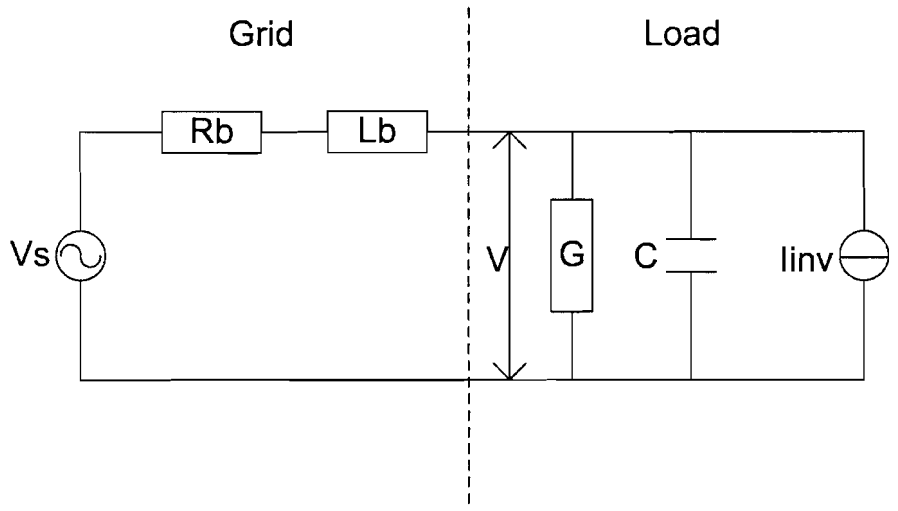

Figure 4.1: Simplest model of grid and load

The grid part of the model consists of:

- A harmonic voltage source V_s modeling the voltage background harmonic distortion.
- The resistance R_b of mostly the LV-cable. R_b is frequency dependent due to skin- and proximity effects.
- The inductance L_b of the cable and the MV/LV-transformer. L_b is frequency dependent due to skin-effects.

The load part of the model consists of:

- A harmonic current source, modeling the harmonic currents of the inverter without the effect of background voltage distortions from the grid.
- A capacitor C, modeling the imaginary part of the power consumed by the load. C may vary with frequency and can be positive as well as negative.
- A resistor R, modeling the real part of the power consumed by the load. R may vary with frequency and can be positive as well as negative.

The transfer function of this circuit is given by:

$$V = \frac{V_s + I_{inv}\left(R_b + j\omega L_b\right)}{1 + \left(R_b + j\omega L_b\right)\cdot\left(G + j\omega C\right)} \tag{4.1}$$

This system will become unstable when the denominator of equation (4.1) becomes zero. This will occur when:

$$\omega = \omega_0 \sqrt{1 - \left(\frac{R_b}{Z_0}\right)^2} \qquad with \quad Z_0 = \sqrt{\frac{L_b}{C}} \text{ and } \omega_0 = \frac{1}{\sqrt{L_b C}} \tag{4.2}$$

and

$$G = -\frac{R_b}{Z_0^2} \qquad with \quad Z_0 = \sqrt{\frac{L_b}{C}} \tag{4.3}$$

Equations (4.2) and (4.3) imply that instability can only occur in very specific circumstances. Due to skin- and proximity-effect in the impedance of the grid and frequency dependency of the load, the resonance frequency is related to the frequency itself. So, as mentioned above, an accurate description in the frequency domain is needed for each of the elements of the model. These will be presented in this chapter.

4.2 Extended harmonic model

The model presented in chapter 4.1 only contains one load and the impedance of the grid to that load. This model can be extended to incorporate more loads and grid topologies. An example of such an extended model is displayed in Figure 4.2.

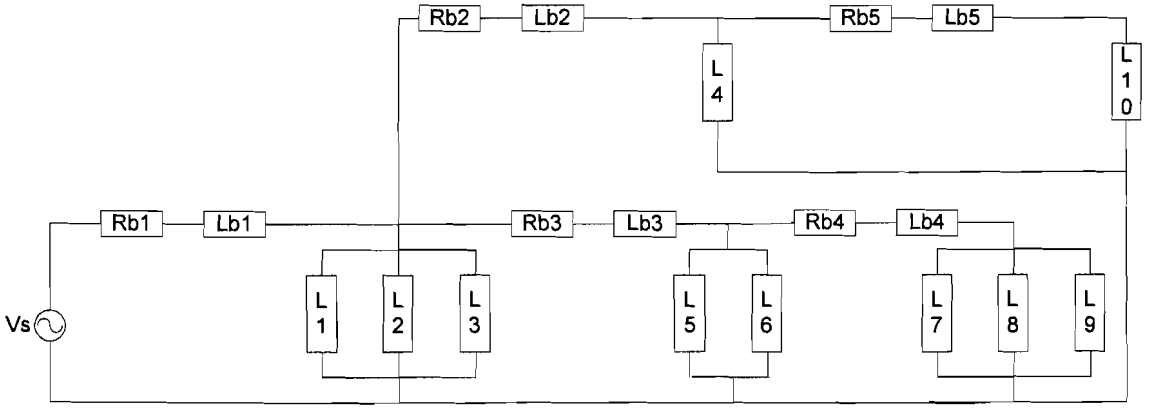

Figure 4.2: Extended harmonic model

For convenience the loads are depicted as one impedance each. These loads still consist of the G, C and I_{inv} as explained in chapter 4.1. The loads can vary from normal resistive loads to complex loads that introduce harmonic currents in the grid.
For the extended model to work it is necessary that the loads can be sufficiently characterized by the G, C and I_{inv} so that the network theory can be applied to them. This will be validated further in this report, where test measurements have been done on some typical consumer loads.

4.3 Modeling the cable

Cables are widely used in the Netherlands for medium-voltage (MV) and low voltage (LV) power distribution. The cables implemented are of various types. The cable model discussed in the following chapters can be used for almost all these types. However it is specified for two of the most common cables used by Continuon for medium voltage and low voltage distribution.
The construction of these cables will be discussed in chapter 4.3.1, followed by a general explanation of the three-phase cable impedance with insight in the cable resistance and inductance in chapter 4.3.2, 4.3.3 and 4.3.4 respectively. Next the practical acquisition of the resistance and reactance of the cable is disclosed in chapter 4.3.5, followed by the measurement results in chapter 4.3.6. Chapter 4.3.6 will then combine these results with the theoretical resistance and inductance to validate the acquired theory with the measurement results.

4.3.1 Cable construction

The cross-sections of the cables are shown in Figure 4.3.

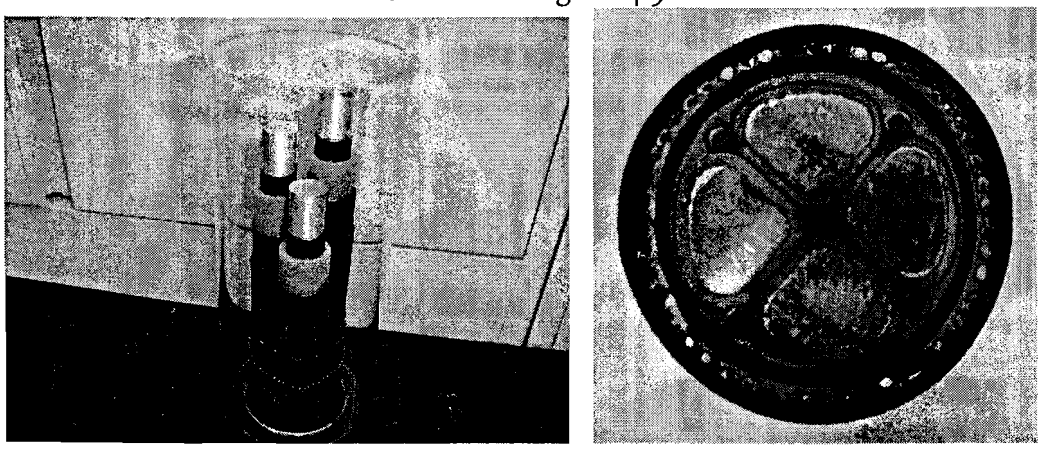

Figure 4.3: Cross-section of medium voltage cable (left) and low voltage cable (right)

The medium voltage cable consists of aluminium, massive, round conductors. The conductor screen is fabricated of weak conducting synthetic material. The isolation is XLPE and the isolation screen is again weak conducting synthetic material. The earth screen consists of round copper wires with an opposite spiral of copper band. More information on this medium voltage cable can be found in Appendix A.
The low voltage cable consists of aluminium massive conductors with a sector formation. The isolation consists of PVC. The earth screen consists of round copper wires. More information on this low voltage cable can be found in Appendix A.

4.3.2 Three-phase cable impedance

The configuration of the three-phase cable is shown in Figure 4.4, where impedances, voltages and currents are identified.

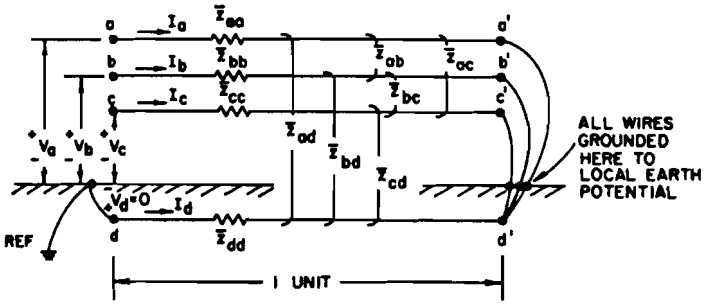

Figure 4.4: Three-phase cable with earth return

All wires are grounded at the remote point a'-b'-c', which implies that:

$$I_d = -(I_a + I_b + I_c) \tag{4.4}$$

Then, the voltage drop equations in the direction of the current flow are as follows:

$$\begin{bmatrix} V_{aa'} \\ V_{bb'} \\ V_{cc'} \\ V_{dd'} \end{bmatrix} = \begin{bmatrix} V_a - V_{a'} \\ V_b - V_{b'} \\ V_c - V_{c'} \\ V_d - V_{d'} \end{bmatrix} = \begin{bmatrix} \overline{z}_{aa} & \overline{z}_{ab} & \overline{z}_{ac} & \overline{z}_{ad} \\ \overline{z}_{ba} & \overline{z}_{bb} & \overline{z}_{bc} & \overline{z}_{bd} \\ \overline{z}_{ca} & \overline{z}_{cb} & \overline{z}_{cc} & \overline{z}_{cd} \\ \overline{z}_{da} & \overline{z}_{db} & \overline{z}_{dc} & \overline{z}_{dd} \end{bmatrix} \begin{bmatrix} I_a \\ I_b \\ I_c \\ I_d \end{bmatrix} \quad \text{V/Unit length} \tag{4.5}$$

These equations are the "primitive voltage equations". The impedance of the cable is usually thought of as the ratio of the voltage to the current seen "looking in" the line at one end. Therefore a voltage reference is selected at the left end of the line and (4.5) is solved for the voltages V_a, V_b and V_c. This can be done since current I_d is known and because it can be stated that:

$$V_{a'} - V_{d'} = 0\,, \qquad V_{b'} - V_{d'} = 0\,, \qquad V_{c'} - V_{d'} = 0 \tag{4.6}$$

for the condition of the connection at the receiving end of the line. Since $V_d = 0$, the fourth equation of (4.5) is subtracted from the first with the result:

$$V_a - \left(V_{a'} - V_{d'}\right) = \left(\overline{z}_{aa} - 2\overline{z}_{ad} + \overline{z}_{dd}\right) I_a + \left(\overline{z}_{ab} - \overline{z}_{ad} - \overline{z}_{bd} + \overline{z}_{dd}\right) I_b + \left(\overline{z}_{ac} - \overline{z}_{ad} - \overline{z}_{cd} + \overline{z}_{dd}\right) I_c \tag{4.7}$$

For convenience this result is written as $V_a = z_{aa}I_a + z_{ab}I_b + z_{ac}I_c$, with newly defined impedances z_{aa}, z_{ab} and z_{ac}. Note that when $I_b = I_c = 0$, z_{aa} is exactly the impedance for a single cable with earth return. If the above operation is repeated for the phases b and c, the result is:

$$\begin{bmatrix} V_a \\ V_b \\ V_c \end{bmatrix} = \begin{bmatrix} z_{aa} & z_{ab} & z_{ac} \\ z_{ba} & z_{bb} & z_{bc} \\ z_{ca} & z_{cb} & z_{cc} \end{bmatrix} \begin{bmatrix} I_a \\ I_b \\ I_c \end{bmatrix} \quad \text{V/Unit length} \tag{4.8}$$

where it is noted that $z_{ba} = z_{ab}$, due to reciproxity of the mutual inductances in a linear, passive, bilateral network. The impedance elements of (4.8) and (4.5) relate to each other as:

Self-impedances:

$$\begin{aligned} z_{aa} &= \overline{z}_{aa} - 2\overline{z}_{ad} + \overline{z}_{dd} && \Omega\text{/unit length} \\ z_{bb} &= \overline{z}_{bb} - 2\overline{z}_{bd} + \overline{z}_{dd} && \Omega\text{/unit length} \\ z_{cc} &= \overline{z}_{cc} - 2\overline{z}_{cd} + \overline{z}_{dd} && \Omega\text{/unit length} \end{aligned} \tag{4.9}$$

Mutual impedances:

$$\begin{aligned} z_{ab} &= \overline{z}_{ab} - \overline{z}_{ad} - \overline{z}_{bd} + \overline{z}_{dd} \quad \Omega/\text{unit length} \\ z_{bc} &= \overline{z}_{bc} - \overline{z}_{bd} - \overline{z}_{cd} + \overline{z}_{dd} \quad \Omega/\text{unit length} \\ z_{ac} &= \overline{z}_{ac} - \overline{z}_{ad} - \overline{z}_{cd} + \overline{z}_{dd} \quad \Omega/\text{unit length} \end{aligned} \tag{4.10}$$

To examine these impedances further the elements of the matrix in (4.5) are split up into their real and imaginary parts. These impedances will be called the primitive impedances.

Primitive self impedances:

$$\begin{aligned} \overline{z}_{aa} &= r_a + j\omega l_a \quad \Omega/\text{unit length} \\ \overline{z}_{bb} &= r_b + j\omega l_b \quad \Omega/\text{unit length} \\ \overline{z}_{cc} &= r_c + j\omega l_c \quad \Omega/\text{unit length} \\ \overline{z}_{dd} &= r_d + j\omega l_d \quad \Omega/\text{unit length} \end{aligned} \tag{4.11}$$

Primitive line-to-line mutual impedances:

$$\begin{aligned} \overline{z}_{ab} &= j\omega l_{ab} \quad \Omega/\text{unit length} \\ \overline{z}_{bc} &= j\omega l_{bc} \quad \Omega/\text{unit length} \\ \overline{z}_{ca} &= j\omega l_{ca} \quad \Omega/\text{unit length} \end{aligned} \tag{4.12}$$

Primitive line-to-earth mutual impedances:

$$\begin{aligned} \overline{z}_{ad} &= j\omega l_{ad} \quad \Omega/\text{unit length} \\ \overline{z}_{bd} &= j\omega l_{bd} \quad \Omega/\text{unit length} \\ \overline{z}_{cd} &= j\omega l_{cd} \quad \Omega/\text{unit length} \end{aligned} \tag{4.13}$$

This leads to:

$$\begin{aligned} z_{aa} &= (r_a + r_d) + j\omega(l_a - 2l_{ad} + l_d) \quad \Omega/\text{unit length} \\ z_{bb} &= (r_b + r_d) + j\omega(l_b - 2l_{bd} + l_d) \quad \Omega/\text{unit length} \\ z_{cc} &= (r_c + r_d) + j\omega(l_c - 2l_{cd} + l_d) \quad \Omega/\text{unit length} \end{aligned} \tag{4.14}$$

4.3.3 Resistance part of the three-phase cable

Cable resistance is a crucial electrical parameter because of its influence on the cable rating. Generally the resistance increases with increasing frequency. This increase is caused by an uneven distribution of the current due to skin and proximity effects. Given that both effects can be considered separately, a general formula for cable resistance at 50Hz is recommended in [1]:

$$R_{50Hz} = R_{dc}\left(1 + y_s + y_p\right)$$

where R = current resistance of conductor at operating temperature (Ω/m) (4.15)
R_{dc} = dc resistance of conductor at operating temperature (Ω/m)
y_s = skin effect factor
y_p = proximity effect factor

with

$$R_{dc} = R_{20}\left[1 + \alpha_{20}\left(T_c - 20\right)\right]$$

where R_{dc} = conductor dc resistance at T°C (Ω/m) (4.16)
R_{20} = conductor dc resistance at 20°C (Ω/m)
α_{20} = temperature coefficient of resistance of the conductor material at 20°C
T_c = conductor temperature (°C)

and

$$y_s = \frac{x_s^4}{192 + 0.8x_s^4}$$

where $x_s^4 = \frac{8\pi f 10^{-7} k_s}{R_{dc}}$ (4.17)
f = frequency (Hz)
k_s = coefficient factor for skin effect which incorporates the type of cable used (values given in Appendix D)

and

$$y_p = \frac{x_p^4}{192+0.8x_p^4}\left(\frac{d_c}{s}\right)^2\left[0.312\left(\frac{d_c}{s}\right)^2 + \frac{1.18}{\frac{x_p^4}{192+0.8x_p^4}+0.27}\right]$$

where $x_p^4 = \frac{8\pi f 10^{-7} k_p}{R_{dc}}$

d_c = is the diameter of the conductor (mm) (4.18)

s = is the distance between conductor axes (mm)

k_p = coefficient factor for proximity effect which incorporates the type of cable used (values given in Appendix D)

The equations for y_s and y_p are correct provided that x_s and x_p do not exceed 2.8. This means that for a study of the resistance of a cable for frequencies up to 2500Hz these equations need to be modified. Therefore the general formulas for skin effect are deducted in Appendix B. This deduction gives a new formula for the resistance of a cable under skin effect:

$$R_{skin} = \frac{R_s}{\sqrt{2}\pi r_0}\left[\frac{Ber(q)Bei'(q) - Bei(q)Ber'(q)}{(Ber'(q))^2 + (Bei'(q))^2}\right] \quad \Omega/m \tag{4.19}$$

This formula can be numerically approached by the following:

$$y_{s,h} = \begin{cases} \dfrac{x_{s,h}^4}{192+0.8x_{s,h}^4} & 0.0 < x_{s,h} \le 2.8 \\ 0.0563x_{s,h}^2 - 0.0177x_{s,h} - 0.136 & 2.8 < x_{s,h} \le 3.8 \\ \dfrac{x_{s,h}}{2\sqrt{2}} - \dfrac{11}{15} & 3.8 < x_{s,h} \end{cases} \tag{4.20}$$

with

$$x_{s,h}^2 = \frac{8\pi f_1 h.10^{-7}}{R_{DC}} \tag{4.21}$$

and

$$R_{skin} = R_{dc}\left(1+y_s\right) \tag{4.22}$$

where f_1 is the fundamental frequency and h is the harmonic order.
Next the formula for the proximity effect* has to be modified in a similar way. This has been done in [10,11]. Also assuming $x_{p,h}^2 = \frac{8\pi f_1 h.10^{-7}}{R_{DC}}$, the factor of proximity effect in a symmetrical 3 phase cable can be expressed as follows:

$$y_{p,h} = \frac{my^2 G_{p,h}}{2 - 5y^2 \frac{II_{p,h}}{12}} \tag{4.23}$$

where m is equal to 2.5, while proximity coefficients $G_{p,h}$ and $H_{p,h}$ are given by:

$$G_{p,h} = \begin{cases} \dfrac{11x_{p,h}^4}{704 + 20x_{p,h}^4} & 0.0 < x_{p,h} \le 2.8 \\ -0.08x_{p,h}^2 + 0.72x_{p,h} - 1.04 & 2.8 < x_{p,h} \le 3.8 \\ \dfrac{x_{p,h}}{4\sqrt{2}} - \dfrac{1}{8} & 3.8 < x_{p,h} \end{cases} \tag{4.24}$$

$$II_{p,h} = \begin{cases} \dfrac{1}{3} \cdot \dfrac{1 + 0.0283x_{p,h}^4}{1 + 0.0042x_{p,h}^4} & 0.0 < x_{p,h} \le 2.8 \\ 0.0384x_{p,h}^2 + 0.119x_{p,h} + 0.095 & 2.8 < x_{p,h} \le 3.8 \\ \dfrac{2x_{p,h} - 4.69}{x_{p,h} - 1.16} & 3.8 < x_{p,h} \end{cases} \tag{4.25}$$

Factor $y_{p,h}$ is also affected by the spacing ratio of $y=d_c/s$, where s is the spacing between conductor axes, and d_c is the diameter of an equivalent circular conductor having the same cross-section and degree of compactness as a shaped conductor. For a multi-core cable, as recommended in [12], both s and d_c are approximately expressed as:

$$\begin{aligned} d_c &= d_s \sqrt{\frac{(4N-1)}{3}} \\ s &= d_c + 2t \end{aligned} \tag{4.26}$$

where d_s and N are respectively the diameter and number of copper strands, and t is the thickness of conductor insulation.

When armour or a sheath is present within the cable, hysteresis losses and additional eddy-current losses are encountered. The factor λ introduced in [2,3] incorporates the extra losses at 50 Hz. By using a generic frequency f instead of 50 Hz, the factor λ is used to approximate the extra losses in a cable at harmonic frequency. This adapted factor λ is given by:

$$\lambda_{2,h} = \frac{0.358 \frac{R_a}{R_h'} \left(\frac{2r_1}{d_a} \right)}{1 + \left(\frac{2.77 R_a x 10^6}{2\pi f_1 h} \right)} \tag{4.27}$$

where R_a and R'_h are respectively the armour/sheath DC resistance and cable harmonic resistance without the armour. r_1 is the circumscribing radius of three-sector shaped conductors in a three-core cable. d_a is the mean diameter of the armour. If a four-core

SWA cable is considered, factor λ_2 in equation (4.27) should be multiplied by 1.02, as recommended in [4].
This steel armour/sheath factor λ effects equation (4.15) as follows:

$$R_h = R_{DC}\left(1 + y_{s,h} + y_{p,h}\right)\left(1 + \lambda_{2,h}\right) \tag{4.28}$$

* *The proximity effect is associated with the magnetic field of two conductors which are close together. If each carries a current in the same direction, the halves of the conductors in close proximity are cut by more magnetic flux then the remote halves. Consequently, the current distribution is not even throughout the cross-section. The remote halves carry a greater proportion. If the currents are in opposite directions the halves in closer proximity carry the greater density of current. In both cases the overall effect results in an increase in the effective resistance of the conductor. The proximity effect decreases with increase in spacing between the cables.*

4.3.4 Inductance part of the three-phase cable

A simple schematic of the cable is shown in Figure 4.5. The current is injected through one of the phases and returns through the sheath. The sheath consists of many copper wires of 1 mm thickness.

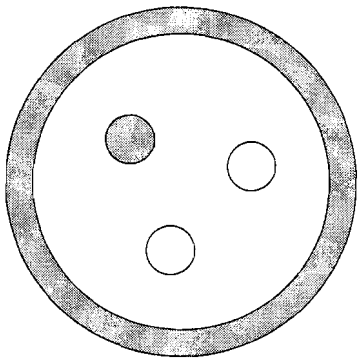

Figure 4.5: Simple cable cross-section

The same as with the resistance part of the cable, the internal inductance is affected by the non-uniform rotational symmetric current density existing for higher frequencies. As mentioned in chapter 4.3.3 this phenomenon is called the "skin-effect". Next to the "skin-effect", the internal inductance of the cable is also affected by the eddy currents induced in the conductors and sheath due to a magnetic field caused by a current in another conductor or sheath. As known from the resistance part of the cable this effect is called the "proximity effect". The last part to incorporate in the inductance is the external inductance, or the inductance due to the time-varying magnetic field in between the two conductors carrying current. This external inductance can be considered frequency independent.

The total inductance can then be expressed as:

$$L_{total} = L_{phase} + L_{ext} + L_{sheath} + L_{proximity} \tag{4.29}$$

with L_{phase} = the internal inductance of the phase carrying current, affected by the skin-effect.

L_{ext} = the external inductance due to the magnetic field in between conductors.

L_{sheath} = the internal inductance of the sheath carrying current ($L_{sheath1}$) plus The inductance of the sheath due to eddy currents induced in the Sheath ($L_{sheath2}$).

$L_{proximity}$ = the inductance caused by eddy currents induced in the phases, because they are in the proximity of another conductor.

Each of these inductances will be calculated below.

4.3.4.1 Inductance due to skin-effect

The skin-effect should be taken into account for every conductor which carries current and for which the skin-depth δ is smaller then the radius of the conductor. The skin depth δ is deducted in Appendix B and equal to:

$$\delta = \sqrt{\frac{2}{\omega\mu\sigma}} \tag{4.30}$$

As can be seen in equation (4.30) the skin-depth is dependent of the frequency. The higher the frequency, the smaller δ. This means the skin-depth will be smallest at the highest frequency of interest. For this study this frequency is the 50th harmonic or 2500 Hz. At this frequency the skin-depth of copper is equal to 1.33 mm. As the conductors in the sheath are made from copper and their radius is 0.5 mm, the skin-effect in the conductors of the sheath can be ignored. This can not be said for the phases themselves. Their radius is 8.55 mm and they are made from aluminium. The skin depth of aluminium at 2500Hz is equal to 1.74 mm, which means the skin-effect can't be ignored for the current carrying phases.

To incorporate this skin-effect for the phases, the formula for the internal inductance of a solid round conductor, thus a phase, is deducted in AppendixB. This deduction results in the following equation for the internal inductance of a solid round conductor (or in this case a phase):

$$L_{phase} = \frac{R_s}{\sqrt{2}\pi r_0 \omega}\left[\frac{Ber(q)Ber'(q) - Bei(q)Bei'(q)}{(Ber'(q))^2 + (Bei'(q))^2}\right] \quad H/m \tag{4.31}$$

4.3.4.2 Inductance due to magnetic field in between conductors

The inductance L_{ext} due to the time-varying magnetic field between the two conductors which carry current is deducted from the external inductance part of a simple coaxial structure.

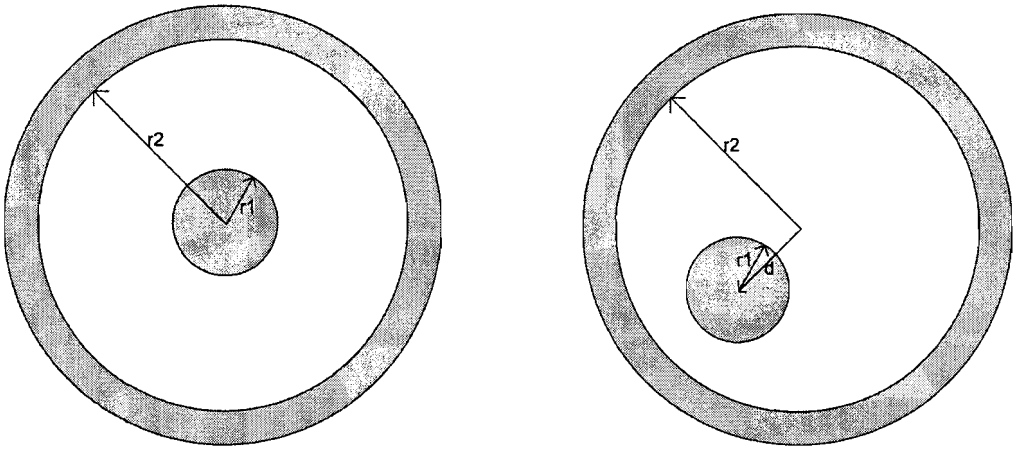

Figure 4.6: Simple coaxial structure

The external inductance of this coaxial structure displayed in Figure 4.6 on the left can be found by using the Ampere-Maxwell law:

$$\oint H \cdot dl = \oiint \left(J + \frac{dD}{dt} \right) \cdot dA \tag{4.32}$$

The displacement current is negligible to the current density J for a good conductor. So equation (4.32) becomes:

$$\oint H \cdot dl = \oiint J \cdot dA \tag{4.33}$$

Outside the conductor this can be written as:

$$\oint H \cdot dl = I_{oms} \tag{4.34}$$

with I_{oms} the total conductor current.
If the conductor radius is taken as r_1 and H is constant in the ϕ direction then equation (4.34) becomes:

$$H \cdot 2\pi \cdot r_1 = I_{oms} \tag{4.35}$$

Introducing the magnetic flux density this results in:

$$B = \frac{\mu_0 \mu_r I_{oms}}{2\pi r_1} \tag{4.36}$$

Now the magnetic flux in the isolation between conductor and sheath can be calculated with Faraday's law:

$$\phi_{oms} = \oiint B \cdot dA = l \int_{r_1}^{r_2} \frac{\mu_0 \mu_r I_{oms}}{2\pi r_1} \cdot dr = \frac{l \mu_0 \mu_r I_{oms}}{2\pi} \ln \frac{r_2}{r_1} \tag{4.37}$$

with r_2 the radius till the sheath.
The last step is to determine L_2 with the calculated flux:

$$L_{ext} = \frac{\phi_{oms}}{I_{oms}} = \frac{\mu_0 \mu_r}{2\pi} \ln \frac{r_2}{r_1} \qquad H/m \tag{4.38}$$

The actual cable structure however is as shown in Figure 4.6 on the right. This influences equation (4.38) in the following way:

$$L_{ext} = \frac{\mu_0 \mu_r}{2\pi} \ln \left\{ \frac{r_2}{r_1} \left[1 - \left(\frac{d}{r_2} \right)^2 \right] \right\} \qquad H/m \tag{4.39}$$

4.3.4.3 Inductance due to proximity effects and losses in sheath

This part of the theory is still a work in progress. The analytical method to calculate the proximity losses is known, but the formulas have not been fully worked out due to time limits. The method and the formulas are discussed in Appendix C. The resulting equation for the inductance of the sheath is:

$$L_{sheath} = L_{sheath1} + L_{sheath2} \tag{4.40}$$

$$L_{sheath1} = -\frac{\mu_0}{2\pi} \sum_{m=1}^{\infty} \frac{1}{m} \left(\frac{a}{r_h} \right)^{2m} U_m \tag{4.41}$$

$$L_{sheath2} = \frac{\mu_0}{2\pi}\frac{d}{r_h}\frac{\delta_m}{2d}\frac{\sinh\left(\frac{2d}{\delta_m}\right)-\sin\left(\frac{2d}{\delta_m}\right)}{\cosh\left(\frac{2d}{\delta_m}\right)-\cos\left(\frac{2d}{\delta_m}\right)} \tag{4.42}$$

The resulting equation for $L_{proximity}$ has not been found due to time limits.

4.3.5 Practical acquisition of resistance and reactance

The goal is to acquire an impedance matrix as in (4.8) for each harmonic till the 50th. For this a single-phase current injection is applied to determine the elements of the impedance matrix. Figure 4.7 shows the lumped parameter model of the cable system under the phase A to neutral (A-N) current injection.

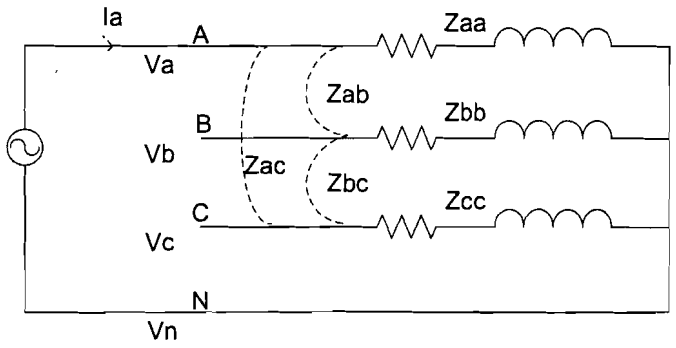

Figure 4.7: Circuit model under the A-N condition

Voltages V_{aa}, V_{ab}, V_{ac} and current I_a are recorded in a measurement with an injection of a sine waveform current for each harmonic. Self and mutual impedance at order h for phase A are calculated as follows:

$$Z_{h,aa} = \left.\frac{V_{h,an}}{I_{h,a}}\right|_{I_b=I_c=0}$$
$$Z_{h,ba} = \left.\frac{V_{h,bn}}{I_{h,a}}\right|_{I_b=I_c=0} \qquad (4.43)$$
$$Z_{h,ca} = \left.\frac{V_{h,cn}}{I_{h,a}}\right|_{I_b=I_c=0}$$

This is repeated for a current injection under B and C until the entire matrix is known. The measurement setup used for this measurement is displayed in Figure 4.8.

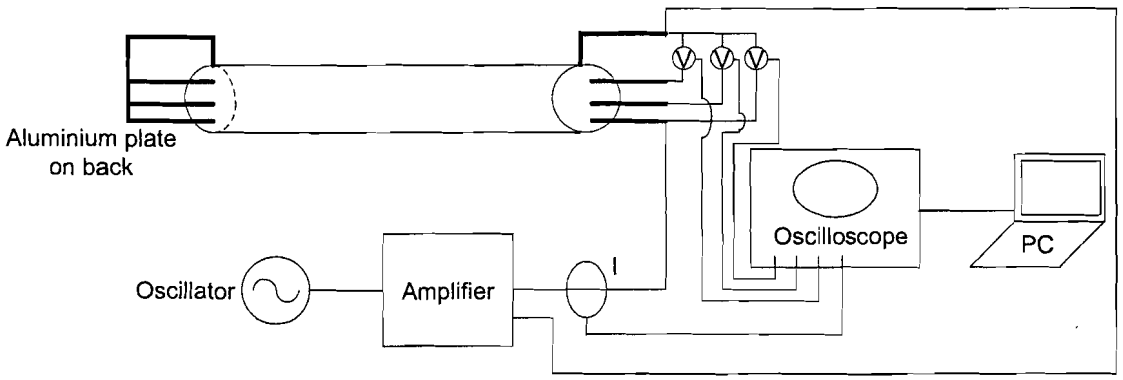

Figure 4.8: Measurement setup

4.3.6 Measurement results

The measurement results will be split up into the results for the medium voltage cable and the low voltage cable.

4.3.6.1 Medium voltage cable

The measurement results acquired with the setup of Figure 4.8 for the medium voltage cable are given in appendix B. These results are for a distance of 1 km cable and include the sheath resistance for each phase, as explained in chapter 4.3.5. The measurement was done at 20°C.
On the diagonal of each matrix the resistance and self-reactance of each phase plus sheath are shown. On the other positions in the matrix the mutual reactance's and sheath resistance are visible.

4.3.6.1.1 Validating 50Hz measured values

To validate the starting point of the measurement the 50Hz measurement values are compared to some values on the Pirelli data-sheets. Recalling from equation (4.9):

$$z_{aa} = \bar{z}_{aa} - 2\bar{z}_{ad} + \bar{z}_{dd} \qquad \Omega/\text{unit length} \tag{4.44}$$

or for the real part:

$$R_{aa} = \bar{R}_{aa} - 2\bar{R}_{ad} + \bar{R}_{dd} \qquad \Omega/\text{unit length} \tag{4.45}$$

$\bar{R}_{ad}$ is negligible to $\bar{R}_{aa}$ and $\bar{R}_{dd}$. So equation (4.45) can be written as:

$$\bar{R}_{aa} \approx R_{aa} - \bar{R}_{dd} \qquad \Omega/\text{unit length} \tag{4.46}$$

In the same way z_{ab} in equation (4.10) can be written as:

$$R_{ab} = \bar{R}_{ab} - \bar{R}_{ad} - \bar{R}_{bd} + \bar{R}_{dd} \qquad \Omega/\text{unit length} \tag{4.47}$$

$\bar{R}_{ab}, \bar{R}_{ad}$ and $\bar{R}_{bd}$ are again negligible against $\bar{R}_{dd}$, so:

$$R_{ab} \approx \bar{R}_{dd} \qquad \Omega/\text{unit length} \tag{4.48}$$

This means that:

$$\bar{R}_{aa} \approx R_{aa} - R_{ab} \qquad \Omega/\text{unit length} \tag{4.49}$$

Applying this equation to the measurement results obtained for 50Hz gives:

$$\bar{R}_{aa} \approx 0.4191 - 0.2938 = 0.1253 \qquad \Omega/\text{km} \tag{4.50}$$

According to the information provided by Pirelli $\bar{R}_{aa}$ should be around 0.125 Ω/km.
Equation (4.50) is just around this value, which means the starting point of the measurement corresponds to the data given by Pirelli.

This validation can be done in a similar way for the reactance of the cable. However the reactance $\bar{X}_{ad}$ can not be neglected. This makes the measured reactance X_{aa} still equal to $\bar{X}_{aa} - 2\bar{X}_{ad} + \bar{X}_{dd}$. Only $\bar{X}_{aa}$ is given by Pirelli, which then makes it impossible to validate the 50 Hz measurements for the reactance.

4.3.6.1.2 Plotting results

Now that the 50Hz measured values are validated the overall results of the measurement can be displayed and discussed. The measured resistances for Z_{aa}, Z_{bb} and Z_{cc} are displayed in Figure 4.9.

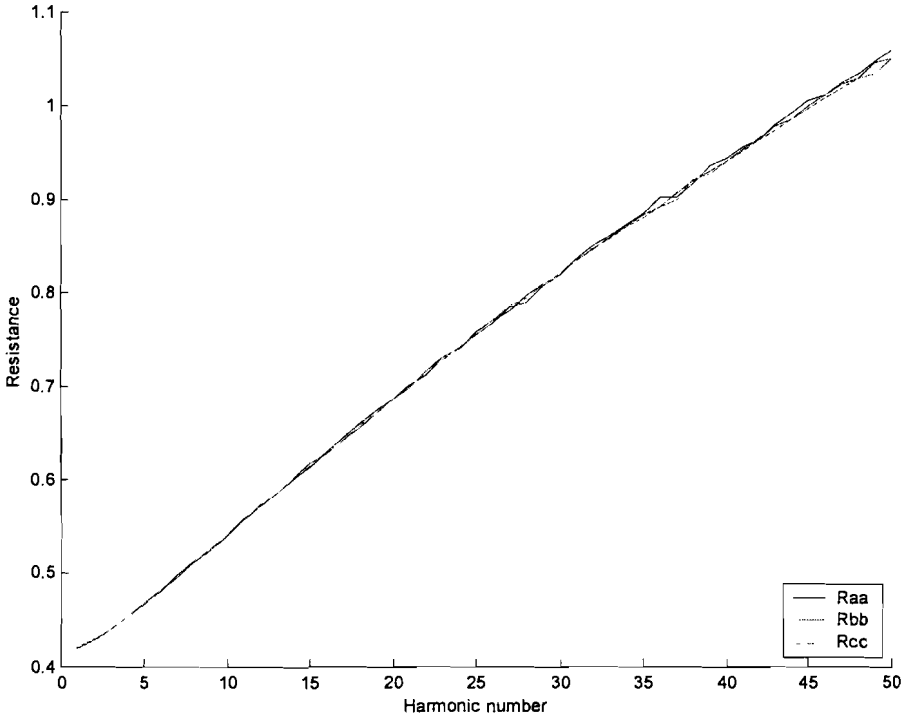

Figure 4.9: Resistance measured for Z_{aa}, Z_{bb} and Z_{cc}

As can be observed the three measurements have the same shape and lie close together, which agrees with the symmetrical build of the cable. Further the resistance increases almost linear in respect to the frequency, which can be ascribed to the skin and proximity effects.

Figure 4.10 shows the measured reactance for Z_{aa}, Z_{bb} and Z_{cc}. Again the three measured lines are close together and have the same shape due to the symmetry of the cable. The interesting thing to observe is that the increase of the reactance is not linear, although it comes close to it. The slight curvature due to the skin effect is easily noticeable. This becomes more distinct when the inductance is plotted, as shown in Figure 4.11.

The irregularity noticed in this figure is the kink in the first few measurements. This kink is caused due to measurement errors. In the low frequency range the cable is almost wholly resistive, as can be observed in the measured matrices in Appendix B. Therefore a slight error in the measured angle between voltage and current introduces large differences in the impedances. Beyond the first few measurements the reactance of the cable increases significantly so that a slight fault in the measured angle doesn't anymore result in a large error in the measured impedance.

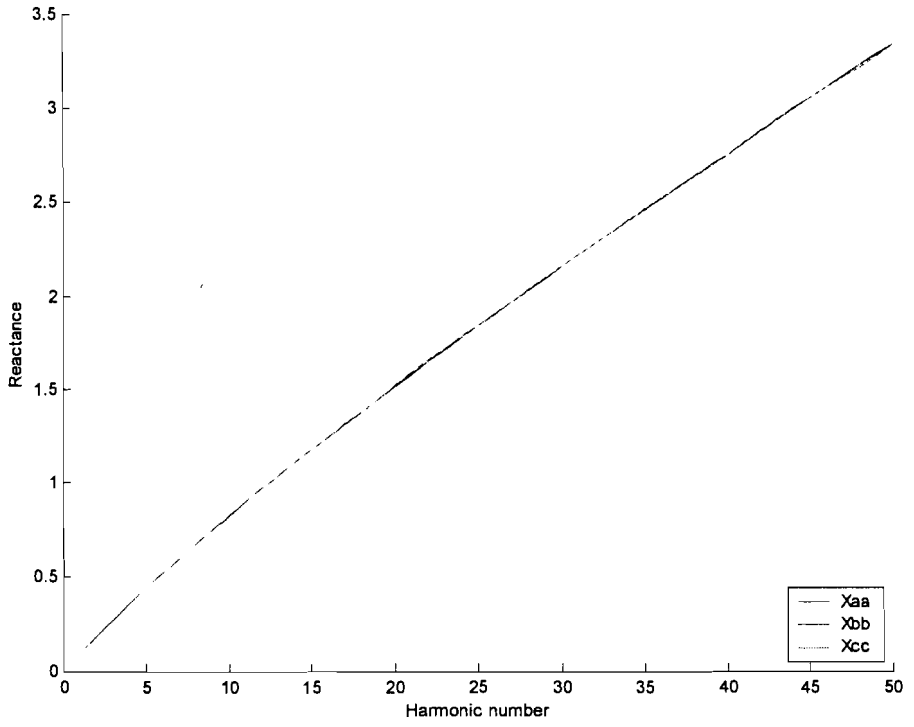

Figure 4.10: Reactance measured for Z_{aa}, Z_{bb} and Z_{cc}

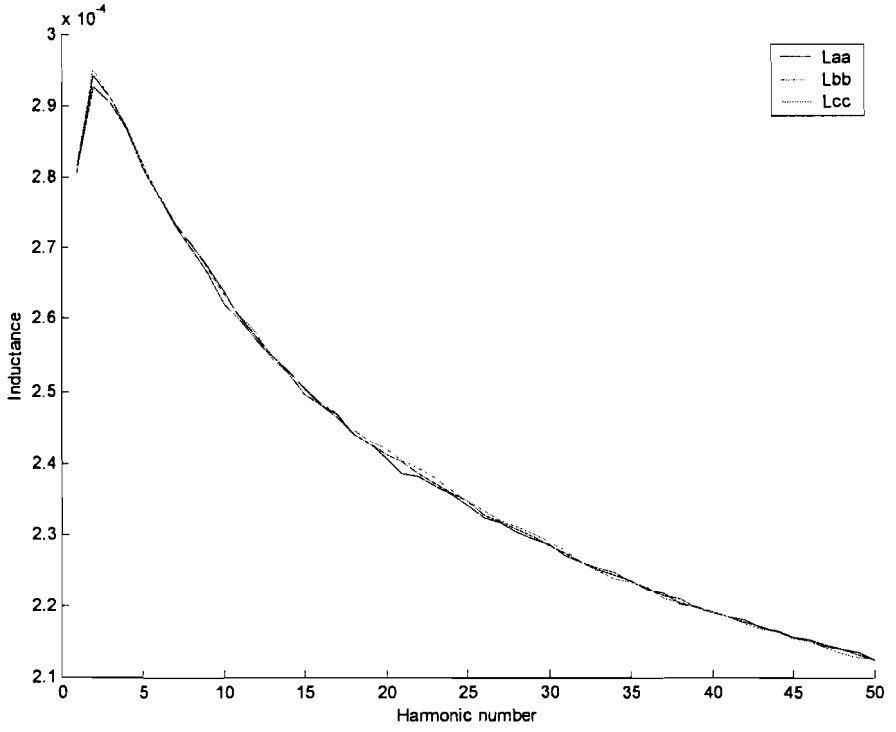

Figure 4.11: Inductance measured for Z_{aa}, Z_{bb} and Z_{cc}

4.3.6.1.3 Comparing measurement results and theory

This chapter compares the measurement results with the acquired theory. Figure 4.12 shows the measured and theoretical resistances.

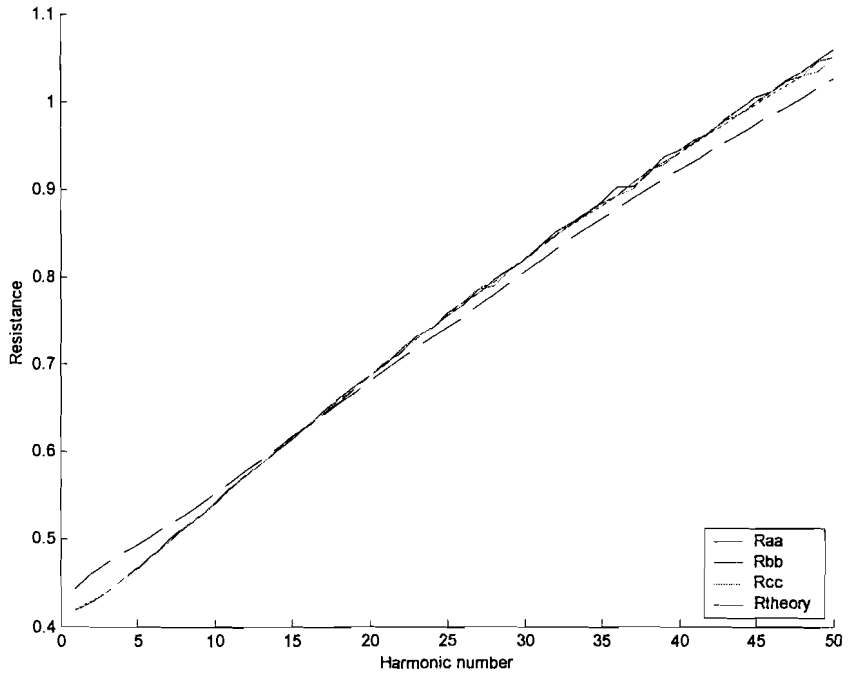

Figure 4.12: Measured resistance and theoretical resistance

As can be observed the theoretical resistance corresponds well with the measured values. The most important differences between the measured and theoretical values are the different starting points and the difference in steepness of the lines. These differences can be ascribed to the discussed measurement difficulties in chapter 4.3.6.1.2 in the low frequency range and the fact that the numerical formulas for the resistance are very sensitive to small changes in its parameters. For example a difference of 2 mm in the diameter of the phase d_c gives the dashed line in Figure 4.13. A change of 4 mm in the mean diameter of the armor d_a gives the dash-dotted line in Figure 4.13. Thus from comparing the theoretical resistance with the measurements it can be concluded that the theoretical resistance corresponds well with the measured resistance.
Figure 4.14 shows the measured and theoretical reactance. For the higher frequencies the two lines show an increasing difference, which becomes more distinct when the inductance is plotted in Figure 4.15.
This difference can be ascribed to the fact that for the calculation of the reactance/inductance the proximity effects and the losses in the sheath are not jet incorporated in the theoretical equations (due to time limits). As now can be seen, it is crucial to incorporate these losses to get a good approximation of the inductance of a cable. As mentioned the losses in the sheath have been fully worked out analytically in chapter 4.3.4.3. These losses only have to be incorporated into the theoretical equations for the current cable to account for them. The proximity losses are another problem. The method to calculate these losses is known (Appendix C), but the equations have not been fully worked out due to time limits. Initial steps have been made from which following equations can be deducted.
Another small problem to consider is the neglection of the back potentials produced by the other phases in step 2 of the analytical approach in Appendix C. In this step only the

back potential of the sheath is considered and the back potentials produced by the other phases as a reaction to the initial potential are ignored to make calculations easier. As the calculated resulting potential is used to calculate the losses in the sheath, this neglection works all the way through to the sheath inductance. For the proximity losses a similar argument can be made. In step 7 of Appendix C the proximity losses are calculated, with a correction for the back potential produced by the sheath. Although this correction for the sheath has been made, the back potential from the third phase is again ignored, causing an error in the resulting inductance. The mentioned errors due to neglection of potentials are very small and can probably be ignored as they will not introduce a large difference between the theory and the measurements. However if a very detailed calculation of the inductance of a cable structure is necessary, software packages like EMTP or finite element based programs can be used.

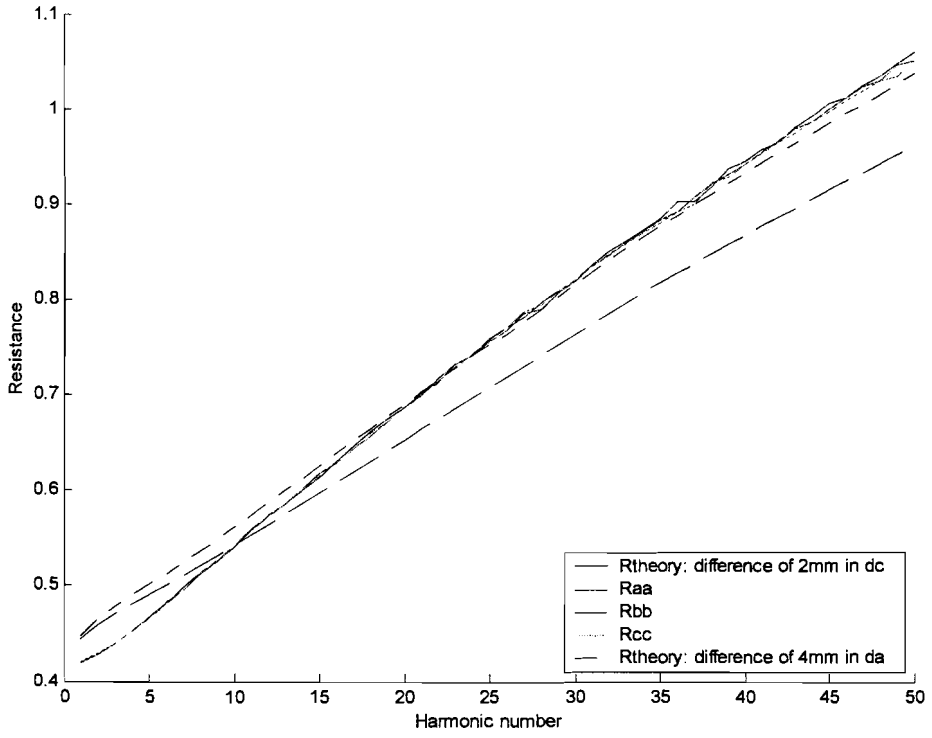

Figure 4.13: Differences in theory of resistance due to small parameter changes

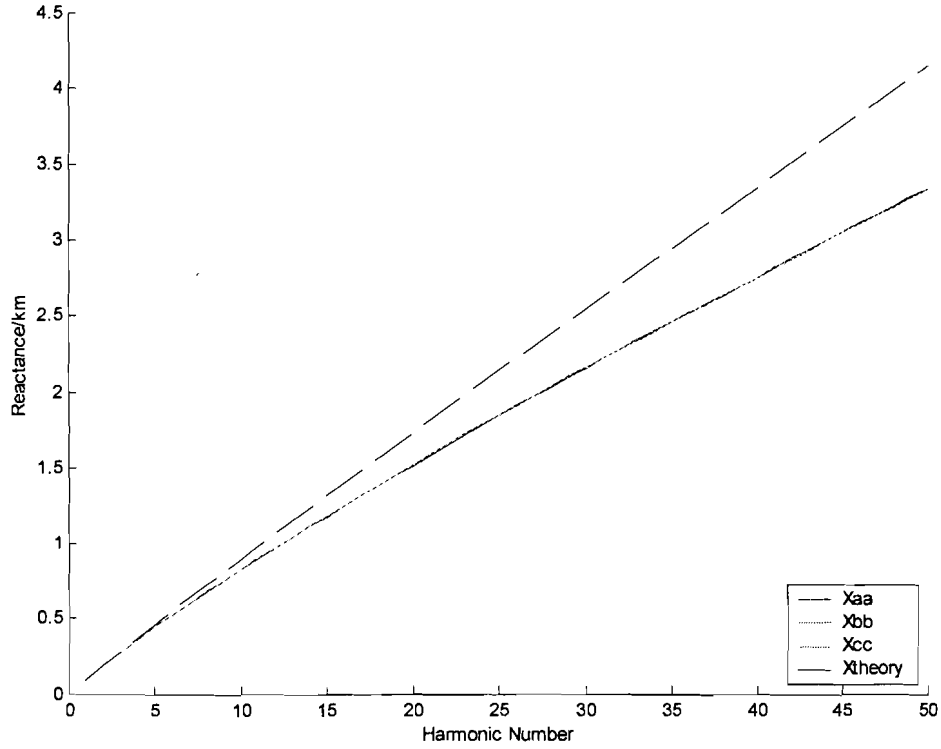

Figure 4.14: Measured reactance and theoretical reactance

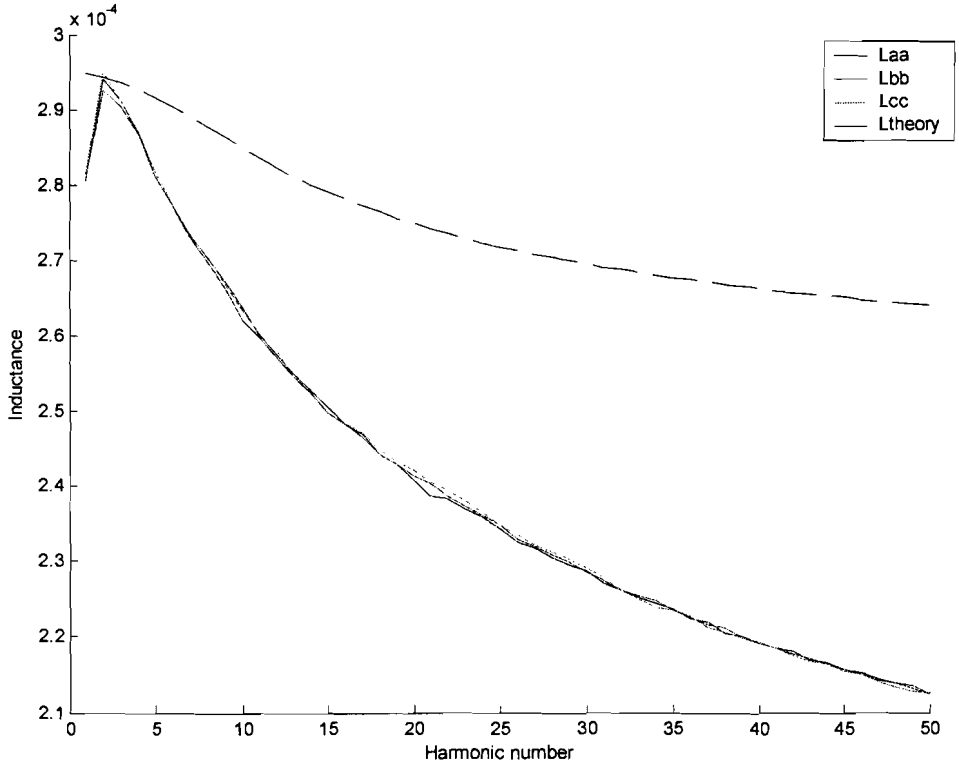

Figure 4.15: Measured inductance and theoretical inductance

4.3.6.2 Low Voltage Cable

The measurement results acquired with the setup of Figure 4.8 for the low voltage cable are given in appendix B. These results are for a distance of 1 km cable and include the sheath resistance for each phase, as explained in chapter 4.3.5. The measurement was done at 0°C

On the diagonal of each matrix the resistance and self-reactance of each phase plus sheath are shown. On the other positions in the matrix the mutual reactance's and sheath resistance are visible.

Only three of the four phases are measured, because measuring all four phases would cause difficulties with the measurement equipment and procedure. However, if these three phases display similarity, as is to be expected with the symmetrical build of the cable, it can be concluded that the fourth will also display this similarity.

4.3.6.2.1 Validating 50Hz measurements

Using the same method as used in chapter 4.3.6.1.1 for the medium voltage cable the 50 Hz impedances can be validated with the Pirelli datasheet. Applying equation (4.49) to the measurements obtained for 50Hz gives:

$$\bar{R}_{aa} \approx R_{aa} - R_{ab} = 0.5879 - 0.3897 = 0.1982 \qquad \Omega/\text{unit length} \tag{4.51}$$

This is for a temperature of 0°C. So calculating the data from Pirelli for the dc resistance of the cable at 20°C back to 0°C with equation (4.16) results in:

$$R_{dc} = R_{20}\left[1+\alpha_{20}\left(T_c - 20\right)\right] = 0.206\left[1+0.00429\left(0-20\right)\right] = 0.1883 \quad \Omega/\text{km} \tag{4.52}$$

Equation (4.52) now gives the dc resistance at a temperature of 0°C. The measured resistance in equation (4.51) is the ac resistance at 50Hz and 0°C. In theory these two values should be close together, with the 50Hz value greater than the dc value. Our measured value is indeed larger and in the vicinity of the dc resistance at 0°C. It can thus be assumed, with the measurement difficulties in mind, that the starting point of the measurement corresponds with the data provided by Pirelli.

This validation can be done in a similar way for the reactance of the cable. However the reactance $\bar{X}_{ad}$ can not be neglected. This makes the measured reactance X_{aa} still equal to $\bar{X}_{aa} - 2\bar{X}_{ad} + \bar{X}_{dd}$. Only $\bar{X}_{aa}$ is given by Pirelli, which then makes it impossible to validate the 50 Hz measurements for the reactance.

4.3.6.2.2 Plotting results

Now that the 50Hz measured values are validated the overall results of the measurement can be displayed and discussed. The measured resistances for Z_{aa}, Z_{bb} and Z_{cc} are displayed in Figure 4.16. As can be observed the three measurements have the same shape and lie close together, which agrees with the symmetrical build of the cable. Further the resistance increases in respect to the frequency, which can be ascribed to the skin and proximity effects. The most important difference noticed is that the lines in Figure 4.16 are more curved then the ones for the medium voltage cable. A reason for this could be the difference in build of the cables. The low voltage cable has shaped conductors as the medium voltage cable has round conductors.

Figure 4.17 shows the measured reactance for Z_{aa}, Z_{bb} and Z_{cc}. As with the medium voltage cable the three measured lines are close together and have the same shape due to the symmetry of the cable. Also the slight curvature due to the skin effect is easily noticeable. This becomes more distinct when the inductance is plotted in Figure 4.18.

The kink in the first few measurements is also caused due to measurement errors as explained for the medium voltage cable.

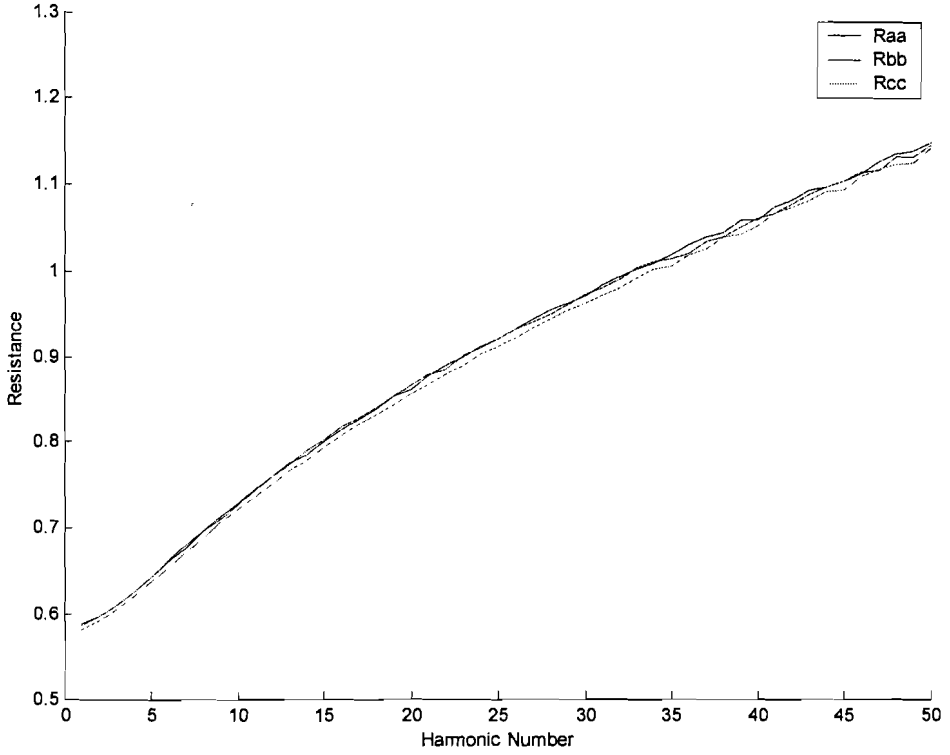

Figure 4.16: Resistance measured for Z_{aa}, Z_{bb} and Z_{cc}

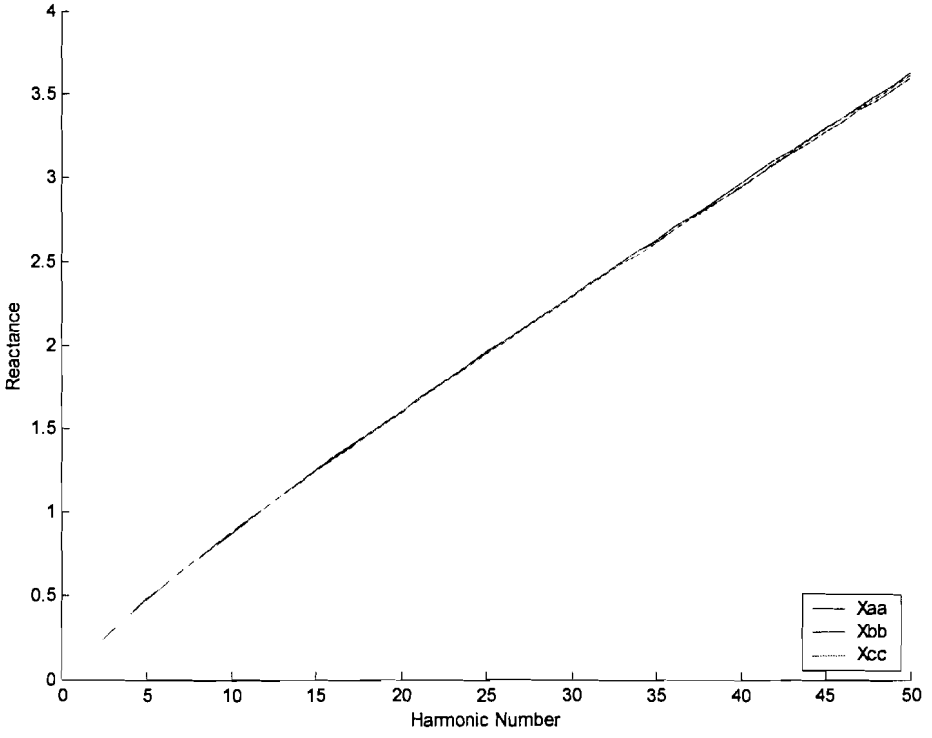

Figure 4.17: Reactance measured for Z_{aa}, Z_{bb} and Z_{cc}

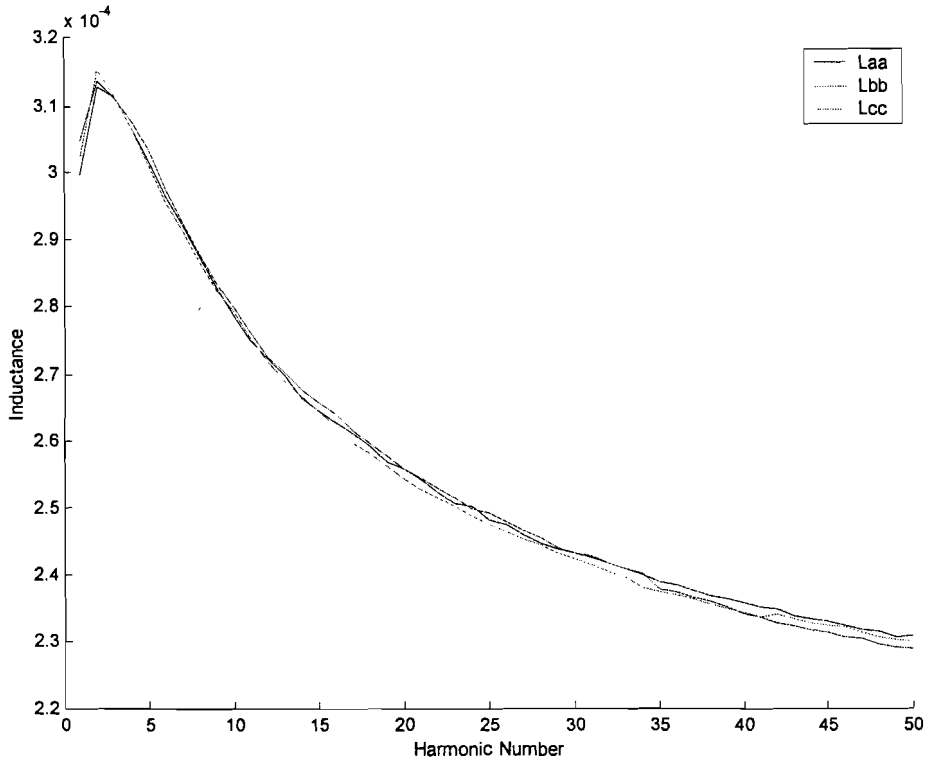

Figure 4.18: Inductance measured for Z_{aa}, Z_{bb} and Z_{cc}

4.3.6.3 Comparing measurement results and theory

Figure 4.19 shows the measured and theoretical resistances.

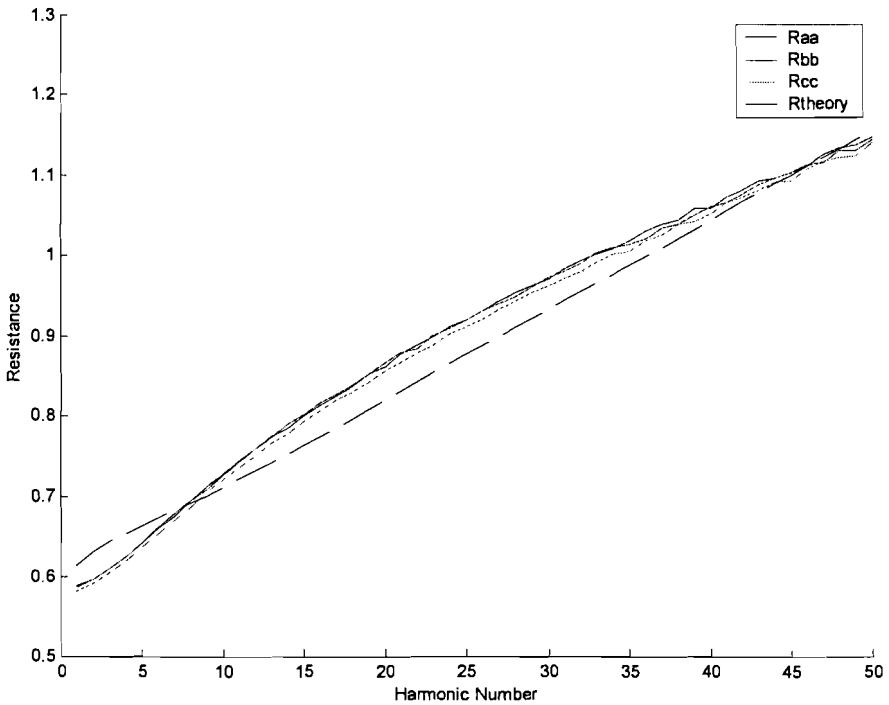

Figure 4.19: Measured resistance and theoretical resistance

The most important difference between the measurements and the theory is the form of the lines. In the theory the frequency and the resistance have an almost linear relationship as for the measurements the frequency and the resistance deviate more to a non-linear relationship. This can be ascribed to the fact that the theory for the resistance of a cable used here is originally derived for circular conductors and a three-phase. As the low voltage cable has four shaped conductors, this probably would be the main cause of difference.
Figure 4.20 shows the measured and theoretical reactance. For the higher frequencies the two lines show an increasing difference, which becomes more distinct when the inductance is plotted in Figure 4.21.
From this figure it is clearly visible that the divergence between the theory and measurements is large for the higher frequencies. This can be ascribed to two aspects. The first aspect is that the theory for the inductance is developed for a three-phase cable with round conductors in contrast to the low voltage cable, which has four shaped conductors. As the difference between the theory and measurements are larger than for the medium voltage cable, this is probably a serious problem.
The second aspect is the same as for the medium voltage cable; for the calculation of the reactance/inductance the proximity effects and the losses in the sheath are not jet incorporated in the theoretical equations (due to time limits). For more information on this aspect see the medium voltage cable.
Thus overall the theoretical inductance does not correspond well with the measured inductance. For a good calculation of the inductance it is recommended to incorporate the missing equations for the losses in the sheath and the proximity effect losses in the calculation of the theoretical inductance or to use software packages like EMTP or finite element based programs to get accurate results.

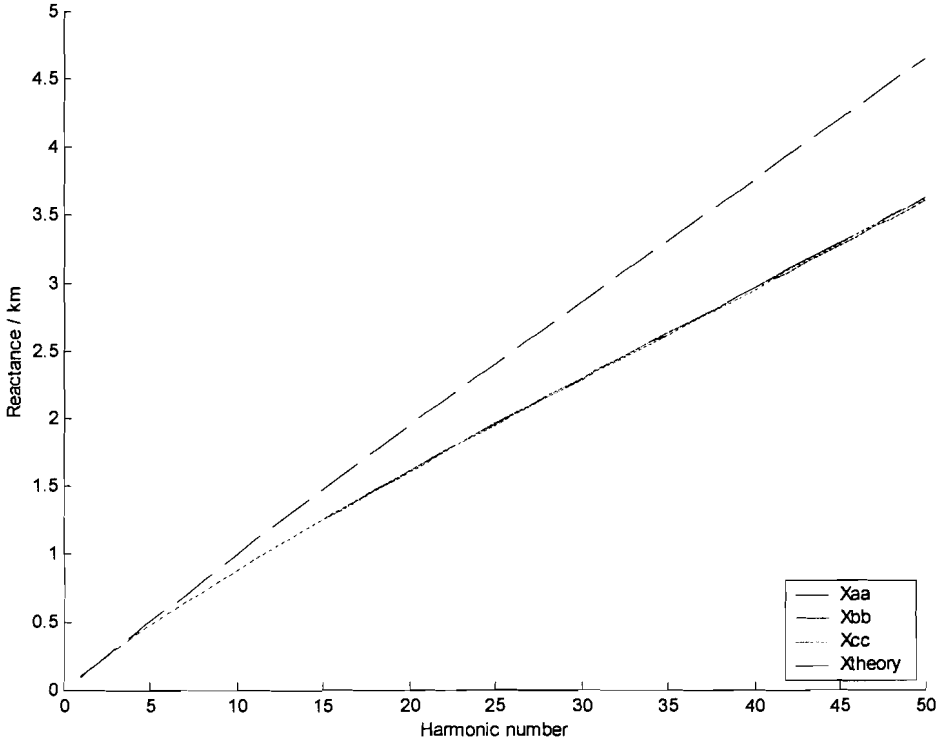

Figure 4.20: Measured and theoretical reactance

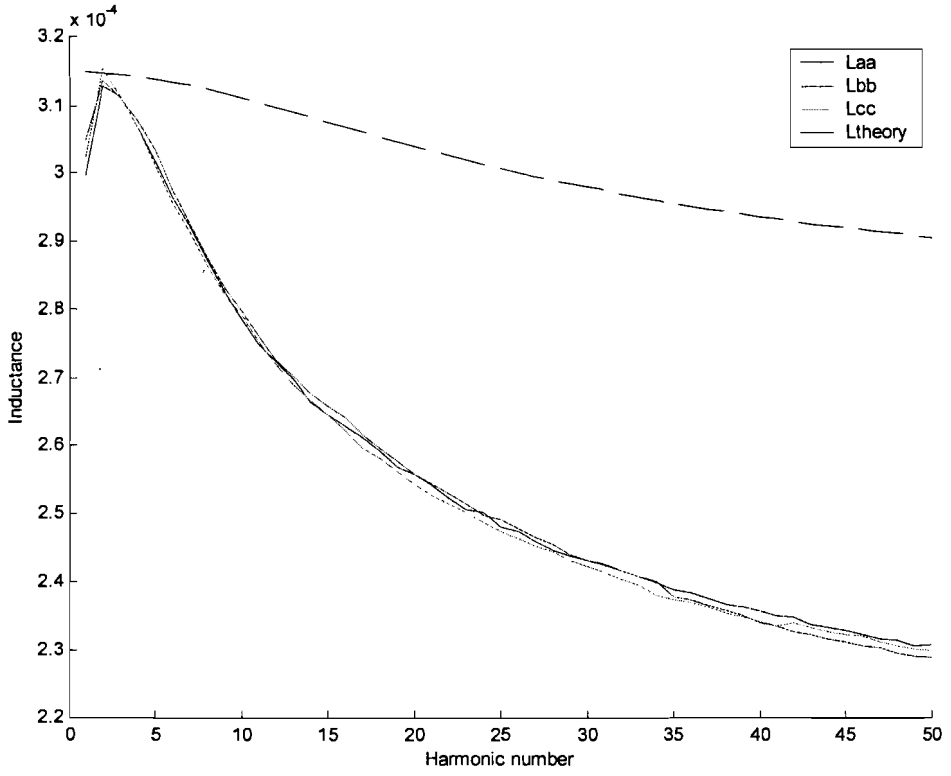

Figure 4.21: Measured and theoretical inductance

4.4 Modeling the loads

In this chapter the modeling of the loads is studied. First, measurement results of standard electrical equipment are presented. This tested equipment consists of common Dutch household appliances like television sets, video recorders, computers, etc. Of each appliance the frequency dependent parameters G, C and I_{inv} are determined. Next to the individual measurements there are measurements done on combinations of the equipment. This gives information on whether or not the summation of the loads is possible for the extended harmonic model of chapter 4.2.
The measurements for the loads were done in collaboration with the Energy Centre of the Netherlands (ECN).
The goal of these measurements is to obtain some inside information on how to deal with this broad scope of devices.

4.4.1 Measurement principles

The equipment is connected to a 5 kW network simulator. This network simulator can be controlled by software to create a harmonically distorted supply voltage. To imitate the behavior of a normal low voltage network a series impedance can be connected to the simulator in accordance with the impedance of a low voltage cable.
The whole of the measurement setup is depicted in Figure 4.22.

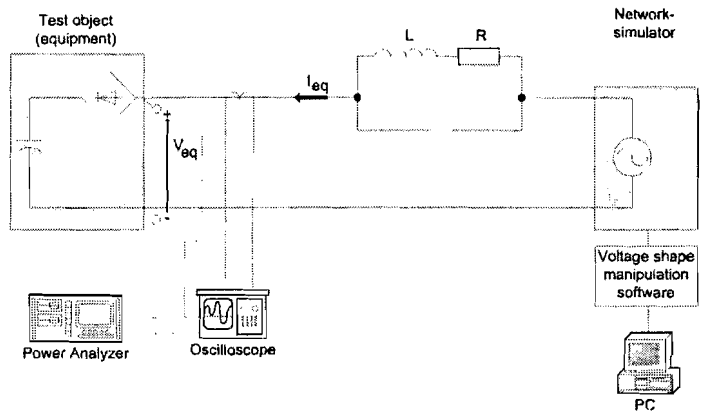

Figure 4.22: Measurement setup for loads

To acquire the G, C and I_{inv} parameters over a frequency range of 2500Hz (50^{th} harmonic), the following is done:

1. Let the grid simulator produce a wave shape without harmonic pollution. Measure voltage, current and power of the device under test for the fundamental frequency and all harmonics up till the 50^{th}.
2. Select all harmonics with a current maximum of 0.1% of the fundamental current.
3. Let the grid simulator produce a wave shape with harmonic distortion. This harmonically distorted wave shape should contain the first harmonic above the fundamental frequency of 50Hz which was selected in 2 and the fundamental frequency.
4. Measure the voltage, current, phase angle between voltage and current and the power of the device under test for the fundamental frequency and all harmonics up till the 50^{th}.
5. Again let the grid simulator produce a wave shape with harmonic distortion as in 3, but now add the second harmonic above the fundamental frequency of 50Hz which was selected in 2.

6. Again measure the voltage, current, phase angle between voltage and current and the power of the device under test for the fundamental frequency and all harmonics up till the 50th.
7. Repeat 5 and 6 for all selected harmonics in 2, using the values for the harmonics shown in Table 5.
8. Calculate for each harmonic n the following quantities:

$$\frac{I}{I_{ref}} = I_n \cdot \frac{U_{ref}}{|P_{ref}|}$$
$$\frac{G_n}{G_{ref}} = \frac{U_{ref}^2 \cdot P_n}{U_n^2 \cdot |P_{ref}|} \qquad (4.53)$$
$$\frac{C_n}{C_{ref}} = \frac{U_{ref}^2 \cdot -P_n \cdot \tan\varphi_n}{U_n^2 \cdot |P_{ref}| \cdot n}$$

with $U_{ref}[V]$ = *The RMS value of the nominal grid voltage. In this case 230V.*
$I_{ref}[A]$ = *The RMS value of the current at* P_{ref}.
$P_{ref}[W]$ = *The nominal AC-power according to the manufacturer.*
$G_{ref}[S]$ = *The conductance that lets a current flow in the grid equal to* I_{ref}.
$C_{ref}[F]$ = *The capacitance that lets a current flow in the grid equal to* I_{ref}.

$U_n[V]$ = *The RMS value of the harmonic voltage (*n^{th} *harmonic).*
$I_n[A]$ = *The RMS value of the harmonic current (*n^{th} *harmonic).*
$U_n[V]$ = *The AC- power of the* n^{th} *harmonic.*
$\Phi_n[°]$ = *The phase angle between voltage and current for the* n^{th} *harmonic.*

9. Present these calculated values in the form of three graphs:
   - I/I_{ref} as function of n
   - G_n/G_{ref} as function of n
   - C_n/C_{ref} as function of n

Harmonic number (n)	Harmonic amplitude (%)	Phase angle (°)
2 to 10	3.0	0
11 to 20	2.5	0
21 to 30	2.0	0
31 to 40	1.5	0
41 to 50	1.0	0

Table 5: Amplitude of the added harmonics

4.4.2 Measurement results for a single load

For 7 common electrical appliances the above measurement method was applied. The method was applied with and without grid impedance. The results will be presented below for each of the appliances.

4.4.2.1 Personal computer

The personal computer studied is a Tulip Vision Line Windows 98 Pentium. The results for the measurement with net impedance are displayed in Figure 4.23(a). The net impedance was equal to 0.309 + j0.155 Ω for the phases and 0.160 + j0.106 Ω for the neutral conductor. The results for the measurement without net impedance are displayed in Figure 4.23(b). The AC-power P_{ref} is equal to 120W.

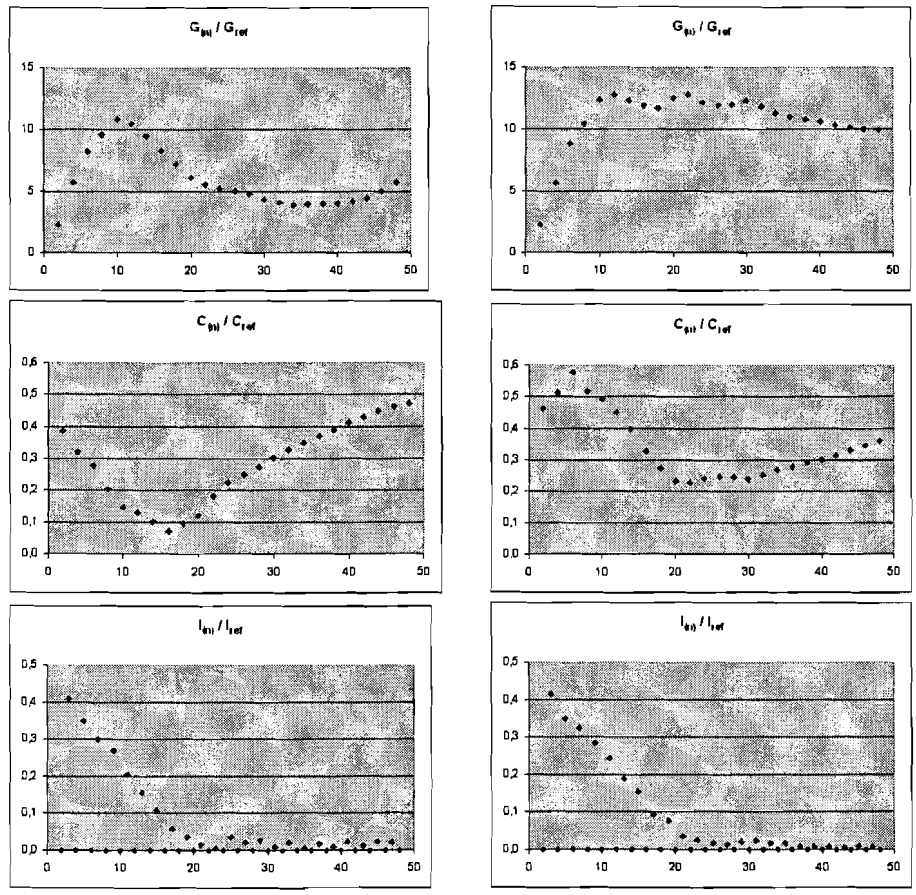

Figure 4.23: Load measurements PC. (a) With net impedance and (b) without net impedance

4.4.2.2 Dimmer with an incandescent lamp

The dimmer/lamp combination was studied at a power of 88W and 44W. The results for the measurement on 88W with net impedance are displayed in Figure 4.24(a). The net impedance was equal to 0.309 + j0.155 Ω for the phases and 0.160 + j0.106 Ω for the neutral conductor for both measurements. The results for the measurement on 88W without net impedance are displayed in Figure 4.24(b) and on 44W in (b). The AC-power P_{ref} is equal to 100W.

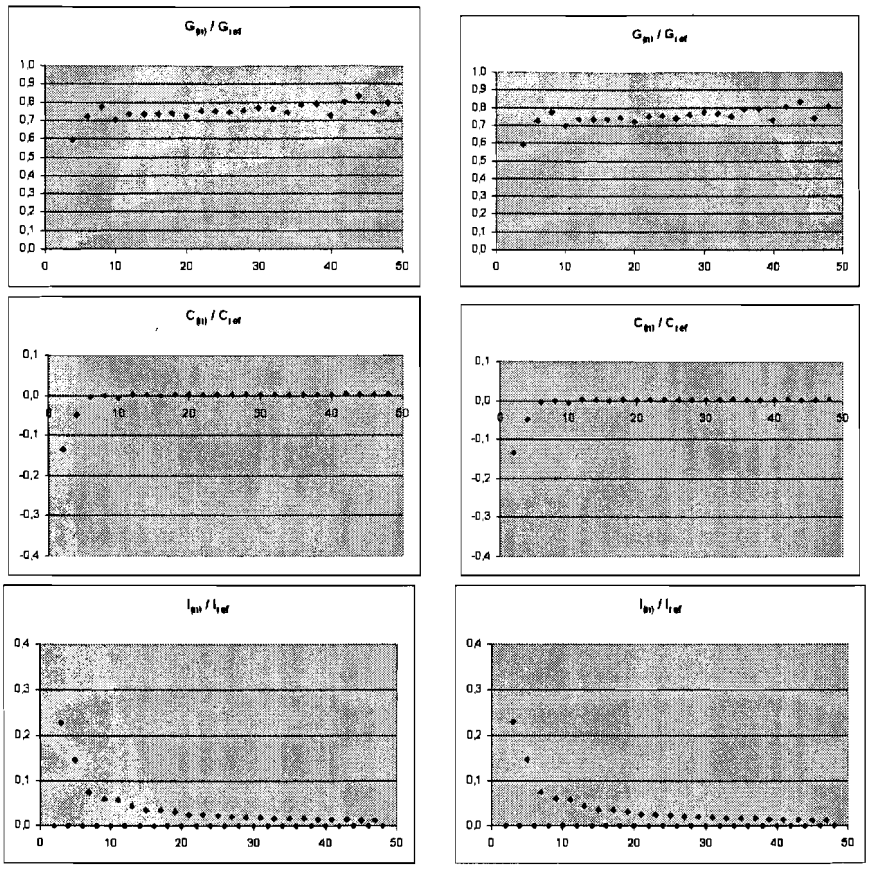

Figure 4.24: Load measurements Dimmer/Lamp 88W. (a) With net impedance and (b) without net impedance

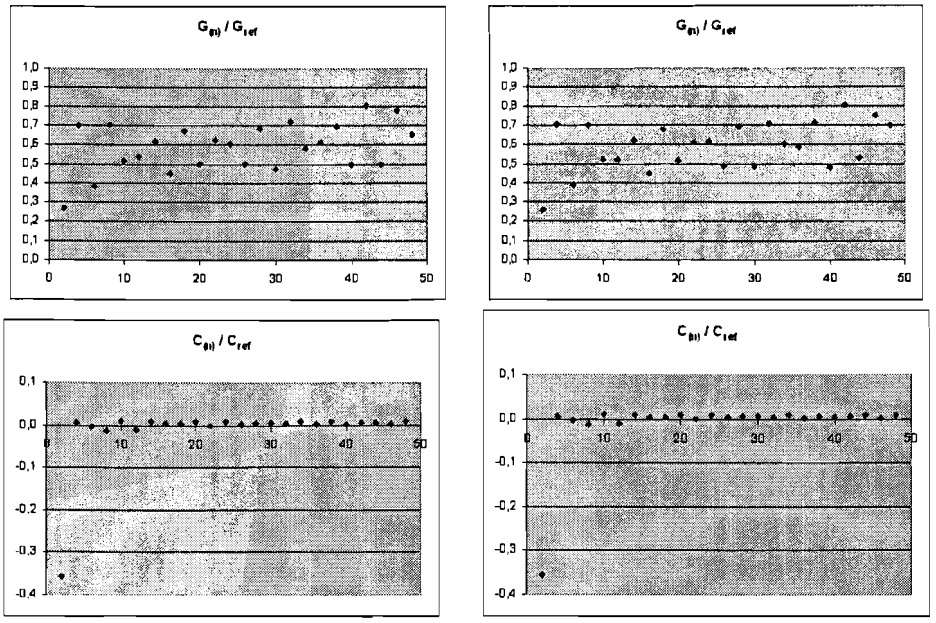

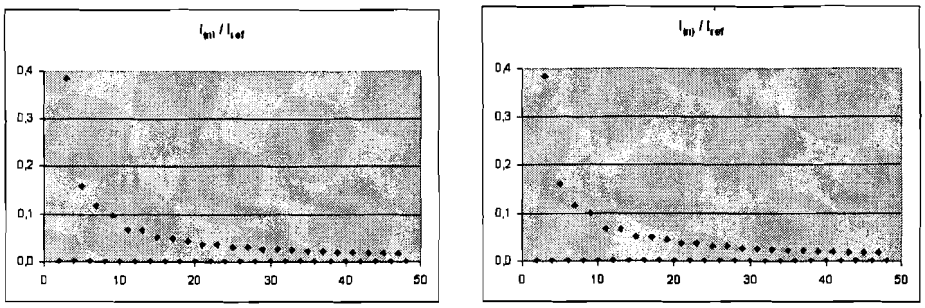

Figure 4.25: Load measurements Dimmer/Lamp 44W. (a) With net impedance and (b) without net impedance

4.4.2.3 Television

The television was studied at normal operation with sound and picture. The results for the measurement with net impedance are displayed in Figure 4.26(a). The net impedance was equal to 0.309 + j0.155 Ω for the phases and 0.160 + j0.106 Ω for the neutral conductor. The results for the measurement without net impedance are displayed in Figure 4.26(b). The AC-power P_{ref} is equal to 39W.

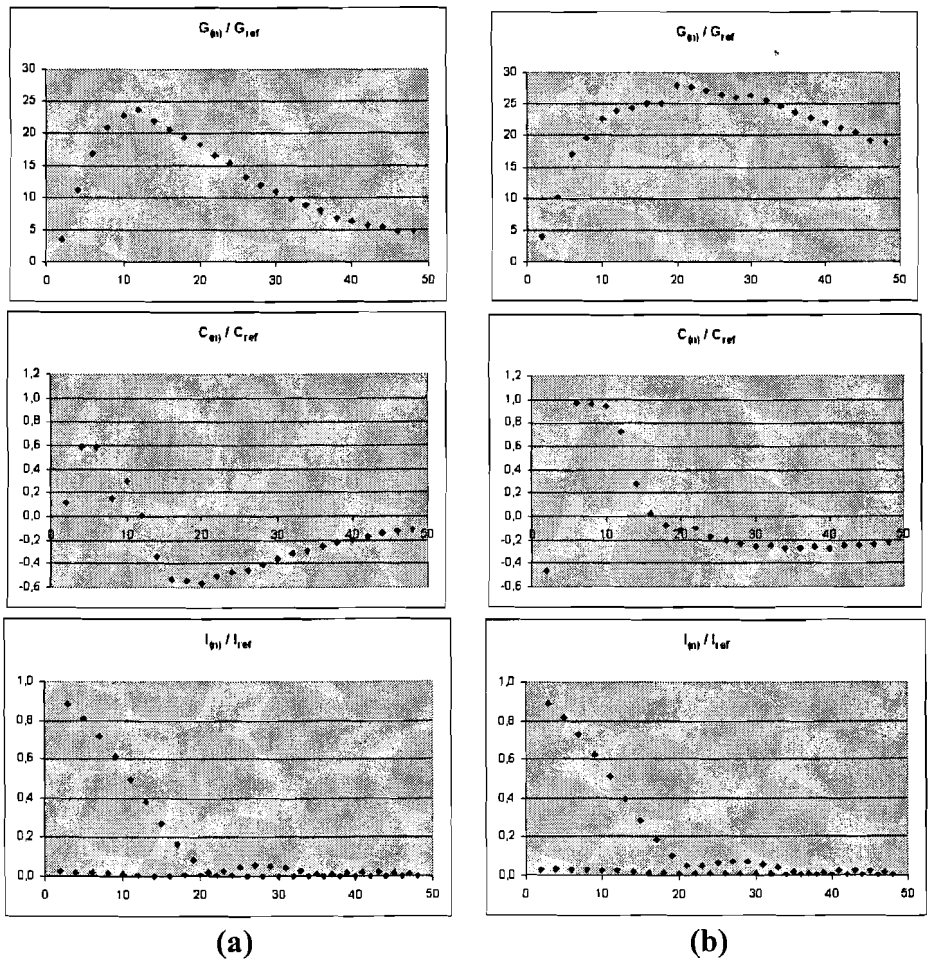

(a) **(b)**

Figure 4.26: Load measurements Television. (a) With net impedance and (b) without net impedance

4.4.2.4 Micro-wave oven

The micro-wave was studied at its full operation power of 1300W. The results for the measurement with net impedance are displayed in Figure 4.27(a). The net impedance was equal to 0.244 + j0.153 Ω for the phases and 0.160 + j0.106 Ω for the neutral conductor. The results for the measurement without net impedance are displayed in Figure 4.27(b). The AC-power P_{ref} is equal to 1300W.

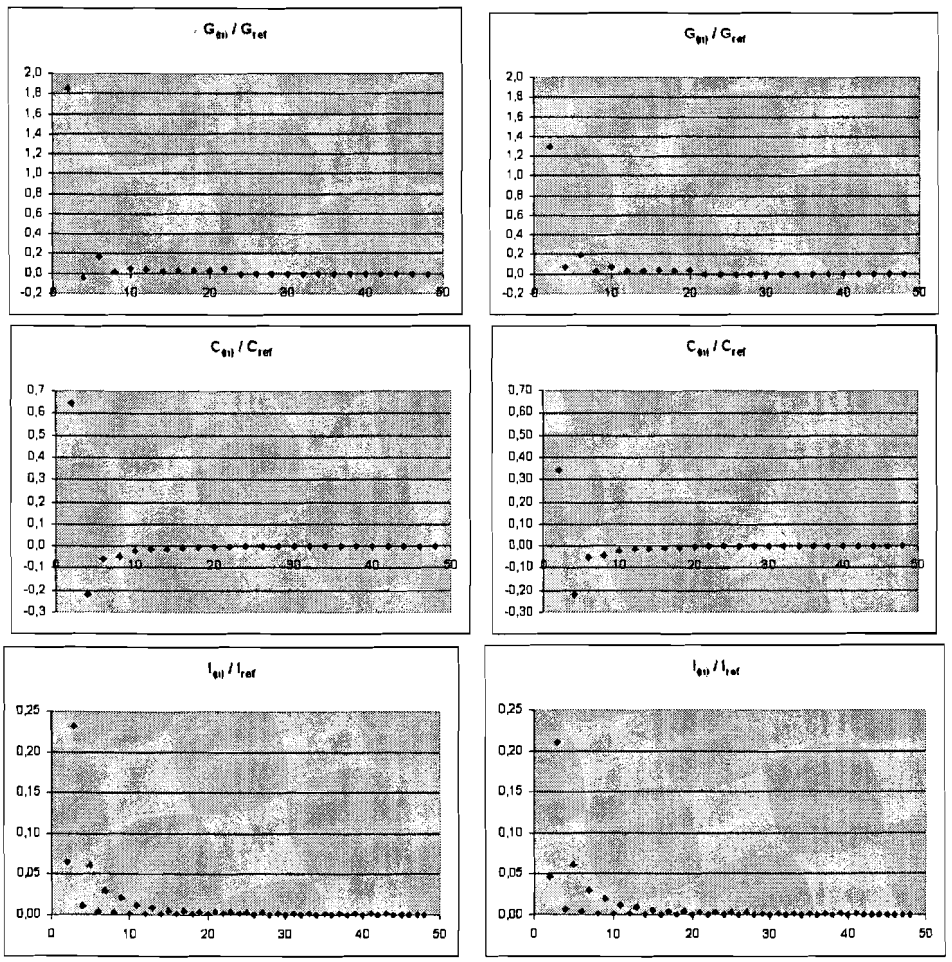

Figure 4.27: Load measurements Micro-wave. (a) With net impedance and (b) without net impedance

4.4.2.5 Video recorder

The video recorder was studied at normal playback. The results for the measurement with net impedance are displayed in Figure 4.28(a). The net impedance was equal to 0.309 + j0.155 Ω for the phases and 0.160 + j0.106 Ω for the neutral conductor. The results for the measurement without net impedance are displayed in Figure 4.28(b). The AC-power P_{ref} is equal to 12W.

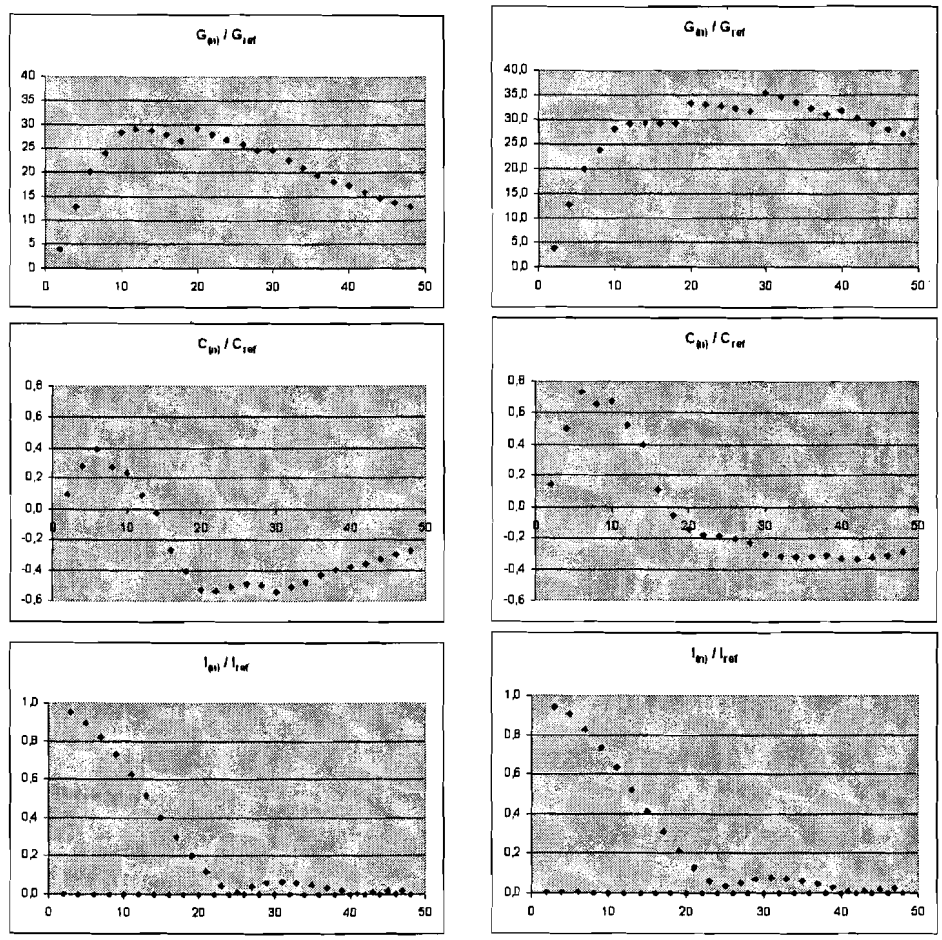

Figure 4.28: Load measurements Video recorder. (a) With net impedance and (b) without net impedance

4.4.2.6 TL lighting

The TL lighting was studied at the on position. The results for the measurement with net impedance are displayed in Figure 4.29(a). The net impedance was equal to 0.309 + j0.155 Ω for the phases and 0.160 + j0.106 Ω for the neutral conductor. The results for the measurement without net impedance are displayed in Figure 4.29(b). The AC-power P_{ref} is equal to 58W.

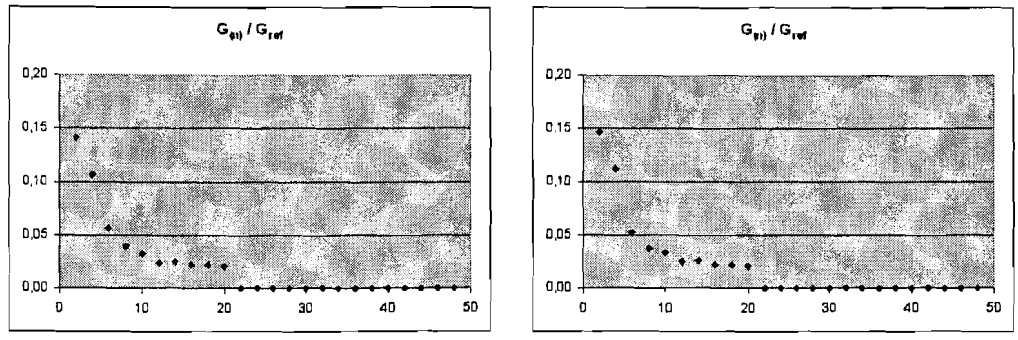

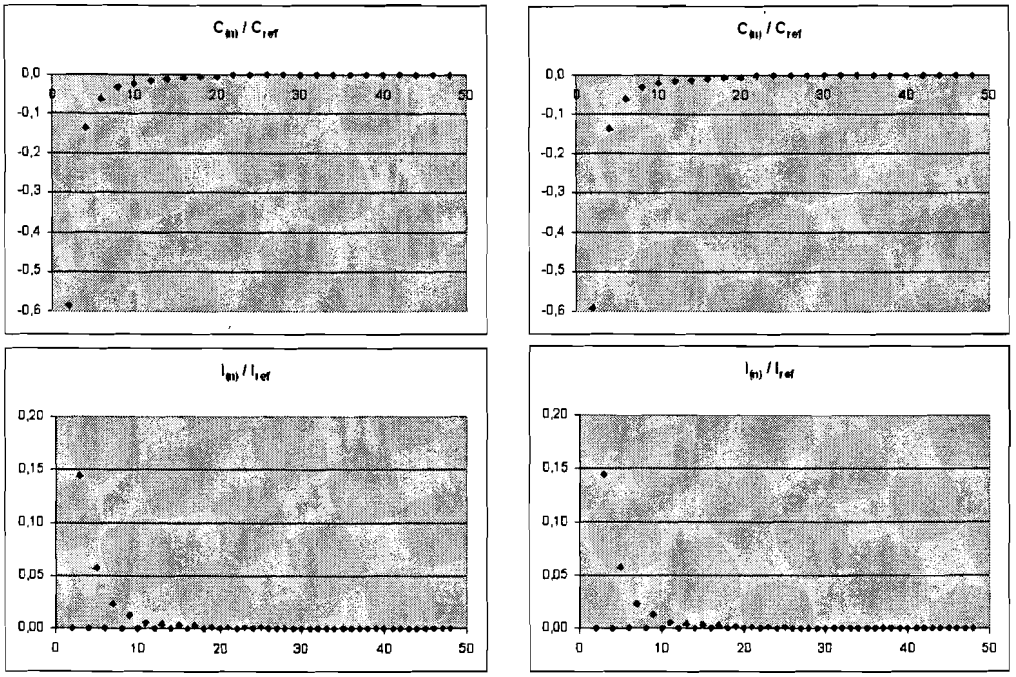

Figure 4.29: Load measurements TL lighting. (a) With net impedance and (b) without net impedance

4.4.2.7 Power factor controller

The results for the measurement with net impedance are displayed in Figure 4.30(a). The net impedance was equal to 0.309 + j0.155 Ω for the phases and 0.160 + j0.106 Ω for the neutral conductor. The results for the measurement without net impedance are displayed in Figure 4.30(b). The AC-power P_{ref} is equal to 80W.

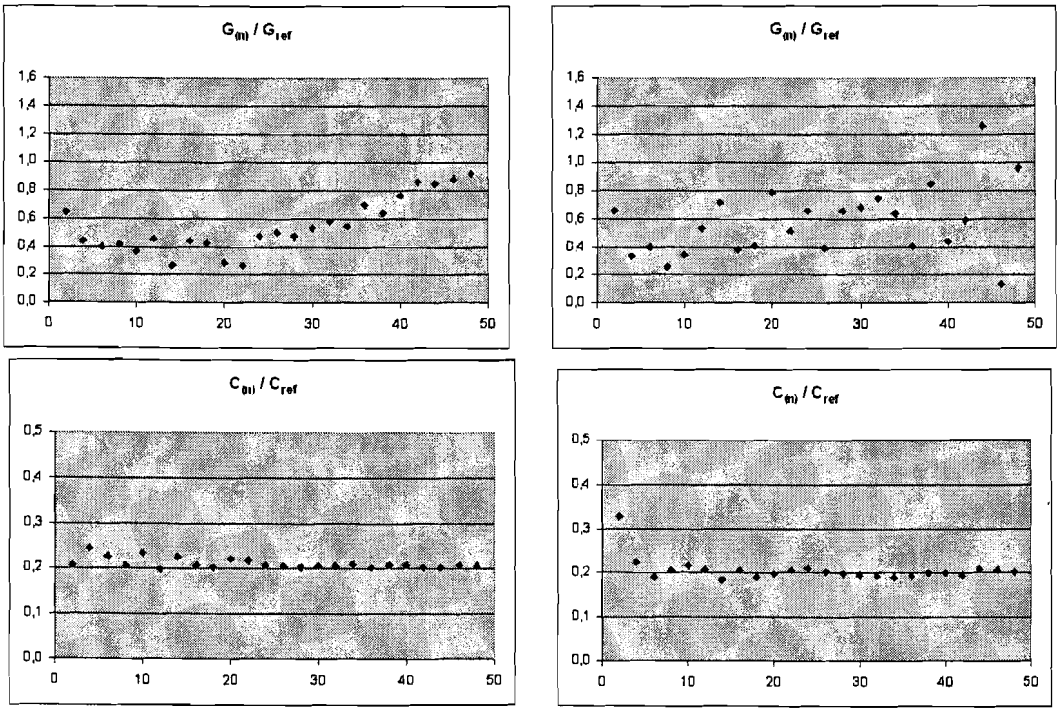

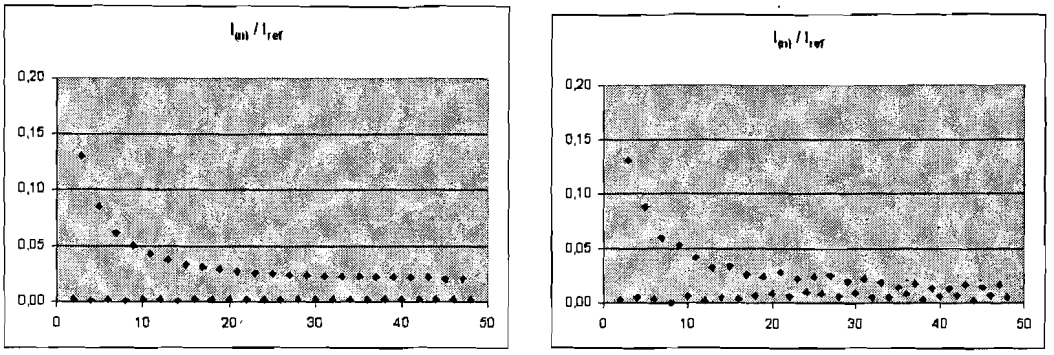

Figure 4.30: Load measurements Power factor controller. (a) With net impedance and (b) without net impedance

4.4.3 Measurement results for multiple loads

For the extended model of chapter 4.2 to work it is necessary that the loads can be sufficiently characterized by the G, C and I_{inv} so that the network theory can be applied to them. To make a start with the validation of this three element model, measurements have been carried out on combinations of the loads in chapter 4.4.2. These loads were connected as displayed in Figure 4.31. If the three elements G, C and I_{inv} are to be treated as network components, the summation of the individual loads at the connection point to the grid must lead to the same result as the measurement done on the combination of them.

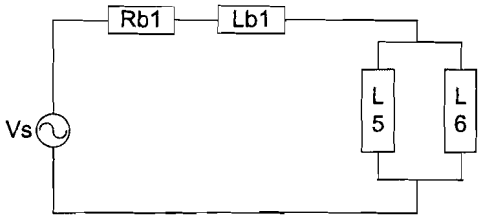

Figure 4.31: Measurement setup for two loads

4.4.3.1 Television and Dimmer with an incandescent lamp

The results for the measurement with net impedance are displayed in Figure 4.32(a) along with the summation of the individual loads. For the measurement the net impedance was equal to 0.309 + j0.155 Ω for the phases and 0.160 + j0.106 Ω for the neutral conductor. The results for the measurement without net impedance are displayed in Figure 4.32(b) along with the summation of the individual loads. The AC-power P_{ref} is equal to 139W for the combination.

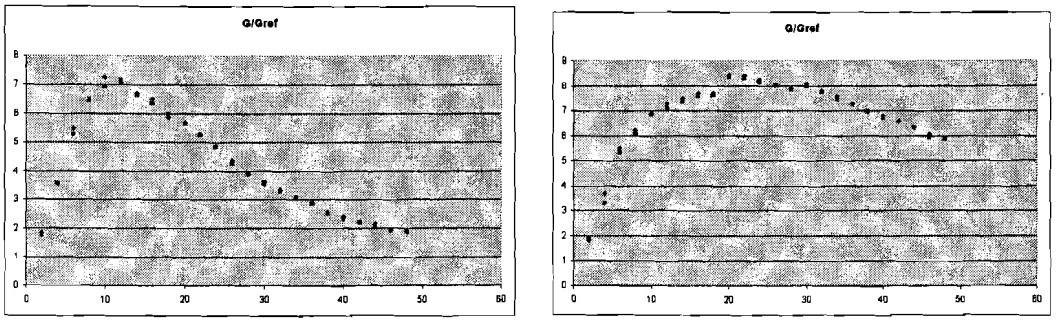

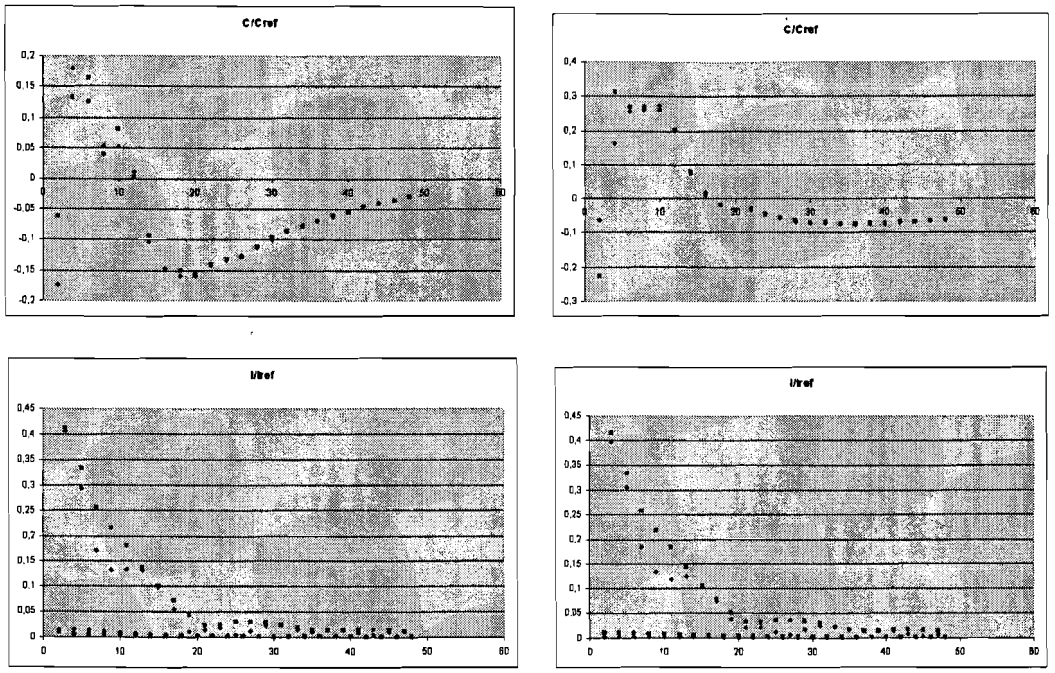

Figure 4.32: Load measurements Television and Dimmer with incandescent lamp in blue. Summation of individual elements in purple. (a) With net impedance and (b) without net impedance.

4.4.3.2 Power factor controller and TL-light

The results for the measurement with net impedance are displayed in (a) along with the summation of the individual loads. For the measurement the net impedance was equal to 0.309 + j0.155 Ω for the phases and 0.160 + j0.106 Ω for the neutral conductor. The results for the measurement without net impedance are displayed in (b) along with the summation of the individual loads. The AC-power P_{ref} is equal to 138W for the combination.

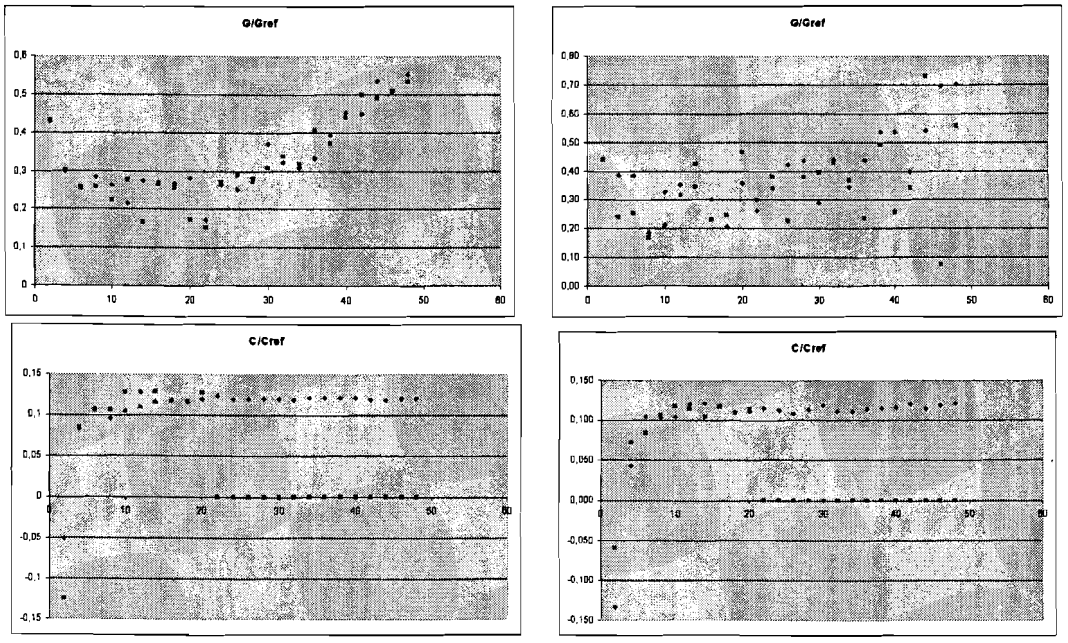

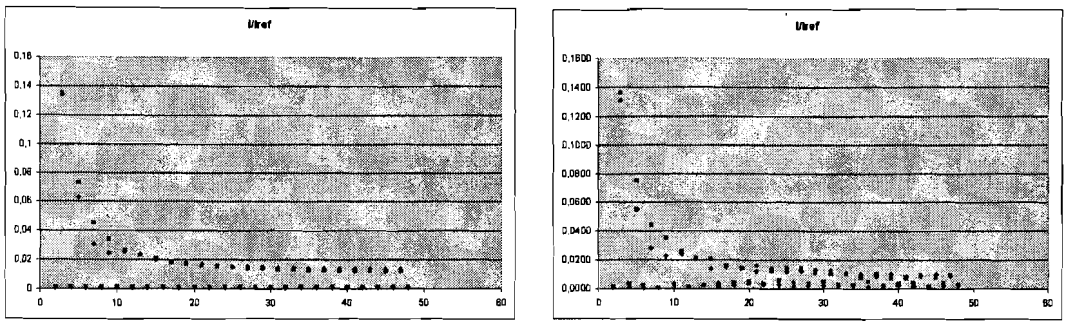

Figure 4.33: Load measurements Power factor controller and TL-light in blue. Summation of individual elements in purple. (a) With net impedance and (b) without net impedance.

4.4.4 Observations

The first thing noticed is that there are differences between the single load measurements with net impedance and without net impedance for the G/Gref and C/Cref measurements. This is most obvious with the personal computer and the television. In these cases the whole "form" of the line changes. This implies the possibility that the load parameters are dependent on grid topologies. As expected the injected harmonic currents of the load under perfect sinusoidal excitation does not differ for the measurements with and without grid impedance.

In the measurements for the dimmer with an incandescent lamp on 88W, both with and without impedance, there are two trends recognizable in the G/Gref graphs. As the points in these graphs are all measured on even harmonics at which the dimmer itself has an emission of less than two percent, these two trends are not due to measurement procedure faults. Next to the dimmer with incandescent lamp the power factor controller also exhibits this behaviour for G/Gref, with the two trends more recognizable in the measurement without net impedance. As there are only two measurements which exhibit this behaviour, it is difficult to draw conclusions from them. Therefore it is recommended to examine this phenomenon more detailed in the future.

Another observation is that G/Gref is positive in every measurement, except for the micro-wave measurement with net impedance where it is negative for the 4^{th} harmonic. As this is the only negative value it can therefore be concluded that the main trend of the element G in the model is that it is positive and thus has the properties of a conductance. This is not observed for the C/Cref measurements. These measurements exhibit both positive and negative values, even in one plot. As a negative capacitance equals an inductance it can be said that element C in the model has different properties ranging from a capacitance to an inductance dependent on which kind of harmonic disturbance there is present in the grid.

For the TL lighting measurement the values above the 22^{nd} harmonic for the C/Cref measurements can be ignored, as something has gone wrong with the measurement at that point.

The last observations made are the differences between the measurements on multiple loads and the theoretical summation of these individual loads. As can be seen in Figure 4.32 and Figure 4.33 these differences can be as large as a factor 1.5. To get more information on the limits between which these summations can be accepted, further experiments have to be done. For these experiments different load and network topologies can be considered to get a total view on the subject.

4.5 Modeling the distribution transformer

As discussed in chapter 3 a distribution transformer can be a source of harmonic disturbance. The harmonics produced can be related to the saturation curve and inrush current of the transformer. Under normal operation conditions however, there is no inrush current and the transformer is operating on a point in the saturation curve so that the harmonics produces by it can be ignored. As a first approach to the problem the transformer can therefore be modeled as a passive element and thus represented by an impedance. This impedance can be deducted from the basic transformer model which is displayed in Figure 4.34. Z(ω) represents the frequency-dependent short-circuit impedance.

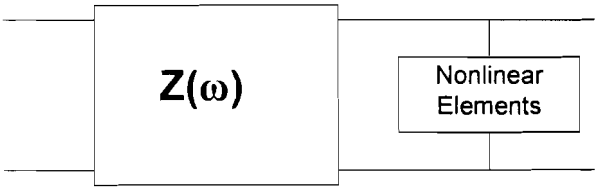

Figure 4.34: Basic transformer equivalent circuit

If needed the non-linear elements can be deducted from measured rms values of voltages and currents and no-load losses. This can be done with help of the conversion technique explained in [5]. At full load it is known that the representation of the nonlinear elements is less important then the representation of the short-circuit impedance and the load. The harmonics produces by the nonlinear elements are small in amplitude compared to the rest. In most applications the nonlinear elements can therefore be ignored.

4.5.1 Single-phase transformer

An ideal single-phase transformer is depicted in Figure 4.35a.

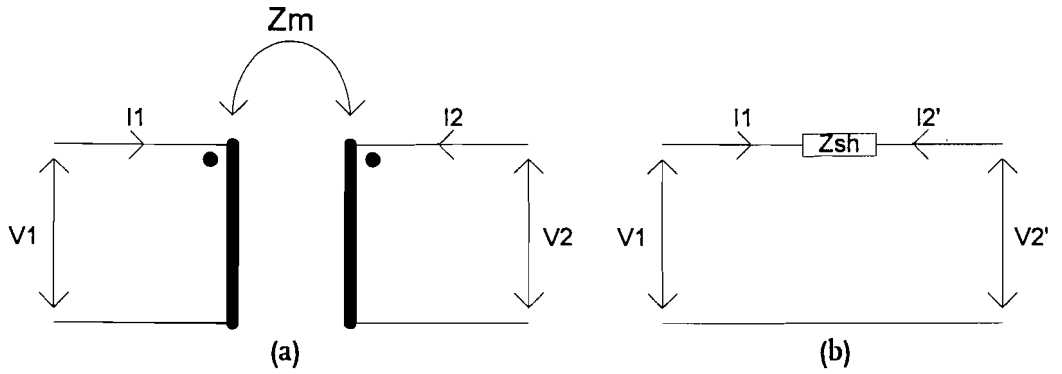

Figure 4.35: (a) Ideal single-phase transformer (b) Equivalent circuit referred to primary

According to [6] this network can be theoretically described by the self and mutual impedances or admittances:

$$\begin{bmatrix} V_1 \\ V_2' \end{bmatrix} = \begin{bmatrix} Z_{11} & Z_{12} \\ Z_{21} & Z_{22} \end{bmatrix} \begin{bmatrix} I_1 \\ I_2' \end{bmatrix} \rightarrow [V]=[Z][I] \quad \text{or} \quad \begin{bmatrix} I_1 \\ I_2' \end{bmatrix} = \begin{bmatrix} Y_{11} & Y_{12} \\ Y_{21} & Y_{22} \end{bmatrix} \begin{bmatrix} V_1 \\ V_2' \end{bmatrix} = [I]=[Y][V] \quad (4.54)$$

with $Z_{12}=Z_{21}=Z_m$ or $Y_{12}=Y_{21}=Y_m=1/Z_m$ and $[Y]=[Z]^{-1}$ and $Z_{11}\approx Z_{22}$. V_2' and I_2' are the secondary voltage and current referred to the primary side, respectively.
Z_m can then be found from an open circuit excitation:

$$Z_m = \left.\frac{V_2'}{I_1}\right|_{I_2'=0} \quad \text{or} \quad Z_m = \left.\frac{V_1}{I_2'}\right|_{I_1=0} \tag{4.55}$$

In practice the magnetic coupling of a transformer is so high that can be stated that Z_m is approximately equal to Z_{11} and thus Z_{22}. The [Z] matrix is then almost singular, which causes problems with its inversion. The short circuit impedances, which are more important then the magnetizing impedances in most cases, get lost. One way to overcome this problem is to directly deduct the [Y] matrix values. These can be found from standard short-circuit tests.
For a single pair of magnetically coupled coils only one short circuit impedance Z_{sh} exists, as shown in Figure 4.35b. From this Y_{sh} can be found with:

$$Y_{sh} = \frac{1}{Z_{sh}} \tag{4.56}$$

To construct Y_{sh} the four elements Y_{11}, Y_{12}, Y_{21} and Y_{22} are needed. These can be obtained directly from Figure 4.35b. The matrix is then found from one short circuit admittance:

$$\begin{bmatrix} I_1 \\ I_2' \end{bmatrix} = \begin{bmatrix} Y_{sh} & -Y_{sh} \\ -Y_{sh} & Y_{sh} \end{bmatrix} \begin{bmatrix} V_1 \\ V_2' \end{bmatrix} \tag{4.57}$$

Z_{sh} is frequency dependent and can be reproduced reasonably well by the circuit depicted in Figure 4.36 as recommended by [7].

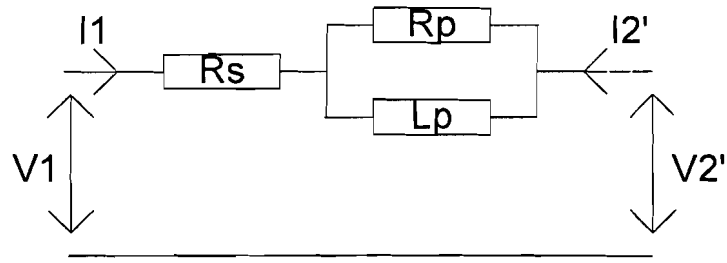

Figure 4.36: Frequency dependent short circuit impedance model of a single phase transformer

R_s is the resistance of the windings at 50Hz. L_p is the leakage inductance of the windings at 50Hz. R_p accounts for the frequency dependent effects. The whole is located in series between two point of the networks connected to the primary and secondary terminals of the transformer considered.

$$L_p = \frac{X_{leakage50Hz}}{2\pi 50} \tag{4.58}$$

Resistances R_s and R_p are constant whatever the frequency, and an estimate can be obtained by the expressions:

$$90 < \frac{U_n^2}{S_N R_s} < 110$$
$$13 < \frac{S_N R_p}{U_N^2} < 30 \qquad (4.59)$$

in which U_N is the rated voltage and S_N the rated power of the transformer.
In this model of Figure 4.36 the stray capacitances of the transformer are neglected. This can only be done if the resonating frequency of the transformer lies far away from the frequency range of interest. For harmonic studies this frequency range of interest is between 50Hz and about 2500Hz. If the transformer resonates in this frequency range, shunt capacitances need to be added in the transformer model of Figure 4.36. These shunt capacitances can be determined by resonance measurements, or taken as typical values from publications or textbooks [8].

4.5.2 Three-phase transformer

Three-phase transformers are best represented in matrix form. It is simple to extend the single-phase transformer formulation to three-phase two winding transformers. Equation (4.56) then becomes:

$$[Y_{sh}] = [Z_{sh}]^{-1} \qquad (4.60)$$

For a short circuit test performed on a two winding transformer, the voltages and currents in each phase of the feeding terminal are related according to:

$$[V_{ABC}] = [Z_{SH}][I_{ABC}] \leftrightarrow \begin{bmatrix} V_A \\ V_B \\ V_C \end{bmatrix} = \begin{bmatrix} Z_{AA} & Z_{AB} & Z_{AC} \\ Z_{BA} & Z_{BB} & Z_{BC} \\ Z_{CA} & Z_{CB} & Z_{CC} \end{bmatrix} \qquad (4.61)$$

To obtain the elements of $[Z_{sh}]$, short-circuit tests are done according to Figure 4.37.

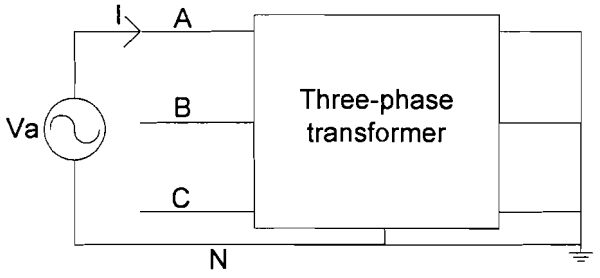

Figure 4.37: Three-phase transformer short-circuit test

Voltages V_a, V_b, V_c and current I per phase are recorded in a measurement with an injection of a sine waveform current. Self and mutual impedance at for phase A are calculated as follows:

$$Z_{AA} = \left.\frac{V_{AN}}{I_A}\right|_{I_B=I_C=0}$$
$$Z_{BA} = \left.\frac{V_{BN}}{I_A}\right|_{I_B=I_C=0} \qquad (4.62)$$
$$Z_{CA} = \left.\frac{V_{CN}}{I_A}\right|_{I_B=I_C=0}$$

The same procedure applies to the other two columns. Due to symmetry reasons only six measurements are required to construct $[Z_{sh}]$. In practice however, $[Z_{sh}]$ is assumed to be balanced ($Z_{AB} = Z_{AC} = Z_{BC}$ and $Z_{AA} = Z_{BB} = Z_{CC}$), which reduces the number of measurements to two.
Frequency dependent effects in the short-circuit impedance are treated the same way as for a single-phase transformer. Here the elements of Figure 4.36 are all matrices.

5 Conclusions and recommendations

The mathematical tool for solving harmonic problems is the theory of Fourier. With this theory an easy transfer can be made from the time domain to the frequency domain, simplifying the analysis of complex harmonic signals.

The main causes of harmonics in the net are non-linear loads. From this collection of non-linear loads the inverters and lighting ballasts are the main sources of harmonic distortion in the net. Other, less significant, causes of harmonic distortion are power transformers and electrical machines. It must be taken in mind that approximately more than 90% of the harmonic distortions in the grid are caused by inverters and the huge numbers of lighting ballasts. Electrical machines and transformers only contribute a small percentage to the total harmonic distortions.

Converters produce harmonics due to the fact that they only draw power from the net for a defined period of time. During the rest of the period the power is sent back into the grid. Power transformers only cause significant harmonic distortion if they are operated near their saturation point or when they are first connected to the grid (inrush current). As this is not the case in a normal grid environment, the harmonic distortion produces by the transformers can be ignored. Electrical machines cause distortion due to non-sinusoidal flux in the air gap, which can be related back to their build.
Most harmonics produced by the above equipment are of the uneven kind and tend to decrease for the higher harmonics.

The resistance part of the harmonic model for the cable corresponds well with the measured values. The inductance part of the model is not jet complete. The inductances due to proximity effects and losses in the sheath still have to be incorporated in the theory. This can be done with the given analytical method.
With the currently used method of measurement and modelling it is possible to expand the model in a simple way to incorporate the capacitance of the cable in it if this is necessary in the future.

A basic theoretical harmonic model for a single-phase and three-phase transformer is given, which can be deducted from 50Hz manufacturer's data. If needed this basic model can be extended to incorporate the non-linear elements of a transformer. The model can also incorporate the resonating of a transformer by adding shunt capacitors to the model. This only has to be done if the transformer resonates in the harmonic frequency range of interest. Also a measurement method is given to validate the given model. It is recommended to carry out these measurements for further validation.

For the load model there are differences between single load measurements with net impedance and without net impedance for the G/Gref and C/Cref measurements. This implies the possibility that the load parameters are dependent on grid topologies.
The main trend of the element G in the model is that it is positive and thus has the properties of a conductance. Element C in the model has different properties ranging from a capacitance to an inductance dependent on which kind of harmonic disturbance there is present in the grid.
There are differences between the measurements on multiple loads and the theoretical summation of these individual loads.
To get more information on the limits between which the model of the load is valid, further experiments have to be done. For these experiments different load and network topologies have to be considered as well as the basic fundamental correctness of the load model.

6 References

[1] CEI/IEC international standard 287-1-1:
Electric cables – Calculation of the current rating –Part 1: Current rating equations (100% load factor) and calculation of losses.
Geneve: CEI/IEC international standard 287-1-1, 1982 (Corrected ed. 1994).

[2] Anders, G.J.
Rating of electric power cables.
New York: IEEE Press, 1997.

[3] IEC publication 228
Conductors of insulated cables.
Geneve: IEC publication 228, 1978.

[4] Du, Y. and J.Burnett
Experimental investigation into harmonic impedance of low-voltage cables.
IEE Proceedings on Generation, Transmission and Distribution, Vol. 147, Issue 6, Nov. 2000, p. 322-328.

[5] Neves, W.L.A. and H.W. Dommel.
On modeling iron core nonlinearities
IEEE Transactions on Power Systems, vol. PWRS-8, pp.417-425, May 1993.

[6] Neves, W.L.A., H.W. Dommel and W. Xu.
Practical Distribution Transformer Models for Harmonic Studies.
IEEE transactions on Power Delivery, vol. 10, no. 2, April 1995.

[7] CIGRE Working group 36.05
Harmonic characteristic parameters, methods of study, estimates of existing values in the network.
Electra No. 77, pp.35-54.

[8] Greenwood, A.
Electrical Transients in Power Systems.
New York: John Wiley & Sons Inc., 1991.

[9] Kaden, H.
Wirbelströme und Schirming in der Nachrichtentechnik
Berlin: Springer-Verlag, 1959.

[10] Moore, G.F.
Electric Cables Handbook.
Bodmin,Cornwall: MPG Books Ltd., 1997.

[11] Anderson, P.M.
Analysis of Faulted Power Systems.
New York: IEEE Press, 1995.

[12] Arillaga, J. and D.A. Bradley, P.S. Bodger
Power system harmonics.
New York: John Wiley & Sons, 1985.

[13] Ramo, S., J.R. Whinnery and T. van Duzer.
Fields and waves in communication electronics.
New York: John Wiley & Sons, 1994.

[14] Cavallini, A. and M. Loggini, G.C. Montanari
Comparison of approximate methods for estimate harmonic currents injected by AC/DC converters.
IEEE Transactions on Industrial Electronics, Vol. 41, Issue 2, 1994, p. 256-264.

[15] Yacamini, R.
Power system harmonics Part 1 Harmonic Sources.
IEEE Power Engineering Journal, Vol. 8, Issue 4, 1994, p. 193-198.

[16] Yacamini, R.
Power system harmonics Part 2 Measurements and calculations.
IEEE Power Engineering Journal, Vol. 9, Issue 1, 1995, p. 51-56.

[17] Yacamini, R.
Power system harmonics Part 3 Problems caused by distorted supplies.
IEEE Power Engineering Journal, Vol. 9, Issue 5, 1995, p. 233-238.

Appendix A: Cable information from Pirelli

PIRELLI

Productinformatie
14/05/2004

Kabeltype	:	**YMeKrvaslqwd 6/10 kV - 3x240 Alrm as70**
Artikelnummer	:	147.6932.60
Voldoet aan	:	NEN 3620 (2003)

Kabelopbouw		
Geleider	:	aluminium, rond massief
Geleiderscherm	:	zwakgeleidend kunststof
Isolatie	:	XLPE
Isolatiescherm	:	zwakgeleidend kunststof
Bedding	:	zwakgeleidend zwelband
Kabelslaan		
Vulling	:	kern en hoeken gevuld
Bedding	:	zwakgeleidend zwelband
Aardscherm	:	ronde koperdraden met tegenspiraal van koperband
Bandage	:	zwakgeleidend zwelband
Buitenmantel	:	rood PE - ST7 (rood PE is niet blijvend UV-bestendig en mag daarom niet langdurig aan zonlicht worden blootgesteld)

Hoofdafmetingen en gewicht		**Nominale dikte**		**Praktijkdiameter**	
Geleider	:			17.1	mm
Isolatie	:	3.4	mm	25.2	mm
Buitenmantel	:	3.2	mm	69	mm
Gewicht per meter	: 4.9 kg			(omschreven cirkel, de kabel heeft een driehoekige vorm, daardoor kan de stempeling plaatselijk onderbroken zijn)	

Mantelstempeling		
PIRELLI NL - jaar	YMeKrvaslqwd 6/10 kV - 3x240 Alrm as70	meterstempeling

Verpakking (voorbeelden)			
Haspeltype	:	P24	hout
Flensdiameter	:	2400	mm
Kerndiameter	:	1400	mm
Bruto breedte	:	1370	mm
lengte	:	500	m
Totaal gewicht ca.	:	3.0	ton

Leginstructies			
Maximale trekkracht aan de kabel met een trekkous	:	14.3	kN
Minimale buigstraal tijdens leggen	:	1.03	m
Minimale buigstraal na installatie	:	0.86	m
Minimum kabellegtemperatuur	:	-10	°C

Electrische gegevens					
Toegekende spanningen U_0/U (U_m)			: 6/10 (12) kV		
Geleider	Gelijkstroomweerstand bij 20 °C, maximaal	:	0.125	Ω/km
	Wisselstroomweerstand bij 90 °C	:	0.161	Ω/km
Toelaatbare kortsluitstroom gedurende 1 sec (adiabatisch 90-250 °C)		:	22.8	kA
Isolatie	Capaciteit	:	0.42	µF/km
	Laadstroom per fase bij U_0 bij 50 Hz	:	0.78	A/km
Aardscherm				
Toelaatbare kortsluitstroom gedurende 1 sec (adiabatisch 80-250 °C)		:	10.4	kA
Kabel				
Continu toelaatbare stroom belasting				
berekend aan de hand van NPR 3626				
1 circuit				
In grond, 1m diep, Tg = 15°C, 0,75 Knm/W		:	350	A
In lucht, Tl = 30°C, géén directe zonnestraling		:	430	A
Bedrijfsreactantie bij 50 Hz		:	0.088	Ω/km

Wijzigingen voorbehouden — *Kabelontwerp*

PIRELLI

Productinformatie

15-04-2003

Kabeltype	:	**VMvK 0,6/1 kV - 4x150 Alsvm**
Artikelnummer	:	141.2681.60
Voldoet aan	:	NEN 3616 (2001)

Kabelopbouw

		Hoofdaders
Geleider	:	aluminium sectorvormig massief
Isolatie *)	:	PVC
Kabelslaan		
Vulmantel	:	rubber
Buitenmantel	:	grijs PVC

*) kleuren volgens NEN 3616: rood - geel - blauw - geel/blauw

Hoofdafmetingen en gewicht		Nominale dikte			Praktijkdiameter	
Geleider	:			(hoogte)	12.6	mm
Isolatie	:	1.8	mm	(hoogte)	16.4	mm
Geslagen aders					36	mm
Vulmantel	:	3.0	mm			
Buitenmantel	:	3.0	mm		49	mm
Gewicht per meter	3.6 kg					

Mantelstempeling

PIRELLI NL - VMvK 0,6/1 kV - 4x150 Alsvm NEN 3616 datum/tijd meterstempeling

Verpakking		standaard	
Haspeltype	:	P18	hout
Flensdiameter	:	1800	mm
Kerndiameter	:	1100	mm
Bruto breedte	:	1080	mm
lengte	:	500	m
Totaal gewicht ca.	:	2100	kg

Leginstructies			
Maximale trekkracht aan de kabel met een trekkous	:	7.2	kN
Minimale buigstraal tijdens leggen	:	0.59	m
Minimale buigstraal na installatie	:	0.49	m

Electrische gegevens

Hoofdader

Geleider	Gelijkstroomweerstand bij 20 °C, maximaal		0.206	Ω/km
	Wisselstroomweerstand bij 90 °C		0.235	Ω/km

Kabel

Continu toelaatbare stroom belasting (gebaseerd op NPR 3107)				
	In grond, 1m diep, Tg = 15°C, 0,50 Km/W		285	A
	In lucht, Tl = 20°C, géén directe zonnestraling	"korte" lengte	285	A
		"lange" lengte	220	A
Bedrijfsreactantie bij 50 Hz			0.079	Ω/km

wijzigingen voorbehouden *Kabelontwerp*

Appendix B: Skin effect

Skin effect in a solid round conductor

When a cable is carrying alternating currents, the distribution of the current is not evenly disposed throughout the cross-section of the conductor. If the conductor is considered to be composed of a large number of concentric circular elements, those at the centre of the conductor will be enveloped by a greater magnetic flux then those on the outside. Consequently, the self-induced back e.m.f. will be greater towards the centre of the conductor, thus causing the current density to be less at the centre then at the conductor surface. This extra concentration of the current at the surface is called the skin effect and it results in an increase in the effective resistance and inductance of the conductor. Figure B.1 shows a schematical representation of this effect. The magnitude of the skin effect is influenced by the frequency, the size of the conductor, the amount of current flowing and the diameter of the conductor.

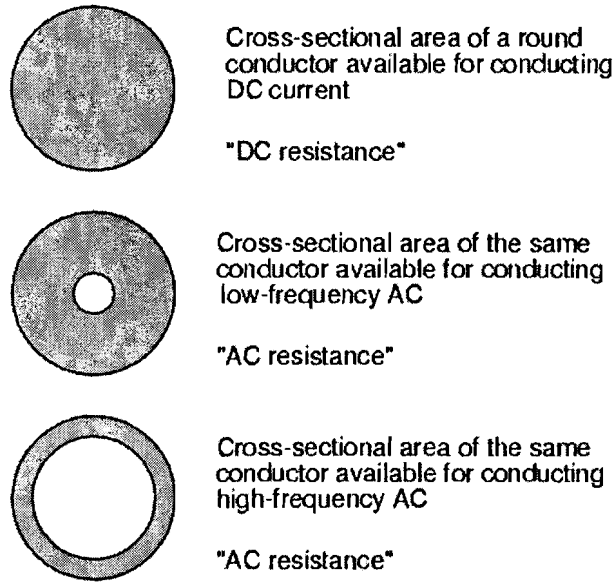

Figure B.1: Skin effect in a cable

For a mathematical study of this skin effect in a round solid conductor, the non-uniform current distribution in the conductor must be found. A conductor is displayed in Figure B.2.

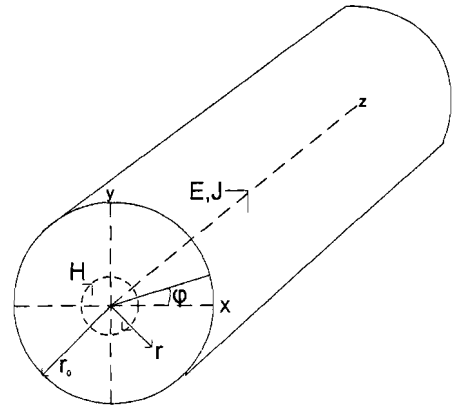

Figure B.2: A good conductor

A good conductor is defined as one for which displacement current is negligible in comparison with conduction current, so that:

$$\nabla \times H = J = \sigma E \tag{0.1}$$

Faraday's law equation in phasor form is:

$$\nabla \times E = -j\omega\mu H \tag{0.2}$$

From equation (0.1) and (0.2) the equation for current density can be derived:

$$\nabla^2 J = j\omega\mu\sigma J \tag{0.3}$$

If the current then is taken in the z direction and no variations with z or angle φ, equation (0.3), expressed in circular coordinates, becomes:

$$\frac{d^2 J_z}{dr^2} + \frac{1}{r}\frac{dJ_z}{dr} + T^2 J_z = 0 \tag{0.4}$$

with

$$T^2 = -j\omega\mu\sigma \qquad or \qquad T = -j^{-1/2}\sqrt{\omega\mu\sigma} = j^{-1/2}\frac{\sqrt{2}}{\delta} \tag{0.5}$$

where δ is the useful parameter called "depth of penetration" or "skin depth". The differential equation (0.4) is a Bessel equation. This means the two independent solutions are:

$$J_z = AJ_0(Tr) + BH_0^{(1)}(Tr) \tag{0.6}$$

For a solid wire r=0 is included in the solution. This makes it necessary for B = 0, since a study of $H_0^{(1)}$ shows that it is infinite at r = 0. Therefore:

$$J_z = AJ_0(Tr) \tag{0.7}$$

The arbitrary constant A may be evaluated in terms of current density at the surface, which is σE_0, with E_0 the surface electric field.

$$J_z = \sigma E_0 \quad \text{at} \quad r_0 \tag{0.8}$$

Then equation (0.7) becomes:

$$J_z = \frac{\sigma E_0}{J_0(Tr_0)} J_0(Tr) \tag{0.9}$$

Now the current distribution is known, the internal impedance (resistance and contribution to reactance from the magnetic flux inside the wire) of a round wire can be found from the total current in the wire and the electrical intensity at the surface.

The total current can be obtained from the magnetic field at the surface, since the line integral of the magnetic field around the outside of the wire must be equal to the total current in the wire:

$$\oint H \cdot dl = I \tag{0.10}$$

or

$$2\pi r_0 \, H_\varphi\Big|_{r=r_0} = I \tag{0.11}$$

Magnetic field is obtained from the electric field by Maxwell's equation:

$$\nabla \times E = -j\omega\mu H \tag{0.12}$$

For a round wire with no variations in z or ϕ, the fields E_z and H_ϕ alone are present, and only r derivatives remain, so equation (0.12) becomes:

$$H_\phi = \frac{1}{j\omega\mu}\frac{dE_z}{dr} \tag{0.13}$$

Electric field is related to the current density via σ. Also, an expression for current density has been obtained in equation (0.9). This makes it possible to write equation (0.13) as:

$$E_z = \frac{J_z}{\sigma} = E_0 \frac{J_0'(Tr)}{J_0(Tr_0)} \tag{0.14}$$

Now equation (0.14) can be substituted in equation (0.13), and with (0.5) it results in:

$$H_\phi = \frac{E_0 T}{j\omega\mu}\frac{J_0'(Tr)}{J_0(Tr_0)} = -\frac{\sigma E_0}{T}\frac{J_0'(Tr)}{J_0(Tr_0)} \tag{0.15}$$

where J'_o denotes $[d/d(Tr)]J_o(Tr)$. From (0.11):

$$I = -\frac{2\pi r_0 \sigma E_0}{T}\frac{J_0'(Tr)}{J_0(Tr_0)} \tag{0.16}$$

The internal impedance is defined as $Z_i = E_z(r_o)/I$. This results in:

$$Z_i = -\frac{TJ_0(Tr_0)}{2\pi r_0 \sigma J_0'(Tr_0)} \tag{0.17}$$

To interpret (0.17) it is useful to break into real and imaginary parts using:

$$J_0(j^{-1/2}v) = Ber(v) + jBei(v) \tag{0.18}$$

and

$$Ber'(v) + jBei'(v) = \frac{d}{dv}(Ber(v) + Bei(v) = j^{-1/2} J_0'(j^{-1/2} v) \tag{0.19}$$

Then equation (0.17) can be written as:

$$Z_i = R + j\omega L_i = \frac{jR_s}{\sqrt{2}\pi r_0}\left[\frac{Ber(q) + jBei(q)}{Ber'(q) + jBei'(q)}\right] \tag{0.20}$$

with

$$R_s = \frac{1}{\sigma\delta} = \sqrt{\frac{\pi f \mu}{\sigma}} \qquad q = \frac{\sqrt{2} r_0}{\delta} \tag{0.21}$$

or

$$\begin{aligned} R_{skin} &= \frac{R_s}{\sqrt{2}\pi r_0}\left[\frac{Ber(q)Bei'(q) - Bei(q)Ber'(q)}{(Ber'(q))^2 + (Bei'(q))^2}\right] \quad \Omega/m \\ \omega L_i &= \frac{R_s}{\sqrt{2}\pi r_0}\left[\frac{Ber(q)Ber'(q) - Bei(q)Bei'(q)}{(Ber'(q))^2 + (Bei'(q))^2}\right] \quad \Omega/m \end{aligned} \tag{0.22}$$

These are the expressions for the resistance and internal reactance of a round wire at any frequency in terms of the parameter q, which is $\sqrt{2}$ times the ratio of the wire radius to depth of penetration.

Appendix C: Inductance due to proximity effects and losses in sheath

This part of the theory is still a work in progress. The analytical method to calculate the proximity losses is known, but the formulas have not been fully worked out for the cable-types due to time limits. The method and the formulas already known will be discussed. Further information will be given on where to find more work on this subject.

First the method used for determining the losses in the cable will be discussed. More information on this method can be found in [9].

Method used for determining losses:

1. Find the initial complex potential induced by the current in the phase.
2. Find the complex back-potential caused by the eddy currents in the sheath. These eddy currents are caused by the initial potential, which means the back-potential from the sheath can be derived from the initial potential.
3. Find the formulation for the electrical field in the sheath.
4. Find the expressions for the undefined variables found in step 1 to 3 from boundary conditions.
5. Calculate the losses caused by the voltage, which is induced in the plane between the phase with the current and the sheath, for the whole cable length. These losses can be calculated with the calculated potentials and electrical field in the sheath. From these losses the inductance due to eddy currents in the sheath can be determined.
6. Calculate the losses in the sheath due to the fact that it is a current carrier.
7. Calculate the losses due to proximity effects between the phases, with corrections for the back-potential from the sheath. From these losses the inductance due to proximity effects between the phases are known.
8. Add the losses in the sheath with the proximity effect losses between the phases, which are corrected with the back-potential from the sheath, to get the total losses due to proximity effects and losses in the sheath.

Now the method is known, an analytical overview will be given.
Consider the cable in Figure C.1.

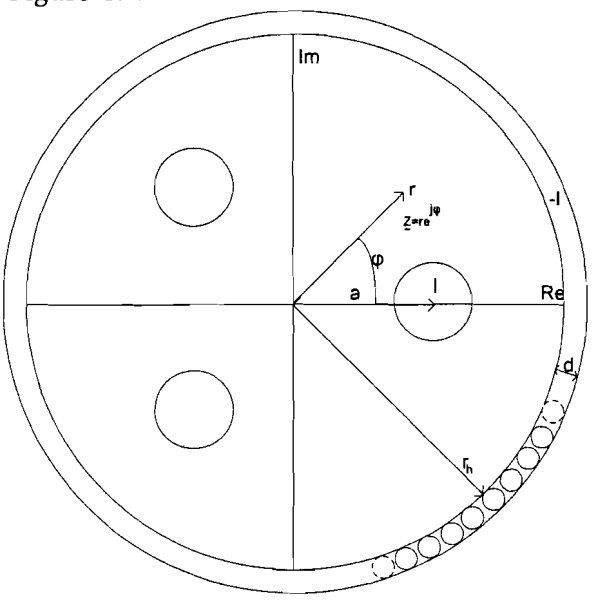

Figure C.1: A schematic of a three phase cable

According to [9] the initial complex potential from the phase with the current can be described as:

$$\underline{Z}_0 = \frac{-iI}{2\pi}\ln(\underline{z}-a) \tag{0.23}$$

With Taylor this can be rewritten in the form:

$$\underline{Z}_0 = \frac{-iI}{2\pi}\left[\ln(-a)+\sum_{m=1}^{\infty}\frac{(-1)^{m-1}}{m}\left(\frac{\underline{z}}{-a}\right)^m\right] \quad \text{for} \quad |\underline{z}|<a \tag{0.24}$$

This means the real initial potential function is equal to:

$$X_0 = \mathrm{Re}(\underline{Z}_0) = \frac{-I}{2\pi}\sum_{m=1}^{\infty}\frac{(-1)^{m-1}}{m}\left(\frac{r}{-a}\right)^m \sin(m\varphi) \tag{0.25}$$

The field described by this initial potential produces a back-potential due to eddy current in the sheath of the form:

$$X_w = \frac{-I}{2\pi}\sum_{m=1}^{\infty}\frac{(-1)^{m-1}}{m}\left(\frac{r_h^2}{-ar}\right)^m W_m \sin(m\varphi) \tag{0.26}$$

with W_m the back-potential factor.
The influence on the total potential of the back-potentials from the two phases without current are ignored for now, as these potentials are very small and only make the analytical calculation more complex.
The imaginary parts of the potentials calculated in equation (0.25) and (0.26) can be found by just replacing $\sin(m\varphi)$ with $-\cos(m\varphi)$. This can be verified by taking the imaginary part of equation (0.24). The complex potential is then equal to:

$$Y = Y_0 + Y_w = \frac{I}{2\pi}\sum_{m=1}^{\infty}\frac{(-1)^{m-1}}{m}\left[\left(\frac{r}{-a}\right)^m + \left(\frac{r_h^2}{-ar}\right)^m W_m\right]\cos(m\varphi) \tag{0.27}$$

Now the total potential in between the sheath and the phases is known, the magnetic fields in this space can be derived from them:

$$\begin{aligned} H_r &= \frac{\partial X}{\partial r} = \frac{I}{2\pi}\sum_{m=1}^{\infty}\frac{(-1)^{m-1}}{(-a)^m}\left[(r)^{m-1} + \frac{r_h^{2m}}{r^{m+1}}W_m\right]\sin(m\varphi) \\ H_r &= \frac{\partial X}{r\partial\varphi} = \frac{I}{2\pi}\sum_{m=1}^{\infty}\frac{(-1)^{m-1}}{(-a)^m}\left[(r)^{m-1} + \frac{r_h^{2m}}{r^{m+1}}W_m\right]\cos(m\varphi) \end{aligned} \tag{0.28}$$

Now the potential and thus the magnetic field in between the phases and the sheath are known, the electrical field in the sheath must be found. In the sheath the following equation must be fulfilled:

$$\Delta E = k_m{}^2 E \quad with \quad k_m = \frac{1+i}{\delta_m} \tag{0.29}$$

If the variables r and φ are separated the electrical field can be described as:

$$E = g(r)\cos(m\varphi) \tag{0.30}$$

If the thickness d of the sheath is presumed small in contrast to the radius r_h, then equation (0.29) in combination with (0.30) leads to:

$$E = E_0 + \sum_{m=1}^{\infty}\left[A_m e^{k_m r} + B_m e^{-k_m r}\right]\cos(m\varphi) \tag{0.31}$$

with E_o the field in the sheath due to fact that it is used as the return conductor. E_o is equal to:

$$E_0 = -IR_{a0}\frac{k_m d}{\sin(k_m d)}\cosh\left(k_m(r - r_h - d)\right) \tag{0.32}$$

with

$$R_{a0} = \frac{1}{2\pi r_h \sigma_h} \tag{0.33}$$

(E_o can be found from a similar analytical approach of a normal coaxial structure. For more information on the derivation of E_o see [9]).

From the electrical field in the sheath the magnetic field in the sheath can be found:

$$\begin{aligned} H_r &= -\frac{1}{i\omega\mu r}\frac{\partial E}{\partial \varphi} = \frac{1}{i\omega\mu r}\sum_{m=1}^{\infty} m\left[A_m e^{k_m r} + B_m e^{-k_m r}\right]\sin(m\varphi) \\ H_\varphi &= \frac{1}{i\omega\mu}\frac{\partial E}{\partial r} = \frac{1}{i\omega\mu}\sum_{m=1}^{\infty} k_m\left[A_m e^{k_m r} - B_m e^{-k_m r}\right]\cos(m\varphi) \end{aligned} \tag{0.34}$$

From the boundary conditions for the magnetic field the missing coefficients A_m, B_m, and W_m can be found. This results in the following equations for the electrical field at the inner boundary of the sheath:

$$(E_w)_{r=r_h} = -\frac{I}{2\pi} i\omega\mu \sum_{m=1}^{\infty}\frac{1}{m}\left[1 - W_m\right]\left(\frac{a}{r_h}\right)^m \cos(m\varphi) \tag{0.35}$$

with

$$W_m = U_m + iV_m = \frac{\frac{1}{2}\left(K_m - \frac{1}{K_m}\right)\sinh(k_m d)}{\cosh(k_m d) + \frac{1}{2}\left(K_m + \frac{1}{K_m}\right)\sinh(k_m d)} \quad \text{and} \quad K_m = \frac{\mu_0}{\mu}\frac{k_m r_h}{m} \tag{0.36}$$

The inductance caused by the voltage, which is induced in the plane between the phase with the current and the sheath, for the whole cable length can now be calculated. This inductance can be calculated with the calculated potentials and electrical field in the sheath with the following equation:

$$\omega\left(L_{ext}+L_{sheath1}\right)=\mathrm{Im}(-i\omega\mu_0\left[\left(Y\right)_{r=r_h}-\left(Y\right)_{r=a+r_i}\right]_{\varphi=0}-\left(E_w\right)_{r=r_h,\varphi=0} \tag{0.37}$$

From this L_h can be extracted:

$$L_{sheath1}=-\frac{\mu_0}{2\pi}\sum_{m=1}^{\infty}\frac{1}{m}\left(\frac{a}{r_h}\right)^{2m}U_m \tag{0.38}$$

Next to these eddy current losses in the sheath, the sheath has also losses due to the fact that it carries a current. These losses can be deducted from E_o and are equal to:

$$L_{sheath2}=\frac{\mu_0}{2\pi}\frac{d}{r_h}\frac{\delta_m}{2d}\frac{\sinh\left(\frac{2d}{\delta_m}\right)-\sin\left(\frac{2d}{\delta_m}\right)}{\cosh\left(\frac{2d}{\delta_m}\right)-\cos\left(\frac{2d}{\delta_m}\right)} \tag{0.39}$$

As with E_o more information on this deduction can be found in [9].

Now that the losses in the sheath are known, the losses due to proximity effects between the phases, with corrections for the back-potential from the sheath can be calculated. Different from the normal proximity effects of two cables discussed in [9], there is a back potential from the sheath which has to be taken into account. This leads to the following equation for the magnetic field:

$$H_a=\frac{I}{4\pi a}+\left(\frac{\partial X_w}{r\partial\varphi}\right)_{r=a,\varphi=0}=\frac{I}{4\pi a}\left(1+2\sum_{m=1}^{\infty}\left(\frac{a}{r_h}\right)^{2m}W_m\right) \tag{0.40}$$

From this magnetic field the losses due to proximity effect can be calculated.
Unfortunately this part of the analytical approach has not been worked out jet.

Appendix D: Measurement results

Medium Voltage Cable

For 50Hz:

0.4191 + 0.0881i 0.2938 + 0.0018i 0.2947 + 0.0019i
0.2919 + 0.0018i 0.4192 + 0.0882i 0.2935 + 0.0009i
0.2922 + 0.0018i 0.2929 + 0.0009i 0.4205 + 0.0885i

For 100Hz:

0.4279 + 0.1848i 0.2942 + 0.0107i 0.2952 + 0.0104i
0.2931 + 0.0103i 0.4279 + 0.1839i 0.2939 + 0.0094i
0.2936 + 0.0096i 0.2933 + 0.0090i 0.4284 + 0.1854i

For 150Hz:

0.4388 + 0.2746i 0.2949 + 0.0174i 0.2958 + 0.0158i
0.2930 + 0.0170i 0.4393 + 0.2737i 0.2944 + 0.0150i
0.2938 + 0.0157i 0.2942 + 0.0148i 0.4400 + 0.2746i

For 200Hz:

0.4527 + 0.3607i 0.2956 + 0.0236i 0.2963 + 0.0216i
0.2939 + 0.0229i 0.4529 + 0.3604i 0.2950 + 0.0204i
0.2946 + 0.0209i 0.2947 + 0.0206i 0.4529 + 0.3609i

For 250Hz:

0.4661 + 0.4429i 0.2963 + 0.0284i 0.2963 + 0.0265i
0.2941 + 0.0280i 0.4681 + 0.4420i 0.2946 + 0.0250i
0.2939 + 0.0261i 0.2944 + 0.0247i 0.4670 + 0.4429i

For 300Hz:

0.4815 + 0.5231i 0.2962 + 0.0335i 0.2965 + 0.0314i
0.2940 + 0.0332i 0.4823 + 0.5226i 0.2947 + 0.0297i
0.2945 + 0.0306i 0.2948 + 0.0294i 0.4815 + 0.5231i

For 350Hz:

0.4989 + 0.6015i 0.2958 + 0.0389i 0.2957 + 0.0357i
0.2938 + 0.0382i 0.4959 + 0.6005i 0.2937 + 0.0337i
0.2940 + 0.0351i 0.2934 + 0.0340i 0.4965 + 0.6009i

For 400Hz:

0.5142 + 0.6794i 0.2953 + 0.0441i 0.2957 + 0.0408i
0.2946 + 0.0429i 0.5125 + 0.6780i 0.2939 + 0.0386i
0.2934 + 0.0404i 0.2937 + 0.0386i 0.5133 + 0.6800i

For 450Hz:

0.5280 + 0.7561i 0.2952 + 0.0497i 0.2945 + 0.0461i
0.2936 + 0.0485i 0.5258 + 0.7529i 0.2926 + 0.0433i
0.2933 + 0.0454i 0.2925 + 0.0437i 0.5271 + 0.7549i

For 500Hz:

0.5419 + 0.8294i 0.2937 + 0.0551i 0.2937 + 0.0501i
0.2922 + 0.0538i 0.5410 + 0.8234i 0.2919 + 0.0479i
0.2917 + 0.0500i 0.2909 + 0.0478i 0.5426 + 0.8281i

For 550Hz:

0.5582 + 0.9002i 0.2931 + 0.0603i 0.2918 + 0.0561i
0.2912 + 0.0592i 0.5572 + 0.8989i 0.2902 + 0.0532i
0.2904 + 0.0548i 0.2903 + 0.0525i 0.5569 + 0.9009i

For 600Hz:

0.5718 + 0.9716i 0.2919 + 0.0662i 0.2914 + 0.0605i
0.2900 + 0.0644i 0.5716 + 0.9704i 0.2893 + 0.0580i
0.2890 + 0.0601i 0.2887 + 0.0585i 0.5729 + 0.9741i

For 650Hz:

0.5860 + 1.0420i 0.2907 + 0.0714i 0.2903 + 0.0658i
0.2890 + 0.0703i 0.5856 + 1.0401i 0.2883 + 0.0631i
0.2880 + 0.0656i 0.2875 + 0.0635i 0.5855 + 1.0405i

For 700Hz:

0.5997 + 1.1131i 0.2898 + 0.0775i 0.2889 + 0.0715i
0.2876 + 0.0764i 0.6011 + 1.1109i 0.2865 + 0.0688i
0.2868 + 0.0713i 0.2863 + 0.0687i 0.6015 + 1.1120i

For 750Hz:

0.6138 + 1.1804i 0.2886 + 0.0825i 0.2874 + 0.0773i
0.2859 + 0.0815i 0.6185 + 1.1768i 0.2848 + 0.0738i
0.2848 + 0.0766i 0.2850 + 0.0735i 0.6154 + 1.1817i

For 800Hz:

0.6304 + 1.2480i 0.2868 + 0.0892i 0.2857 + 0.0830i
0.2854 + 0.0871i 0.6280 + 1.2473i 0.2828 + 0.0795i
0.2841 + 0.0820i 0.2828 + 0.0799i 0.6287 + 1.2487i

For 850Hz:

0.6458 + 1.3180i 0.2859 + 0.0952i 0.2844 + 0.0887i
0.2842 + 0.0934i 0.6439 + 1.3169i 0.2814 + 0.0851i
0.2825 + 0.0881i 0.2813 + 0.0854i 0.6431 + 1.3191i

For 900Hz:

0.6610 + 1.3813i 0.2847 + 0.1012i 0.2832 + 0.0942i
0.2828 + 0.0992i 0.6576 + 1.3812i 0.2799 + 0.0902i
0.2812 + 0.0936i 0.2799 + 0.0910i 0.6595 + 1.3839i

For 950Hz:

0.6752 + 1.4491i 0.2833 + 0.1077i 0.2811 + 0.1006i
0.2816 + 0.1053i 0.6723 + 1.4490i 0.2779 + 0.0965i
0.2798 + 0.0994i 0.2782 + 0.0969i 0.6715 + 1.4516i

For 1000Hz:

0.6864 + 1.5122i 0.2822 + 0.1140i 0.2800 + 0.1066i
0.2796 + 0.1115i 0.6869 + 1.5158i 0.2768 + 0.1024i
0.2775 + 0.1056i 0.2770 + 0.1029i 0.6870 + 1.5211i

For 1050Hz:

0.7010 + 1.5739i 0.2805 + 0.1211i 0.2786 + 0.1132i
0.2780 + 0.1175i 0.6986 + 1.5853i 0.2751 + 0.1089i
0.2755 + 0.1113i 0.2749 + 0.1093i 0.6996 + 1.5875i

For 1100Hz:

0.7126 + 1.6461i 0.2794 + 0.1268i 0.2769 + 0.1192i
0.2773 + 0.1243i 0.7160 + 1.6495i 0.2734 + 0.1150i
0.2747 + 0.1177i 0.2734 + 0.1150i 0.7138 + 1.6541i

For 1150Hz:

0.7311 + 1.7119i 0.2780 + 0.1333i 0.2757 + 0.1251i
0.2761 + 0.1302i 0.7306 + 1.7144i 0.2720 + 0.1206i
0.2735 + 0.1233i 0.2720 + 0.1211i 0.7278 + 1.7196i

For 1200Hz:

0.7407 + 1.7782i 0.2765 + 0.1402i 0.2741 + 0.1317i
0.2743 + 0.1379i 0.7407 + 1.7793i 0.2699 + 0.1272i
0.2715 + 0.1309i 0.2700 + 0.1277i 0.7415 + 1.7825i

For 1250Hz:

0.7589 + 1.8397i 0.2755 + 0.1468i 0.2726 + 0.1374i
0.2735 + 0.1437i 0.7557 + 1.8435i 0.2685 + 0.1328i
0.2705 + 0.1364i 0.2686 + 0.1339i 0.7562 + 1.8447i

For 1300Hz:

0.7696 + 1.8997i 0.2738 + 0.1533i 0.2709 + 0.1445i
0.2721 + 0.1500i 0.7668 + 1.9026i 0.2667 + 0.1394i
0.2689 + 0.1426i 0.2670 + 0.1402i 0.7694 + 1.9076i

For 1350Hz:

0.7811 + 1.9660i 0.2732 + 0.1599i 0.2700 + 0.1506i
0.2709 + 0.1573i 0.7845 + 1.9677i 0.2654 + 0.1457i
0.2673 + 0.1497i 0.2659 + 0.1462i 0.7864 + 1.9696i

For 1400Hz:

0.7962 + 2.0273i 0.2699 + 0.1669i 0.2683 + 0.1574i
0.2695 + 0.1640i 0.7902 + 2.0308i 0.2638 + 0.1524i
0.2662 + 0.1559i 0.2632 + 0.1533i 0.7940 + 2.0339i

For 1450Hz:

0.8083 + 2.0901i 0.2694 + 0.1731i 0.2670 + 0.1642i
0.2683 + 0.1709i 0.8079 + 2.0934i 0.2623 + 0.1588i
0.2648 + 0.1629i 0.2622 + 0.1593i 0.8088 + 2.0973i

For 1500Hz:

0.8210 + 2.1555i 0.2682 + 0.1800i 0.2656 + 0.1709i
0.2674 + 0.1780i 0.8199 + 2.1527i 0.2609 + 0.1656i
0.2638 + 0.1700i 0.2610 + 0.1661i 0.8206 + 2.1587i

For 1550Hz:

0.8354 + 2.2121i 0.2673 + 0.1866i 0.2642 + 0.1777i
0.2663 + 0.1844i 0.8336 + 2.2152i 0.2591 + 0.1724i
0.2621 + 0.1763i 0.2598 + 0.1725i 0.8336 + 2.2188i

For 1600Hz:

0.8501 + 2.2732i 0.2661 + 0.1940i 0.2621 + 0.1834i
0.2651 + 0.1908i 0.8455 + 2.2747i 0.2579 + 0.1786i
0.2613 + 0.1823i 0.2580 + 0.1795i 0.8470 + 2.2744i

For 1650Hz:

0.8610 + 2.3342i 0.2647 + 0.2004i 0.2608 + 0.1902i
0.2639 + 0.1981i 0.8596 + 2.3363i 0.2561 + 0.1855i
0.2600 + 0.1899i 0.2567 + 0.1861i 0.8577 + 2.3339i

For 1700Hz:

0.8725 + 2.3969i 0.2635 + 0.2081i 0.2594 + 0.1970i
0.2631 + 0.2051i 0.8718 + 2.4025i 0.2548 + 0.1918i
0.2588 + 0.1965i 0.2553 + 0.1934i 0.8699 + 2.3918i

For 1750Hz:

0.8843 + 2.4600i 0.2623 + 0.2148i 0.2582 + 0.2046i
0.2614 + 0.2125i 0.8831 + 2.4569i 0.2535 + 0.1993i
0.2575 + 0.2037i 0.2535 + 0.1997i 0.8799 + 2.4575i

For 1800Hz:

0.9021 + 2.5137i 0.2614 + 0.2217i 0.2573 + 0.2115i
0.2610 + 0.2185i 0.8928 + 2.5176i 0.2521 + 0.2062i
0.2564 + 0.2097i 0.2526 + 0.2064i 0.8921 + 2.5185i

For 1850Hz:

0.9026 + 2.5792i 0.2602 + 0.2286i 0.2549 + 0.2185i
0.2587 + 0.2271i 0.9076 + 2.5756i 0.2505 + 0.2128i
0.2545 + 0.2173i 0.2511 + 0.2135i 0.8994 + 2.5716i

For 1900Hz:

0.9171 + 2.6322i 0.2595 + 0.2364i 0.2552 + 0.2250i
0.2580 + 0.2332i 0.9204 + 2.6407i 0.2499 + 0.2196i
0.2536 + 0.2238i 0.2501 + 0.2209i 0.9213 + 2.6336i

For 1950Hz:

0.9366 + 2.6962i 0.2582 + 0.2428i 0.2535 + 0.2322i
0.2580 + 0.2402i 0.9307 + 2.6946i 0.2484 + 0.2271i
0.2530 + 0.2310i 0.2487 + 0.2271i 0.9284 + 2.6939i

For 2000Hz:

0.9446 + 2.7522i 0.2570 + 0.2500i 0.2523 + 0.2396i
0.2566 + 0.2471i 0.9412 + 2.7535i 0.2472 + 0.2342i
0.2516 + 0.2381i 0.2474 + 0.2343i 0.9416 + 2.7549i

For 2050Hz:

0.9557 + 2.8143i 0.2564 + 0.2575i 0.2515 + 0.2465i
0.2557 + 0.2545i 0.9536 + 2.8148i 0.2459 + 0.2413i
0.2509 + 0.2449i 0.2465 + 0.2415i 0.9524 + 2.8156i

For 2100Hz:

0.9643 + 2.8790i 0.2554 + 0.2650i 0.2503 + 0.2534i
0.2546 + 0.2623i 0.9657 + 2.8735i 0.2452 + 0.2477i
0.2501 + 0.2526i 0.2452 + 0.2488i 0.9632 + 2.8710i

For 2150Hz:

0.9806 + 2.9323i 0.2549 + 0.2724i 0.2495 + 0.2603i
0.2541 + 0.2688i 0.9782 + 2.9350i 0.2437 + 0.2548i
0.2488 + 0.2591i 0.2441 + 0.2557i 0.9745 + 2.9290i

For 2200Hz:

0.9924 + 2.9954i 0.2534 + 0.2798i 0.2485 + 0.2681i
0.2535 + 0.2761i 0.9867 + 2.9918i 0.2428 + 0.2622i
0.2489 + 0.2666i 0.2431 + 0.2627i 0.9862 + 2.9903i

For 2250Hz:

1.0049 + 3.0490i 0.2525 + 0.2864i 0.2475 + 0.2750i
0.2529 + 0.2828i 0.9994 + 3.0485i 0.2416 + 0.2693i
0.2476 + 0.2730i 0.2418 + 0.2697i 0.9968 + 3.0469i

For 2300Hz:

1.0107 + 3.1118i 0.2518 + 0.2942i 0.2463 + 0.2818i
0.2514 + 0.2908i 1.0108 + 3.1082i 0.2404 + 0.2761i
0.2460 + 0.2812i 0.2412 + 0.2770i 1.0090 + 3.1068i

For 2350Hz:

1.0243 + 3.1661i 0.2511 + 0.3014i 0.2458 + 0.2890i
0.2506 + 0.2977i 1.0239 + 3.1647i 0.2391 + 0.2838i
0.2455 + 0.2875i 0.2396 + 0.2840i 1.0191 + 3.1621i

For 2400Hz:

1.0337 + 3.2256i 0.2501 + 0.3085i 0.2438 + 0.2963i
0.2496 + 0.3051i 1.0295 + 3.2264i 0.2381 + 0.2903i
0.2442 + 0.2948i 0.2387 + 0.2917i 1.0296 + 3.2169i

For 2450Hz:

1.0476 + 3.2860i 0.2497 + 0.3160i 0.2432 + 0.3038i
0.2492 + 0.3123i 1.0457 + 3.2828i 0.2368 + 0.2978i
0.2442 + 0.3022i 0.2387 + 0.2984i 1.0333 + 3.2752i

For 2500Hz:

1.0594 + 3.3375i 0.2485 + 0.3232i 0.2429 + 0.3107i
0.2480 + 0.3197i 1.0500 + 3.3369i 0.2365 + 0.3052i
0.2433 + 0.3091i 0.2367 + 0.3051i 1.0504 + 3.3382i

Low Voltage Cable

For 50Hz:

0.5879 + 0.0988i 0.3897 + 0.0344i 0.3887 + 0.0098i
0.3904 + 0.0344i 0.5868 + 0.1005i 0.3921 + 0.0321i
0.3857 + 0.0133i 0.3883 + 0.0367i 0.5817 + 0.0996i

For 100Hz:

0.5967 + 0.2064i 0.3927 + 0.0731i 0.3881 + 0.0298i
0.3935 + 0.0740i 0.5957 + 0.2069i 0.3947 + 0.0750i
0.3853 + 0.0311i 0.3916 + 0.0750i 0.5907 + 0.2080i

For 150Hz:

0.6104 + 0.3081i 0.3973 + 0.1098i 0.3874 + 0.0467i
0.3979 + 0.1105i 0.6099 + 0.3078i 0.3997 + 0.1112i
0.3846 + 0.0476i 0.3959 + 0.1110i 0.6044 + 0.3079i

For 200Hz:

0.6243 + 0.4044i 0.4022 + 0.1448i 0.3860 + 0.0641i
0.4026 + 0.1458i 0.6258 + 0.4060i 0.4041 + 0.1469i
0.3835 + 0.0652i 0.4004 + 0.1461i 0.6193 + 0.4045i

For 250Hz:

0.6417 + 0.4977i 0.4071 + 0.1789i 0.3855 + 0.0811i
0.4076 + 0.1794i 0.6425 + 0.5003i 0.4091 + 0.1807i
0.3830 + 0.0823i 0.4055 + 0.1803i 0.6368 + 0.4965i

For 300Hz:

0.6613 + 0.5866i 0.4122 + 0.2110i 0.3844 + 0.0984i
0.4124 + 0.2114i 0.6621 + 0.5888i 0.4138 + 0.2131i
0.3817 + 0.0995i 0.4112 + 0.2124i 0.6545 + 0.5850i

For 350Hz:

0.6766 + 0.6744i 0.4169 + 0.2419i 0.3832 + 0.1160i
0.4164 + 0.2427i 0.6800 + 0.6756i 0.4176 + 0.2452i
0.3810 + 0.1161i 0.4156 + 0.2443i 0.6709 + 0.6725i

For 400Hz:

0.6967 + 0.7579i 0.4200 + 0.2732i 0.3823 + 0.1333i
0.4207 + 0.2733i 0.6968 + 0.7589i 0.4211 + 0.2758i
0.3805 + 0.1338i 0.4187 + 0.2750i 0.6885 + 0.7556i

For 450Hz:

0.7130 + 0.8389i 0.4235 + 0.3032i 0.3819 + 0.1506i
0.4239 + 0.3039i 0.7108 + 0.8407i 0.4260 + 0.3062i

0.3792 + 0.1515i 0.4218 + 0.3060i 0.7073 + 0.8376i

For 500Hz:

0.7287 + 0.9188i 0.4265 + 0.3338i 0.3808 + 0.1690i
0.4272 + 0.3335i 0.7281 + 0.9228i 0.4282 + 0.3377i
0.3787 + 0.1690i 0.4250 + 0.3369i 0.7218 + 0.9207i

For 550Hz:

0.7435 + 0.9974i 0.4292 + 0.3639i 0.3800 + 0.1860i
0.4295 + 0.3643i 0.7429 + 1.0023i 0.4307 + 0.3680i
0.3771 + 0.1869i 0.4275 + 0.3676i 0.7363 + 0.9986i

For 600Hz:

0.7590 + 1.0783i 0.4326 + 0.3936i 0.3788 + 0.2033i
0.4329 + 0.3946i 0.7593 + 1.0788i 0.4335 + 0.3974i
0.3771 + 0.2048i 0.4309 + 0.3975i 0.7517 + 1.0765i

For 650Hz:

0.7742 + 1.1564i 0.4352 + 0.4241i 0.3782 + 0.2209i
0.4349 + 0.4252i 0.7735 + 1.1590i 0.4360 + 0.4281i
0.3757 + 0.2230i 0.4330 + 0.4284i 0.7661 + 1.1534i

For 700Hz:

0.7859 + 1.2303i 0.4376 + 0.4532i 0.3769 + 0.2392i
0.4366 + 0.4531i 0.7903 + 1.2364i 0.4372 + 0.4591i
0.3749 + 0.2389i 0.4362 + 0.4575i 0.7790 + 1.2307i

For 750Hz:

0.8007 + 1.3081i 0.4388 + 0.4840i 0.3769 + 0.2571i
0.4393 + 0.4833i 0.8017 + 1.3153i 0.4409 + 0.4900i
0.3744 + 0.2572i 0.4371 + 0.4895i 0.7944 + 1.3090i

For 800Hz:

0.8138 + 1.3864i 0.4410 + 0.5149i 0.3755 + 0.2745i
0.4401 + 0.5144i 0.8169 + 1.3937i 0.4416 + 0.5198i
0.3732 + 0.2755i 0.4396 + 0.5195i 0.8068 + 1.3833i

For 850Hz:

0.8255 + 1.4636i 0.4415 + 0.5435i 0.3743 + 0.2924i
0.4428 + 0.5439i 0.8269 + 1.4660i 0.4435 + 0.5495i
0.3728 + 0.2932i 0.4401 + 0.5490i 0.8210 + 1.4559i

For 900Hz:

0.8386 + 1.5388i 0.4437 + 0.5728i 0.3735 + 0.3110i
0.4433 + 0.5744i 0.8392 + 1.5413i 0.4458 + 0.5806i
0.3715 + 0.3108i 0.4425 + 0.5792i 0.8304 + 1.5320i

For 950Hz:

0.8532 + 1.6101i 0.4458 + 0.6025i 0.3725 + 0.3287i
0.4452 + 0.6028i 0.8539 + 1.6142i 0.4462 + 0.6103i
0.3704 + 0.3287i 0.4441 + 0.6089i 0.8423 + 1.6050i

For 1000Hz:

0.8611 + 1.6868i 0.4466 + 0.6311i 0.3719 + 0.3457i
0.4466 + 0.6337i 0.8667 + 1.6875i 0.4492 + 0.6398i
0.3701 + 0.3475i 0.4471 + 0.6386i 0.8559 + 1.6767i

For 1050Hz:

0.8768 + 1.7606i 0.4487 + 0.6614i 0.3715 + 0.3647i
0.4498 + 0.6653i 0.8780 + 1.7630i 0.4509 + 0.6715i
0.3698 + 0.3654i 0.4477 + 0.6699i 0.8674 + 1.7511i

For 1100Hz:

0.8883 + 1.8308i 0.4485 + 0.6903i 0.3706 + 0.3829i
0.4508 + 0.6939i 0.8842 + 1.8351i 0.4534 + 0.7029i
0.3683 + 0.3843i 0.4458 + 0.6988i 0.8780 + 1.8247i

For 1150Hz:

0.8991 + 1.9022i 0.4528 + 0.7199i 0.3698 + 0.4012i
0.4519 + 0.7231i 0.9010 + 1.9078i 0.4541 + 0.7313i
0.3679 + 0.4012i 0.4512 + 0.7290i 0.8881 + 1.8986i

For 1200Hz:

0.9104 + 1.9805i 0.4530 + 0.7491i 0.3695 + 0.4186i
0.4531 + 0.7495i 0.9099 + 1.9781i 0.4561 + 0.7623i
0.3672 + 0.4199i 0.4531 + 0.7596i 0.9020 + 1.9693i

For 1250Hz:

0.9202 + 2.0460i 0.4553 + 0.7808i 0.3682 + 0.4372i
0.4528 + 0.7766i 0.9202 + 2.0546i 0.4572 + 0.7920i
0.3659 + 0.4361i 0.4556 + 0.7893i 0.9111 + 2.0411i

For 1300Hz:

0.9312 + 2.1219i 0.4555 + 0.8100i 0.3672 + 0.4551i
0.4540 + 0.8103i 0.9322 + 2.1249i 0.4573 + 0.8227i
0.3649 + 0.4561i 0.4563 + 0.8193i 0.9211 + 2.1133i

For 1350Hz:

0.9439 + 2.1904i 0.4571 + 0.8392i 0.3676 + 0.4727i
0.4542 + 0.8344i 0.9395 + 2.1961i 0.4617 + 0.8545i
0.3636 + 0.4719i 0.4554 + 0.8487i 0.9336 + 2.1853i

For 1400Hz:

0.9536 + 2.2604i 0.4580 + 0.8694i 0.3655 + 0.4921i
0.4587 + 0.8674i 0.9492 + 2.2675i 0.4612 + 0.8839i
0.3655 + 0.4910i 0.4579 + 0.8784i 0.9430 + 2.2574i

For 1450Hz:

0.9615 + 2.3333i 0.4596 + 0.8979i 0.3655 + 0.5093i
0.4583 + 0.8958i 0.9611 + 2.3353i 0.4630 + 0.9102i
0.3630 + 0.5087i 0.4588 + 0.9075i 0.9540 + 2.3255i

For 1500Hz:

0.9705 + 2.4060i 0.4631 + 0.9273i 0.3644 + 0.5275i
0.4604 + 0.9249i 0.9725 + 2.4068i 0.4632 + 0.9422i
0.3613 + 0.5265i 0.4616 + 0.9375i 0.9618 + 2.3976i

For 1550Hz:

0.9819 + 2.4805i 0.4629 + 0.9589i 0.3630 + 0.5462i
0.4646 + 0.9547i 0.9790 + 2.4819i 0.4649 + 0.9721i
0.3628 + 0.5451i 0.4637 + 0.9702i 0.9708 + 2.4683i

For 1600Hz:

0.9931 + 2.5513i 0.4659 + 0.9872i 0.3630 + 0.5653i
0.4646 + 0.9845i 0.9895 + 2.5505i 0.4659 + 0.9976i
0.3618 + 0.5634i 0.4648 + 0.9985i 0.9798 + 2.5370i

For 1650Hz:

1.0015 + 2.6211i 0.4685 + 1.0167i 0.3629 + 0.5832i
0.4655 + 1.0159i 1.0027 + 2.6206i 0.4665 + 1.0304i
0.3616 + 0.5823i 0.4674 + 1.0290i 0.9906 + 2.6088i

For 1700Hz:

1.0083 + 2.6909i 0.4677 + 1.0459i 0.3623 + 0.5999i
0.4667 + 1.0438i 1.0096 + 2.6933i 0.4683 + 1.0535i
0.3604 + 0.5997i 0.4683 + 1.0587i 1.0005 + 2.6701i

For 1750Hz:

1.0189 + 2.7582i 0.4714 + 1.0759i 0.3612 + 0.6189i
0.4673 + 1.0722i 1.0133 + 2.7456i 0.4691 + 1.0836i
0.3596 + 0.6175i 0.4695 + 1.0873i 1.0051 + 2.7421i

For 1800Hz:

1.0309 + 2.8321i 0.4696 + 1.1065i 0.3622 + 0.6379i
0.4710 + 1.1029i 1.0195 + 2.8185i 0.4736 + 1.1167i
0.3602 + 0.6372i 0.4685 + 1.1180i 1.0186 + 2.8158i

For 1850Hz:

1.0379 + 2.9017i 0.4735 + 1.1370i 0.3600 + 0.6565i
0.4689 + 1.1328i 1.0329 + 2.8883i 0.4684 + 1.1468i
0.3587 + 0.6541i 0.4742 + 1.1468i 1.0245 + 2.8853i

For 1900Hz:

1.0443 + 2.9695i 0.4747 + 1.1646i 0.3603 + 0.6739i
0.4710 + 1.1593i 1.0384 + 2.9575i 0.4723 + 1.1760i
0.3577 + 0.6729i 0.4735 + 1.1777i 1.0379 + 2.9515i

For 1950Hz:

1.0584 + 3.0403i 0.4757 + 1.1942i 0.3594 + 0.6923i
0.4768 + 1.1914i 1.0503 + 3.0236i 0.4739 + 1.2037i
0.3605 + 0.6917i 0.4756 + 1.2048i 1.0417 + 3.0227i

For 2000Hz:

1.0592 + 3.1116i 0.4788 + 1.2223i 0.3586 + 0.7113i
0.4759 + 1.2172i 1.0603 + 3.0894i 0.4759 + 1.2354i
0.3577 + 0.7073i 0.4766 + 1.2326i 1.0522 + 3.0910i

For 2050Hz:

1.0727 + 3.1806i 0.4808 + 1.2527i 0.3609 + 0.7307i
0.4757 + 1.2514i 1.0659 + 3.1606i 0.4814 + 1.2640i
0.3581 + 0.7290i 0.4757 + 1.2641i 1.0663 + 3.1597i

For 2100Hz:

1.0818 + 3.2528i 0.4805 + 1.2799i 0.3582 + 0.7468i
0.4823 + 1.2764i 1.0767 + 3.2252i 0.4767 + 1.2904i
0.3588 + 0.7440i 0.4783 + 1.2926i 1.0727 + 3.2417i

For 2150Hz:

1.0939 + 3.3176i 0.4836 + 1.3108i 0.3564 + 0.7671i
0.4860 + 1.3057i 1.0881 + 3.2966i 0.4797 + 1.3245i
0.3600 + 0.7616i 0.4814 + 1.3199i 1.0811 + 3.3110i

For 2200Hz:

1.0968 + 3.3873i 0.4838 + 1.3406i 0.3557 + 0.7833i
0.4851 + 1.3347i 1.0974 + 3.3631i 0.4787 + 1.3521i
0.3594 + 0.7806i 0.4832 + 1.3506i 1.0921 + 3.3783i

For 2250Hz:

1.1041 + 3.4594i 0.4866 + 1.3673i 0.3562 + 0.8014i
0.4833 + 1.3619i 1.1038 + 3.4325i 0.4793 + 1.3823i
0.3560 + 0.7989i 0.4827 + 1.3796i 1.0939 + 3.4500i

For 2300Hz:

1.1115 + 3.5260i 0.4890 + 1.3985i 0.3572 + 0.8215i
0.4812 + 1.3986i 1.1132 + 3.5008i 0.4826 + 1.4108i
0.3560 + 0.8213i 0.4864 + 1.4073i 1.1087 + 3.5217i

For 2350Hz:

1.1254 + 3.5915i 0.4860 + 1.4297i 0.3566 + 0.8381i
0.4888 + 1.4176i 1.1155 + 3.5732i 0.4834 + 1.4361i
0.3564 + 0.8326i 0.4864 + 1.4378i 1.1165 + 3.5859i

For 2400Hz:

1.1333 + 3.6658i 0.4890 + 1.4551i 0.3569 + 0.8575i
0.4890 + 1.4497i 1.1303 + 3.6351i 0.4891 + 1.4656i
0.3553 + 0.8530i 0.4905 + 1.4674i 1.1227 + 3.6528i

For 2450Hz:

1.1379 + 3.7270i 0.4930 + 1.4840i 0.3579 + 0.8741i
0.4908 + 1.4763i 1.1312 + 3.7042i 0.4872 + 1.4949i
0.3562 + 0.8697i 0.4872 + 1.4959i 1.1242 + 3.7200i

For 2500Hz:

1.1480 + 3.8064i 0.4927 + 1.5157i 0.3551 + 0.8949i
0.4919 + 1.5133i 1.1444 + 3.7771i 0.4921 + 1.5303i
0.3565 + 0.8919i 0.4911 + 1.5270i 1.1417 + 3.7939i

Paper UPEC 2005

BEHAVIOR OF DEVICES AND GRID COMPONENTS IN THE FREQUENCY DOMAIN

M.A.J.T.Hooijmans, J.F.G.Cobben, W.L.Kling

Electrical Power Systems, Technical University Eindhoven, The Netherlands.

7

ABSTRACT

Analyzing harmonics in a LV- and MV-grid, thereby considering non-linear loads and special loads as grid-connected PV-systems, is difficult due to the interaction between these components. Furthermore the characteristics of most (grid) components depend on frequency. To make a proper estimation of a possible harmonic problem there is a need for a characteristic description of these components and a proper calculation model. The characteristics of the most important grid component (cable) and several devices are measured and used for calculation in the developed model for harmonic calculations.

1 INTRODUCTION

Harmonic distortion is caused by electrical equipment with non-linear current/voltage characteristics. This equipment injects harmonic currents into the grid. These harmonic currents induce harmonic voltages in the grid impedances, which are superimposed upon the existing supply voltage. Usually these harmonic voltages are no problem, because they are relatively small compared to the amplitude of the fundamental voltage. However, it is possible that resonance circuits amplify the voltage harmonics to such an extent that they have a relatively large influence on the fundamental voltage. This results in a distorted supply voltage. At the current time the impact of these harmonic voltages on the Dutch net and loads has not been fully worked out. As a first step for harmonic calculations, models of the net and the most common loads are necessary. Therefore research has been done into the modeling of different network elements for harmonics.

2. THE HARMONIC MODEL

The harmonic model is shown in Figure 1.
The grid part of the model consists of:

- A harmonic voltage source V_s modelling the voltage background harmonic distortion.
- The resistance R_b of mostly the LV-cable. R_b is frequency dependent due to skin- and proximity- effects.
- The inductance L_b of the cable and the MV/LV transformer. L_b is frequency dependent due to skin- and proximity- effects.

The load part of the model consists of:

- A harmonic current source, modelling the harmonic currents of the load without the effect of background voltage distortions from the grid.
- A capacitor C, modelling the imaginary part of the power consumed by the load. C may vary with frequency and can be positive as well as negative.
- A resistor R, modelling the real part of the power consumed by the load. R may vary with frequency and can be positive as well as negative.

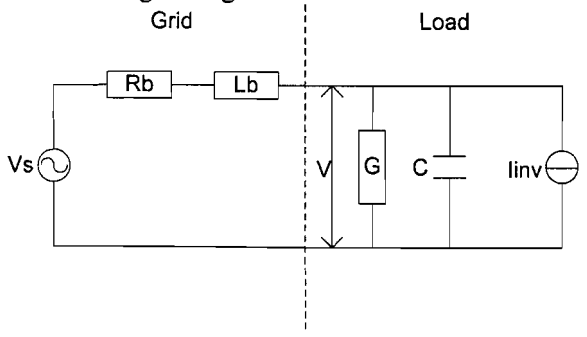

Figure 2: Harmonic model

The transfer function of this circuit is given by:

$$V = \frac{V_s + I_{inv}\left(R_b + j\omega L_b\right)}{1 + \left(R_b + j\omega L_b\right)\cdot\left(G + j\omega C\right)} \qquad (1)$$

This system will become unstable when the denominator of equation (1) becomes zero. This will occur when:

$$\omega = \omega_0\sqrt{1-\left(\frac{R_b}{Z_0}\right)^2} \qquad with \quad Z_0 = \sqrt{\frac{L_b}{C}} \text{ and } \omega_0 = \frac{1}{\sqrt{L_b C}} \qquad (2)$$

and

$$G = -\frac{R_b}{Z_0^2} \qquad with \quad Z_0 = \sqrt{\frac{L_b}{C}} \qquad (3)$$

Equations (2) and (3) imply that instability can only occur in very specific circumstances. Due to skin- and

proximity-effects in the impedance of the grid and frequency dependency of the load, the resonance frequency is related to the frequency itself. Thus an accurate description in the frequency domain is needed for each of the elements of the model to make a proper estimation of a possible harmonic problem.

3 THE EXTENDED HARMONIC MODEL

The model presented only contains one load and the impedance of the grid to that load. This model can be extended to incorporate more loads and grid topologies. An example of such an extended model is displayed in Figure 3.

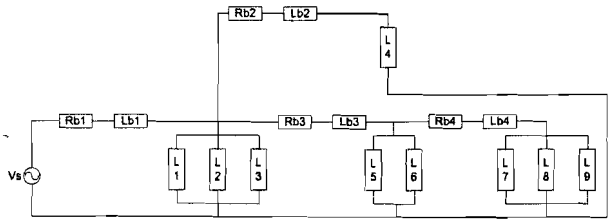

Figure 3: Extended harmonic model

For convenience the loads are depicted as one impedance each. These loads still consist of the G, C and I_{inv} as explained. The loads can vary from normal linear loads (then there is no I_{inv}) to complex loads that introduce harmonic currents in the grid.

4 THE CABLE MODEL

The configuration of a three-phase cable is shown in Figure 4, where impedances, voltages and currents are identified.

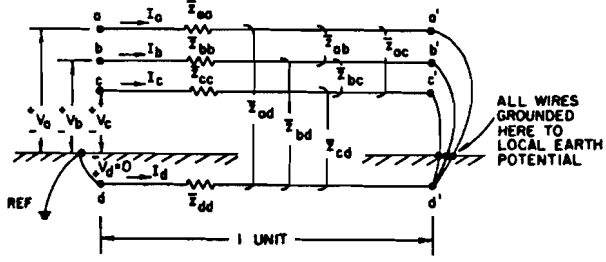

Figure 4: Three-phase cable

This configuration can be described by (after reducing the original matrix with the reference selected):

$$\begin{bmatrix} V_a \\ V_b \\ V_c \end{bmatrix} = \begin{bmatrix} z_{aa} & z_{ab} & z_{ac} \\ z_{ba} & z_{bb} & z_{bc} \\ z_{ca} & z_{cb} & z_{cc} \end{bmatrix} \begin{bmatrix} I_a \\ I_b \\ I_c \end{bmatrix}$$

where it is noted that $z_{ba} = z_{ab}$, due to reciprocity of the mutual inductances in a linear, passive, bilateral network.

4.1 Cable Resistance

Cable resistance is a crucial electrical parameter because of its influence on the cable rating. Generally the resistance increases with increasing frequency. This increase is caused by an uneven distribution of the current due to skin and proximity effects. Given that both effects can be considered separately, a general formula for cable resistance is recommended in [1]. This formula is extended to calculate the resistance at a harmonic frequency:

$$R_h = R_{DC}\left(1 + y_{s,h} + y_{p,h}\right)\left(1 + \lambda_{2,h}\right) \tag{5}$$

where R_h is the current resistance of the conductor at operating temperature and R_{dc} is the DC resistance of the conductor at operating temperature. $Y_{s,h}$ and $y_{p,h}$ are factors of skin and proximity effects, respectively. $\lambda_{2,h}$ is a factor of losses in the sheath of the cable.
The extended formula for $y_{s,h}$ is equal to:

$$y_{s,h} = \begin{cases} \dfrac{x_{s,h}^4}{192 + 0.8x_{s,h}^4} & 0.0 < x_{s,h} \le 2.8 \\ 0.0563x_{s,h}^2 - 0.0177x_{s,h} - 0.136 & 2.8 < x_{s,h} \le 3.8 \\ \dfrac{x_{s,h}}{2\sqrt{2}} - \dfrac{11}{15} & 3.8 < x_{s,h} \end{cases} \tag{6}$$

with

$$x_{s,h}^2 = \frac{8\pi f_1 h.10^{-7}}{R_{DC}} \tag{7}$$

where f_1 is the fundamental frequency and h is the harmonic order. The extended formula for $y_{p,h}$ is equal to:

$$y_{p,h} = \frac{my^2 G_{p,h}}{2 - 5y^2 \dfrac{II_{p,h}}{12}} \tag{8}$$

where m is equal to 2.5, while proximity coefficients $G_{p,h}$ and $II_{p,h}$ are given by:

$$G_{p,h} = \begin{cases} \dfrac{11x_{p,h}^4}{704 + 20x_{p,h}^4} & 0.0 < x_{p,h} \le 2.8 \\ -0.08x_{p,h}^2 + 0.72x_{p,h} - 1.04 & 2.8 < x_{p,h} \le 3.8 \\ \dfrac{x_{p,h}}{4\sqrt{2}} - \dfrac{1}{8} & 3.8 < x_{p,h} \end{cases} \tag{9}$$

$$II_{p,h}(4) = \begin{cases} \dfrac{1}{3}\dfrac{1 + 0.0283x_{p,h}^4}{1 + 0.0042x_{p,h}^4} & 0.0 < x_{p,h} \le 2.8 \\ 0.0384x_{p,h}^2 + 0.119x_{p,h} + 0.095 & 2.8 < x_{p,h} \le 3.8 \\ \dfrac{2x_{p,h} - 4.69}{x_{p,h} - 1.16} & 3.8 < x_{p,h} \end{cases} \tag{10}$$

Factor $y_{p,h}$ is also affected by the spacing ratio of $y=d_c/s$, where s is the spacing between conductor axes, and d_c is the diameter of an equivalent circular conductor having the same cross-section and degree of compactness as a shaped conductor.

When armour or a sheath is present within the cable, hysteresis losses and additional eddy-current losses are encountered. The factor λ introduced in [2] incorporates the extra losses at 50 Hz. By using a generic frequency f instead of 50 Hz, the factor λ is used to approximate the extra losses in a cable at harmonic frequency. This adapted factor λ is given by:

$$\lambda_{2,h} = \frac{0.358\frac{R_a}{R_h'}\left(\frac{2r_1}{d_a}\right)}{1+\left(\frac{2.77R_a x10^6}{2\pi f_1 h}\right)} \quad (11)$$

where R_a and R'_h are respectively the armour/sheath DC resistance and cable harmonic resistance without the armour. r_1 is the circumscribing radius of three-sector shaped conductors in a three-core cable. d_a is the mean diameter of the armour.

4.2 Cable Inductance

The total cable inductance can be expressed as:

$$L_{total} = L_{phase} + L_{ext} + L_{sheath} + L_{proximity} \quad (12)$$

with:

- L_{phase} the internal inductance of the phases carrying current, affected by the skin-effect.
- L_{ext} the external inductance due to the magnetic field in between conductors.
- L_{sheath} the internal inductance of the sheath carrying current ($L_{sheath1}$) plus the inductance of the sheath due to eddy currents induced in the sheath by a magnetic field ($L_{sheath2}$).
- $L_{proximity}$ the inductance due to eddy currents induced in each of the phases by an external magnetic field.

Formulas have been worked out for each of these inductances in [3] and [6], except for $L_{proximity}$.

4.3 Cable Measurement

The goal is to acquire an impedance matrix as in (4) for each harmonic till the 50th. For this a single-phase current injection is applied to determine the elements of the impedance matrix. Figure 5 shows the lumped parameter model of the cable system under the phase A to neutral (A-N) current injection.

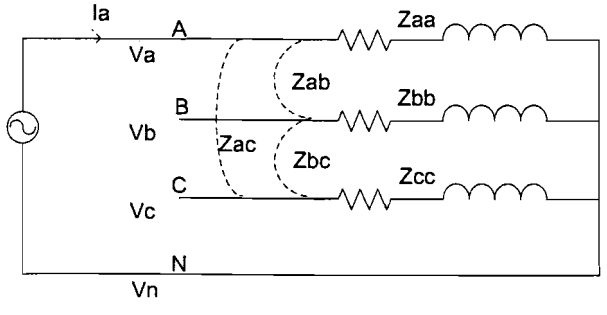

Figure 5: Circuit model

Voltages V_{aa}, V_{ab}, V_{ac} and current I_a are recorded in a measurement with an injection of a sine waveform current for each harmonic. Self and mutual impedance at order h for phase A are calculated as follows:

$$Z_{h,aa} = \left.\frac{V_{h,an}}{I_{h,a}}\right|_{I_b=I_c=0} \quad Z_{h,ba} = \left.\frac{V_{h,bn}}{I_{h,a}}\right|_{I_b=I_c=0} \quad Z_{h,ca} = \left.\frac{V_{h,cn}}{I_{h,a}}\right|_{I_b=I_c=0} \quad (13)$$

This is repeated for a current injection under B and C until the entire matrix is known. The measurement setup used for this measurement is displayed in Figure 6.

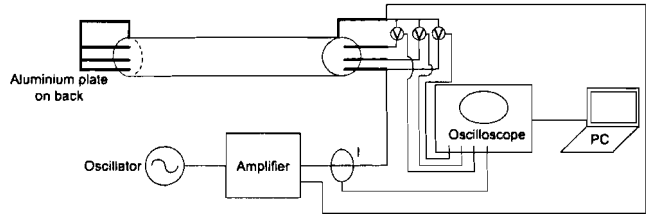

Figure 6: Measurement setup

4.4 Cable results

Measurement results for two frequently used cable types plus theoretical results with the described theory are shown in Figure 7 and 7.

The theoretical resistance corresponds well with the measured values for the MVC and reasonably well with the LVC. The differences can be ascribed to the differences in cable structure. The resistance rises in a linear way with frequency.

The reactance increases with frequency, but not in a linear way. As can be observed it curves slightly down. This means the inductance decreases for an increasing harmonic order. The difference between the theoretical and measured reactance's can be ascribed to the fact that the inductance $L_{proximity}$ has not jet been introduced in the theory.

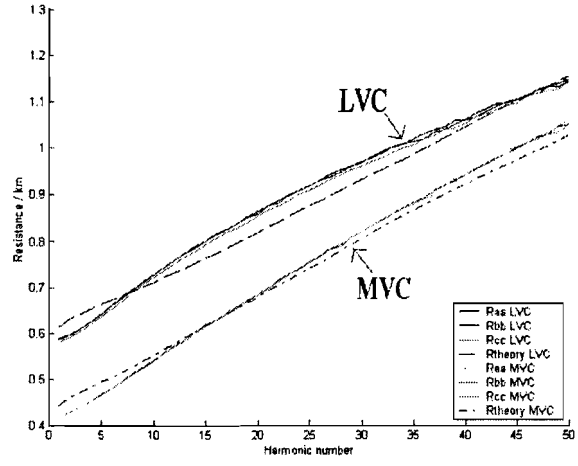

Figure 6: Resisitance medium Voltage Cable 3x240 Alrm as 70 and Low Voltage Cable 4x150 Alsvm

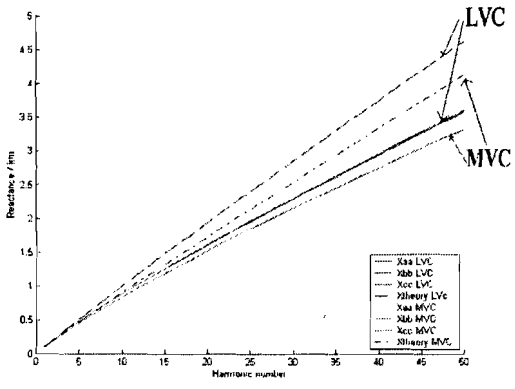

Figure 7: Reactance MV and LV Cable

5. THE LOADS

Measurement results of some standard electrical equipment are displayed in figure 8 and figure 9.

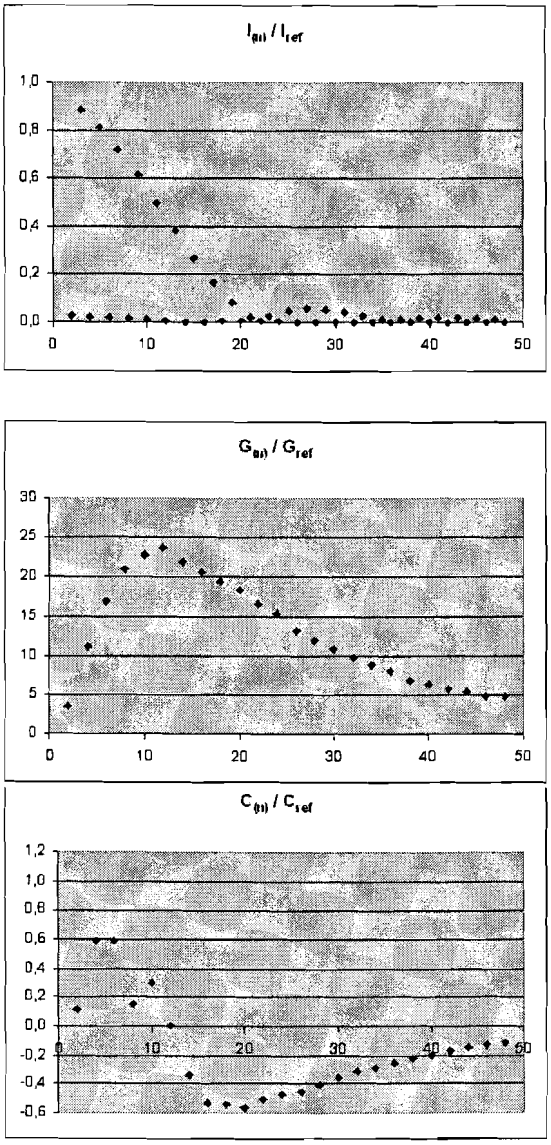

Figure 8: Load measurements results TV

The total tested equipment consists of common Dutch household appliances like television sets, video recorders, computers, etc. Of each appliance the frequency frequency dependent parameters G, C and I_{inv} were determined. Next to the individual measurements there were measurements done on combinations of the equipment. More information on the measurement procedure can be found in [3].

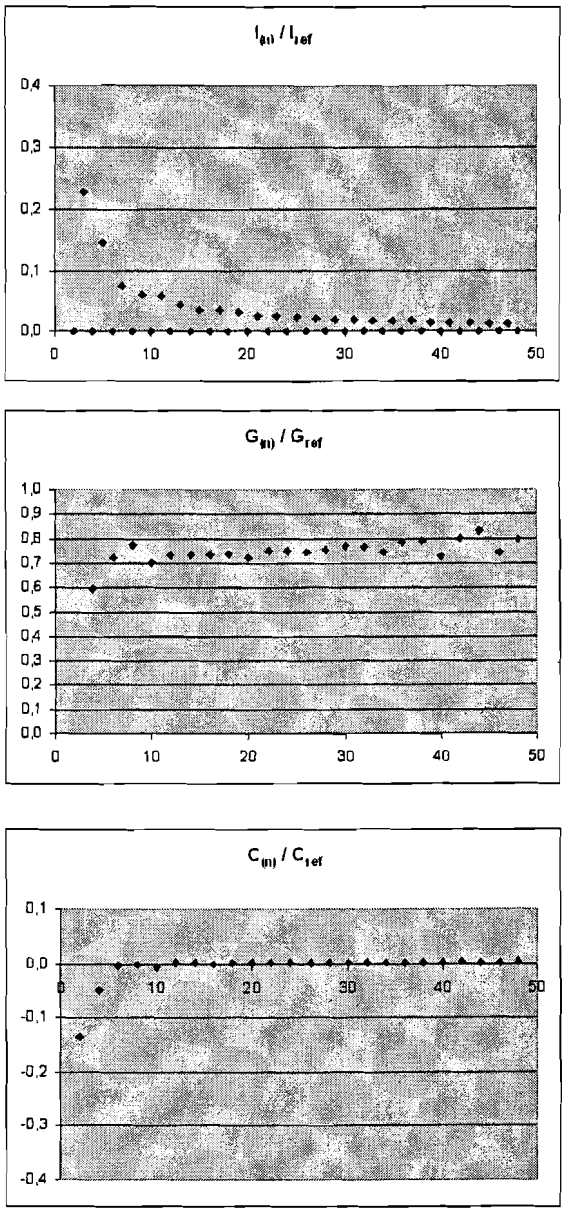

Figure 9: Load measurements results Dimmer with incandescent light

The television was studied at normal operation with sound and picture. The dimmer/lamp combination was studied at a power of 88W. As expected, the G and C can vary from positive to negative.

7. CONCLUSIONS

A basic harmonic model is presented. Theoretical values of cable resistance and inductance are given as well as measured values. A basic transformer model is discussed, which incorporates the harmonic behavior of this grid element up to 2500Hz. The parameters for this transformer model can be derived from 50Hz manufacturer's data. As last measurement results are given for different common load types which are most common in the Dutch grid.

8. REFERENCES

1. 'Electric cables – Calculation of the current rating – Part 1: Current rating equations (100% load factor) and calculation of losses', CEI/IEC international standard 287-1-1, 1982 (Corrected ed. 1994).
2. Anders, G.J., 'Rating of electric power cables', IEEE Press New York, 1997.
3. Hooijmans, M.A.J.T., 'Harmonic behavior and modeling of grid components and devices', MSc Thesis, Eindhoven University of Technology, May 2005.
4. Neves, W.L.A. and Dommel, H.W., 'On modeling iron core nonlinearities', IEEE Transactions on Power Systems, vol. PWRS-8, pp.417-425, May 1993.
5. CIGRE Working group 36.05, 'Harmonic characteristic parameters, methods of study, estimates of existing values in the network', Electra No. 77, pp.35-54.
6. Kaden, H., 'Wirbelströme und Schirming in der Nachrichtentechnik', Springer-Verlag Berlin, 1959.

Contact: J.F.G.Cobben
Eindhoven University of Technology
P.O. Box 513
5600 MB Eindhoven
The Netherlands
j.f.g.cobben@tue.nl